Optimization of Power Systems with Voltage Security Constraints

by

William D. Rosehart

A thesis presented to the University of Waterloo
in fulfillment of the
thesis requirement for the degree of
Doctor of Philosophy
in
Electrical and Computer Engineering

Waterloo, Ontario, Canada 2000

©William D. Rosehart, 2000

National Library of Canada
Acquisitions and Bibliographic Services
395 Wellington Street
Ottawa ON K1A 0N4
Canada

Bibliothèque nationale du Canada
Acquisitions et services bibliographiques
395, rue Wellington
Ottawa ON K1A 0N4
Canada

Your file Votre référence

Our file Notre référence

The author has granted a non-exclusive licence allowing the National Library of Canada to reproduce, loan, distribute or sell copies of this thesis in microform, paper or electronic formats.

L'auteur a accordé une licence non exclusive permettant à la Bibliothèque nationale du Canada de reproduire, prêter, distribuer ou vendre des copies de cette thèse sous la forme de microfiche/film, de reproduction sur papier ou sur format électronique.

The author retains ownership of the copyright in this thesis. Neither the thesis nor substantial extracts from it may be printed or otherwise reproduced without the author's permission.

L'auteur conserve la propriété du droit d'auteur qui protège cette thèse. Ni la thèse ni des extraits substantiels de celle-ci ne doivent être imprimés ou autrement reproduits sans son autorisation.

0-612-60563-9

Canada

The University of Waterloo requires the signatures of all persons using or photocopying this thesis. Please sign below, and give address and date.

Abstract

As open access market principles are applied to power systems, significant changes in their operation and control are occurring. In the new marketplace, power systems are operating under higher loading conditions as market influences demand greater attention to operating cost versus stability margins. Since stability continues to be a basic requirement in the operation of any power system, new tools are being considered to analyze the effect of stability on the operating cost of the system, so that system stability can be incorporated into the costs of operating the system.

In this thesis, new optimal power flow (OPF) formulations are proposed based on multi-objective methodologies to optimize active and reactive power dispatch while maximizing voltage security in power systems. The effects of minimizing operating costs, minimizing reactive power generation and/or maximizing voltage stability margins are analyzed. Results obtained using the proposed Voltage Stability Constrained OPF formulations are compared and analyzed to suggest possible ways of costing voltage security in power systems.

When considering voltage stability margins, the importance of system modeling becomes critical, since it has been demonstrated, based on bifurcation analysis, that modeling can have a significant effect of the behavior of power systems, especially at high loading levels. Therefore, this thesis also examines the effects of detailed generator models and several exponential load models. Furthermore, because of its influence on voltage stability, a Static Var Compensator model is also incorporated into the optimization problems.

ACKNOWLEDGMENTS

I would first like to thank and acknowledge Prof. Claudio Cañizares for his guidance and support since my undergraduate degree. I will always remember Claudio, as more than just a supervisor, during my degree, we ran races together and even tried to climb a mountain together. I also greatly acknowledge Prof. Victor Hugo Quintana, my co-supervisor, for his support in both my research and professional development. Since I started my Ph.D. degree, Prof. Quintana has always provided me with great resources and wise advice.

Also greatly appreciated is the excellent work environment created by my colleagues. The "Lab" has gone through a few generations since I arrived. I would like to thank Ian for creating "party lab" while we worked on assignments and research, Mansour's and Andre's help at the start and for showing me that a Ph.D. can be completed. I would like to thank Zeno for showing me the ropes when I first arrived, as well as Leon for software and power system tutorials. Of course, I am greatly appreciative of having Edvina as my "office-mate" for so many years. I enjoyed everything from our technical debates to planning dinners for hiking and canoe trips. I have come to greatly enjoy the company of Mithulan and Hong in the "Lab". Hong has managed to keep the computers happy, and I have greatly enjoyed my many technical and not so technical discussions with Mithulan.

Outside of the "Lab", there have been many people who deserve my appreciation and acknowledgment. Prof. John Reeve, taught me my first graduate course, and has always been able to point to the importance of engineering in our work. I am very grateful to Prof. David Wang, who adopted me in the controls group and Prof. Vannelli who has encouraged and supported my research throughout my degree. June and Gord guided me through my teaching terms and taught me many valuable lessons. Rodrigo and Marcelino have been good friends and colleagues. Their help in understanding the mysteries of optimization has been greatly appreciated. I am indebted to Geraldo, for providing me a basis from which I could develop so much.

Of course, it would not have been possible to finish my Ph.D. without the support of many close friends and my family. Jan has been a great friend over the years. Gilbert and Laleh have also been great friends. I greatly enjoyed our time together in the E&CE GSA Council. I think it will be a long time before another council works together so well. The support of my family has been invaluable, my father and my mother have always supported and encouraged my studies.

Dedication

To the birds in the tree outside my window
for making sure I got to school each day.

In loving memory of my Grandmother.

Contents

1 Introduction **1**

1.1 Background 2

1.1.1 Optimization Techniques 2

1.1.2 Modeling 4

1.2 Research Motivation and Objectives 5

1.3 Implementation Methods 6

1.4 Outline of the Thesis 7

2 Optimal Power Flow and Optimization Techniques **9**

2.1 Introduction 10

2.2 Optimal Power Flow 11

2.3 Logarithmic-Barrier Interior Point Method 12

2.3.1 Associated Problem and Optimality Conditions 12

2.4 Higher Order Primal-Dual Interior Point Algorithms 15

2.4.1 Predictor-Corrector Interior Point Methods 15

2.5 Summary 17

3 Voltage Stability **18**

3.1 Introduction 19

3.2 Bifurcation Analysis 19

3.3 Saddle-node Bifurcations 21

3.4 Limit-Induced Bifurcations 25

3.5 Bifurcation Analysis Methods 28

3.5.1 Continuation Methods 28

3.5.2 Direct Methods 31

3.6 Optimization Based Voltage Stability Analysis 32

3.6.1 System Model 32

3.6.2 Effects of Control Parameters on Bifurcation Diagrams 33

3.6.3 Optimization Based Direct Method 35
3.6.4 Maximum Distance to Collapse Problem 36
3.6.5 Maximum Distance to Saddle-node Bifurcation 38
3.7 Summary 40

4 Voltage Stability Constrained Optimal Power Flow **42**
4.1 Introduction 43
4.1.1 OPF and Voltage Stability Criteria 46
4.1.2 Limit-induced Versus Saddle-node Bifurcations 47
4.1.3 Modified Maximum Distance to Collapse 50
4.2 VSC-OPF Formulations 52
4.2.1 Hybrid VSC-OPF Formulation 54
4.2.2 Linear Combination VSC-OPF Formulation 55
4.2.3 Fixed Stability Margin VSC-OPF 56
4.2.4 Goal Programming VSC-OPF Formulation 56
4.2.5 VSC-OPF with Reactive Power Pricing Formulation 57
4.3 Numerical Analysis 59
4.3.1 Modified Maximum Distance to Collapse Formulation 59
4.3.2 Hybrid VSC-OPF Formulation 63
4.3.3 Linear Combinations VSC-OPF 69
4.3.4 Fixed Stability Margin VSC-OPF 74
4.3.5 Goal Programming VSC-OPF 75
4.3.6 VSC-OPF with Reactive Power Pricing 75
4.4 Cost of Voltage Stability 80
4.5 Numerical Implementation 83
4.6 Summary of Results 85

5 Power System Modeling **86**
5.1 Introduction 87
5.2 Generator Model 87
5.2.1 Generator Limits 88
5.3 Load Models 91
5.4 Static Var Compensator (SVC) 92
5.5 Numerical Analysis 96
5.5.1 Detailed Generator Model 96
5.5.2 Exponential Load Models 101
5.5.3 Static Var Compensator 111

5.6 Summary of Results 115

6 Conclusions **117**

6.1 Summary and Contributions 118

6.2 Directions for Future Work 120

Bibliography **121**

List of Tables

4.1 Results of reactive power limits on various system variables for the 57-bus system (at λ_* for $\lambda_p = 0.95$) 63

5.1 Maximum Loading (λ_*) for the 57-bus system found by applying the Maximum Distance to Collapse formulation using the detailed generator model 99

5.2 Maximum Loading λ_* for the 57-bus system found for the Maximum Distance to Collapse formulation. 104

5.3 Maximum Loading λ_* for the 118-bus system found for the Maximum Distance to Collapse formulation. 105

List of Figures

3.1 Generator-infinite bus system. 22
3.2 Bifurcation diagram for generator-infinite bus example. 24
3.3 Illustration of limit induced instability. 26
3.4 Bifurcation diagram for generator-infinite bus example. 27
3.5 Illustration of continuation algorithm. 29
3.6 Bifurcation diagram for the IEEE 14-bus system. 33
3.7 Single line diagram of the IEEE 14-bus system. 34
3.8 Generator-infinite bus single line diagram. 37
3.9 3-bus system single line diagram. 40

4.1 Single line diagram of the 57-bus system. 44
4.2 Single line diagram of the 118-bus system. 45
4.3 Maximum loading versus current operating point using the Maximum Distance to Collapse problem for the 57-bus test system. 60
4.4 Maximum loading versus current operating point using the Maximum Distance to Collapse problem for the 118-bus test system. 61
4.5 Change in voltage magnitude at Bus 30 versus λ_p for the 57-bus test system. 62
4.6 Generation costs versus current operating point applying the Hybrid VSC-OPF problem for the 57-bus test system. 64
4.7 Maximum loading point versus current operating point applying the Hybrid VSC-OPF problem for the 57-bus test system. 65
4.8 Generator cost versus current operating point for the 57-bus test system with operational limits on both the current and maximum loading point. . 67
4.9 Maximum loading point versus current operating point for the 57-bus test system with operational limits on both the current and maximum loading point. 68
4.10 Operating costs versus weighting factor ω_1 for the Linear Combination formulation applied to the 57-bus test system for $\lambda_p = 0.9$. 69
4.11 Maximum loading versus weighting factor ω_1 for the Linear Combination formulation applied to the 57-bus test system for $\lambda_p = 0.9$. 70

4.12 Operating costs versus current operating point for the Linear Combinations formulation, Maximum Distance to Collapse and traditional OPF for the 57-bus test system. 71
4.13 Maximum loading point versus current operating point for the Linear Combinations and Maximum Distance to Collapse formulations for the 57-bus test system. 72
4.14 Operating costs versus current operating point for the Linear Combination and traditional OPF formulations for the 118-bus test system. 73
4.15 Cost versus current operating point for the Fixed Stability Margin and traditional OPF formulations for the 118-bus test system. 74
4.16 Cost versus current operating point for the Goal Programming ($\omega_2 = 0.001$, $\omega_3 = 1 - \omega_1$) and traditional OPF formulations for the 57-bus test system. 76
4.17 Maximum loading point versus current operating point for the Goal Programming ($\omega_2 = 0.001$, $\omega_3 = 1 - \omega_1$), traditional OPF and Maximum Distance to Collapse formulations for the 57-bus test system. 77
4.18 Cost versus current operating point for the Goal Programming formulation considering reactive power costs ($\omega_2 = 0.001$, $\omega_3 = 1 - \omega_1$, $\omega_4 = \omega_5 = 0.3$) and traditional OPF formulation for the 57-bus test system. 78
4.19 Maximum loading point versus current operating point for Goal Programming formulation considering reactive power costs ($\omega_2 = 0.001$, $\omega_3 = 1 - \omega_1$, $\omega_4 = \omega_5 = 0.3$), traditional OPF and Maximum Distance to Collapse formulations for the 57-bus test system. 79
4.20 Difference in operating cost (solid line) when applying the Maximum Distance to Collapse formulation ($\times$) versus a traditional OPF ($*$) formulation for the 57-bus system. 81
4.21 Percent change in operating costs (solid line) and stability margin (dashed line) when applying the Maximum Distance to Collapse formulation versus a traditional OPF formulation for the 57-bus system. 82
4.22 Difference in operating cost (solid line) when applying the Fixed Stability Margin VSC-OPF formulation ($\times$) versus a traditional OPF ($*$) formulation for the 57-bus system. 83
4.23 Percent change in operating costs when applying the Fixed Stability Margin VSC-OPF formulation versus a traditional OPF formulation for the 57-bus system. 84

5.1 Capability curve for synchronous generator. 90
5.2 Implemented capability curve for synchronous generator. 91
5.3 Common structure for SVC. 93
5.4 SVC steady state circuit representation. 94
5.5 Typical steady state V-I characteristics of a SVC. 95

5.6 Cost versus current loading point for the 57-bus system when minimizing cost. 97
5.7 Difference in operating costs between the detailed generator model and the traditional PV generator model for the 57-bus system. 98
5.8 Maximum loading versus current loading point for the 57-bus system when solving the Maximum Distance to Collapse formulation. 100
5.9 Cost versus current loading point for the 57-bus system when solving the traditional OPF problem. 102
5.10 Cost versus current loading point for the 118-bus system when solving the traditional OPF problem. 103
5.11 Maximum loading versus current loading point for the 57-bus system when maximizing the distance to collapse. 106
5.12 Maximum loading versus current loading point for the 118-bus system when maximizing the distance to collapse. 107
5.13 Maximum loading versus current loading point for the modified 57-bus system when maximizing the distance to collapse with generator real and reactive power limits at the critical point. 109
5.14 Maximum loading versus current loading point for the modified 57-bus system when maximizing the distance to collapse with operating limits at the critical point. 110
5.15 Difference in total operating costs with a SVC placed at Bus 31 of the 57-bus system versus no SVC when solving the traditional OPF problem. . 112
5.16 Difference in maximum loading point with a SVC placed at Bus 31 of the 57-bus system versus no SVC when solving the Modified Maximum Distance to Collapse formulation with no limits at the maximum loading point. 113
5.17 Difference in maximum loading point with a SVC placed at Bus 31 of the 57-bus system versus no SVC when solving the Modified Maximum Distance to Collapse formulation with operating limits at the maximum loading point. 114
5.18 Difference in total operating costs with a SVC placed at Bus 31 of the 57-bus system versus no SVC when solving the Fixed Stability Margin VSC-OPF formulation (dashed line) and the traditional OPF problem (solid line) with operating limits at the maximum loading point. 115

List of Terms

Acronyms:

DAE	:	Differential-Algebraic Equations
FACTS	:	Flexible AC Transmission Systems
IEEE	:	Institute of Electrical and Electronics Engineers
IP	:	Interior-Point
KKT	:	Karush Kuhn Tucker
NLP	:	Non-linear Programming
OPF	:	Optimal Power Flow
P	:	Real Power
PC-IP	:	Predictor-Corrector Interior-Point
PD-IP	:	Primal-Dual Interior-Point
Q	:	Reactive power
S	:	Apparent power
SLP	:	Sequential Linear Programming
SQP	:	Sequential Quadratic Programming
SVC	:	Static Var Compensator
VSC-OPF	:	Voltage Stability Constrained Optimal Power Flow
pf	:	Power factor
p.u.	:	Per unit

Sub-scripts:

$*$	:	Maximum point
aff	:	Affine step
cen	:	Centering step
cor	:	Corrector step
0	:	Equilibrium point
p	:	Current point

Scalars:

β	:	Goal programming variable
λ	:	Bifurcation variable
μ	:	Barrier parameter
M	:	Number of algebraic variables
N	:	Number of differential variables
k	:	Iteration number
l	:	Continuation method step size scalar
m	:	Number of independent variables
n	:	Number of dependent variables

p	:	Number of independent constraints
q	:	Total number of dependent and independent variables
s	:	Slack variable
ω	:	Weighting factor

Vectors:

γ	:	Dual variable vector
ν	:	Dual variable vector
ρ	:	Vector of independent variables
χ	:	Systems variables
$\underline{\chi}$	:	Systems variables lower limits
$\overline{\chi}$	:	Systems variables upper limits
$\mathbb{1}$	:	Vector of ones
$\underline{\mathbf{H}}$	:	Inequality constraints lower limits
$\overline{\mathbf{H}}$	:	Inequality constraints upper limits
$\mathbf{s}$	:	Vector of slack variables
$\mathbf{v}$	:	Normalized left eigenvector
$\mathbf{w}$	:	Normalized right eigenvector
$\mathbf{x}$	:	Vector of dependent variables
$\mathbf{y}$	:	Lagrangian vector
τ	:	Vector of algebraic variables
$\mathbf{z}$	:	Vector of differential variables

Matrices:

$\mathbf{D_x}$	:	Matrix operator $\partial/\partial x$
$\mathbf{S}$	:	Diagonal matrix of slack variables
Υ	:	Diagonal matrix of dual variables

Functions:

∇	:	Gradient function
$\mathbf{f}_d(\cdot)$	:	Set of differential equations used to model the system
$\mathbf{f}_a(\cdot)$	:	Set of algebraic equations used to model the system
$\mathbf{s}(\cdot)$	:	Reformulated set of differential equations used to model the system
$\mathbf{c}(\cdot)$	:	Continuation method phase condition equation
$g(\cdot)$	:	Traditional OPF objective function
$F(\cdot)$	:	Load flow equations
$G(\cdot)$	:	Objective function
$H(\cdot)$	:	Transmission line limits inequalities
$J(\cdot)$	:	Jacobian function
$L_\mu(\cdot)$	:	Lagrangian function

Power System Components

Generators

δ	:	Generator bus voltage angle with respect to the infinite bus
ω	:	Angular frequency of generator
I_a	:	Armature current
I_d	:	Direct axis component of I_a
I_q	:	Quadrature axis component of I_a
D	:	Machine damping
E_f	:	Field voltage
$M_{inertia}$	:	Machine Inertia
P_{gen}	:	Generator active power
P_m	:	Mechanical Power
P_{elec}	:	Electric power
Q_{gen}	:	Generator reactive power
Q_{limit}	:	Upper limit on generator reactive power
R_a	:	Armature resistance
S	:	Apparent power
X_d	:	Armature direct axis synchronous reactance
X_q	:	Armature quadrature axis synchronous reactance
V_d	:	Direct axis component of V_a
V_{gen}	:	Generator terminal voltage
V_q	:	Quadrature axis component of V_a

Static Loads

P_0	:	Reference real power consumed at the reference voltage V_0
Q_0	:	Reference imaginary power consumed at the reference voltage V_0
V_0	:	Reference voltage to set voltage dependency of loads
ϱ_1	:	Scalar used to set the exponential voltage dependency of the real part of the load
ϱ_2	:	Scalar used to set the exponential voltage dependency of the imaginary part of the load

Static Var Compensators

α	:	Thyristor valves firing angle
B_e	:	Total SVC equivalent susceptance
I_{SVC}	:	SVC controller RMS current magnitude
Q_{SVC}	:	SVC controller reactive power output
V_i	:	Magnitude of voltage at system bus that SVC controls
V_{REF}	:	Desired or reference voltage for the SVC controller

V_{SVC}	:	SVC controller RMS voltage magnitude
X_C	:	Fundamental frequency reactance of the SVC capacitor
X_e	:	Total SVC equivalent impedance
X_{SL}	:	SVC control slope
X_L	:	Fundamental frequency reactance of the SVC inductor without thyristor control
X_{TH}	:	Reactance of the step-down transformer
X_v	:	Thyristor controlled reactor (TCR) fundamental frequency variable inductance

Chapter 1

Introduction

1.1 Background

As open access market principles are applied to power systems, significant changes in their operation and control are occurring. In the new marketplace, power systems are operating under higher loading conditions as market influences demand greater attention to operating cost versus stability margin. Since stability continues to be a basic requirement in the operation of any power system, new tools are being considered to analyze the effect of stability on the operating cost of the system, so that system stability can be incorporated into the costs of operating the system.

1.1.1 Optimization Techniques

As systems are being operated with reduced stability margins [1, 2], there has been several new voltage collapse events throughout the world [1, 2]. Thus, the incorporation of voltage stability criteria in the operation of power systems has become essential [3]. In recent years, the application of optimization techniques to voltage stability problems has been gaining interest. It is possible to restate many voltage collapse problems as optimization problems. Although bifurcation methods are very well developed, the use of optimization based techniques has many advantages, including the ability to incorporate limits and determine control actions on certain system variables to improve the stability margin [4, 5, 6]. New voltage stability analysis techniques have been introduced using optimization methods in voltage collapse analysis (e.g., [4, 5, 6, 7, 8, 9, 10, 11, 12, 13, 14, 15, 16, 17]).

Possible applications of optimization techniques to voltage collapse analysis are discussed in [4]. In [5], an Interior Point (IP) optimization technique is used to determine the optimal generator settings that maximize the distance to voltage collapse. In [6], applications of optimization techniques to voltage collapse studies are presented with theoretical and some numerical analysis. Furthermore, [6] includes a technique to incorporate voltage stability into traditional optimal power flow (OPF) formulations. In [10], optimal shunt and series compensation parameter settings are calculated to maximize the distance to a saddle-node bifurcation which can be associated, in some cases, with voltage collapse. In [11], a voltage-collapse point computation problem is formulated as an optimization problem, allowing the use of optimization techniques and tools. In [12], the reactive power margin from the point of view of voltage collapse is determined using Interior Point (IP) methods; the authors used a barrier function to incorporate limits. In [13], the authors determine the closest bifurcation to the current operating point on the hyperspace of bifurcation points. A similar approach is taken in [14] where the direct method which traditionally has been used to determine bifurcation points [18], is reformulated as an optimization problem. In [15], the maximum loadability of a power system is examined using Interior Point methods.

Voltage stability has long been accepted as an important aspect of power system analysis. With open-market principles being applied to many systems, the value of security is now receiving more attention. In [19], a Monte-Carlo assessment of the value of system security is presented, primarily considering security issues due to unplanned outages. In [20], a procedure for VAR planning is given that incorporates stability analysis. In [8, 9], a two stage approach is taken to determine candidate buses for reactive power support based on a proposed optimization technique to determine the voltage stability limit considering some constraints at the current operating point and the point of collapse. A formulation to incorporate transient stability into an OPF formulation is given in [16]. Finally, in [7], several Voltage Stability Constrained Optimal Power Flow (VSC-OPF) formulations are proposed considering both the current loading point and the maximum loading point into the formulation, so that voltage stability margins can be considered in

the OPF problem.

1.1.2 Modeling

In voltage stability and bifurcation analysis of power systems, detailed system models have been shown to have a significant effect on the equilibrium points and their characteristics [21, 22]. The differences among equilibrium points become more apparent when a system is heavily loaded and the devices approach their operating limits. Traditional models, where generators are modeled using limits on reactive power, real power, and voltage magnitudes, may fail to provide an accurate representation of the power system in certain conditions. In [22], reactive power limits are shown to play a significant role in discrepancies between detailed and non-detailed generator models. Generator ratings and limits in non-detailed models are incorporated using limits on their voltage and power levels, whereas detailed models tend to place limits on the armature current and field voltage, as these accurately reflect the actual operating limits of the machine. In [17], generator excitation limits are incorporated into an optimization based maximum distance to collapse formulation.

In [21], the effects of various loading models on the occurrence of saddle-node bifurcations are presented. In [8], the effects of load modeling in optimization based voltage stability studies are discussed.

The application of Flexible AC Transmission Systems (FACTS) controllers, which are based on power electronic switches, in power systems has been increasing [23]. These controllers provide reactive power compensation, which can increase the maximum transfer capability of a power network [24, 25]. Steady-state models for the Static Var Compensator (SVC) FACTS controller, presented in [24], allows for their incorporation into both load flow analysis and optimization.

1.2 Research Motivation and Objectives

As loading levels in a power system increase, the stability margin, i.e., the distance to collapse, generally decreases. Control actions can be taken to increase the available transfer capability of the system, but this may result in increased operating costs. These increased costs may be considered as the costs of enforcing voltage stability constraints.

The main motivation of the thesis is to examine how to incorporate voltage stability criteria into a traditional OPF problem to account for the stability "level" of the system while considering operating costs. Most optimization based voltage stability analysis methods (e.g., [15, 26]) consider only the stability margin. Incorporating operating costs and voltage stability criteria into one integrated formulation allows one to account for stability into the overall operating costs.

When considering voltage stability margins the importance of system modeling becomes critical, since it has been demonstrated, based on bifurcation analysis, that modeling can have a significant effect on the behavior of power systems [21, 22, 27], especially at high loading levels. Therefore, in this research, a detailed generator model and several static load models are incorporated into OPF formulations. Furthermore, because of its influence in voltage stability, a Static Var Compensator (SVC) model is also incorporated into the OPF formulations.

From the above discussions, the main objectives of the thesis research are as follows:

- Extending the *maximum distance to collapse* algorithm (e.g., [15, 26]) to consider feasibility and limits at both the current operating point and the collapse (maximum) loading point. This allows for the examination of voltage collapse through both saddle-node bifurcations [18, 28, 29] and limit-induced bifurcations [30].

- Development of Voltage Stability Constrained Optimal Power Flow (VSC-OPF) formulations that incorporate voltage stability margins to consider the influence of stability on the traditional OPF problem.

- Incorporation of detailed generator models in the OPF and VSC-OPF formulations to improve the accuracy of the system's model. Since equilibrium points are effected by modeling differences, especially when systems become heavily loaded and generator limits are approached, the accurate representation of these limits, particularly armature current and field voltage limits, in the OPF and VSC-OPF formulations is considered and analyzed.

- Incorporation of exponential load models into both the OPF and VSC-OPF formulations to study the effect of load modeling on the characteristics of the solutions obtained from these problems.

- Incorporation of a load-flow model of the Static Var Compensator (SVC), a Flexible AC Transmission System controller, into the OPF and VSC-OPF formulations to analyze its effect on these problems.

- Implementation of the proposed formulations by testing them using several systems to gain insight into their characteristics and how limits effect the solutions.

1.3 Implementation Methods

The OPF and VSC-OPF problems are solved using a Predictor-Corrector Primal-Dual Logarithmic Barrier Interior Point (IP) method. This method has been successfully applied to optimal power flow problems and has been shown to be very efficient [31, 32].

The Predictor-Corrector IP method was implemented using a combination of MAPLE [33] and MATLAB [34] programming. System models are constructed symbolically in MAPLE, then differentiation tools in MAPLE are used to calculate the vectors and matrices required for the optimization method. The set of equations describing the models are exported to text files using an export tool in MAPLE [33], and are then modified into MATLAB format using a script file written in MATLAB to form data files. MATLAB routines were written to access the data files to generate the required vectors and matrices

for numerical analysis; sparse matrix routines are used to manipulate and store the data. Although, this method of implementing the proposed algorithms and models has limitations when dealing with a large system, it is extremely well suited to investigate different models since derivatives, partial derivatives, and Jacobians can all be symbolically formed in MAPLE .

1.4 Outline of the Thesis

The remaining chapters of the thesis are organized as follows:

Chapter 2 provides a generic formulation of the Optimal Power Flow (OPF) problem. This is followed by an introduction to the nonlinear Interior Point method used to solve the problems considered in this thesis.

Chapter 3 gives some of the basic components of Voltage Stability, presented with illustrative examples, focusing first on saddle-node and then on limit-induced bifurcations. Two traditional bifurcation analysis methods, continuation and direct methods, are reviewed. Finally, the chapter includes an examination of some existing optimization based approaches used for voltage stability analysis.

Chapter 4 presents several of the main research contributions of the thesis. First, a modification of the Maximum Distance to Collapse problem is presented along with a generic non-linear optimization formulation to incorporate voltage stability into a traditional OPF problem. Second, an analysis to determine when the maximum loading point of the system will correspond to a saddle-node bifurcation, based on the application of the maximum distance to collapse problem and the KKT optimality conditions [35] is given. Third, five novel VSC-OPF formulations are presented together

with a discussion of the advantages and disadvantages of each formulation. The results obtained from applying the Modified Maximum Distance to Collapse problem and the various VSC-OPF problems to several test systems are presented and discussed.

Chapter 5 presents the remaining research contributions of the thesis. A detailed generator model, different static load models and a Static Var Compensator (SVC) model are proposed for inclusion into the OPF and VSC-OPF formulations. A discussion on the results obtained from solving the OPF and VSC-OPF problems for several test systems that include the different models is presented.

Chapter 6 summarizes the work presented in the thesis. The main contributions of the thesis are highlighted, and a list of potential research directions to study further the issue of the incorporation of stability criteria into OPF problems is given.

Chapter 2

Optimal Power Flow and Optimization Techniques

2.1 Introduction

The OPF problem introduced in the early 1960's by Carpentier has grown into a powerful tool for power system operation and planning. In general, the OPF problem is a nonlinear programming (NLP) problem that is used to determine the "optimal" control parameter settings to minimize a desired objective function, subject to certain system constraints [36, 37, 38]. Because of the restructuring of power system utilities [39], different OPF problems are now being considered. Furthermore, there has been great interest in voltage stability issues and their possible relationship with optimization methods [4, 5, 10, 11, 12, 13, 15].

The development of numerical analysis techniques and algorithms, particularly Interior Point (IP) methods, allows large and difficult problems to be solved with reasonable computational effort [37, 40]. Power systems are one of the areas where IP methods have been successfully applied (e.g., [37, 41, 42, 43, 44]).

The objective of this chapter is to briefly introduce the OPF problem and provide a description of the Interior Point (IP) method used for solving the NLP problems presented in this thesis.

The remainder of the chapter is structured as follows: First, the OPF problem is briefly introduced. Then, a Primal-Dual Interior-Point (PD-IP) method is presented and is extended to a Predictor-Corrector Interior Point (PC-IP) method. Since the main contribution of this thesis focuses on voltage stability constrained optimal power flow

formulations, the IP methods used here are briefly described, giving the appropriate references where details of the optimization problems and solution techniques can be found.

2.2 Optimal Power Flow

With the introduction of diverse objective functions, the OPF problem represents a variety of optimization problems [38], which includes, for example, active power cost optimization and active power loss minimization [37]. OPF problems are generally formulated as nonlinear programming problems (NLP) as follows:

$$\begin{aligned} \min \quad & \mathbf{G}(\chi) \\ \text{s.t.} : \quad & \mathbf{F}(\chi) = \mathbf{0} \\ & \underline{\mathbf{H}} \leq \mathbf{H}(\chi) \leq \overline{\mathbf{H}} \\ & \underline{\chi} \leq \chi \leq \overline{\chi} \end{aligned} \tag{2.1}$$

where generally $\mathbf{F}(\chi) : \Re^q \rightarrow \Re^m$ represents the load flow equations, $\mathbf{H}(\chi) : \Re^q \rightarrow \Re^p$ usually stands for transmission line limits, with lower and upper limits represented by $\underline{\mathbf{H}}$ and $\overline{\mathbf{H}}$, respectively. The vector of system variables, denoted by $\chi \in \Re^q$, typically includes voltage magnitudes and angles, generator power levels and transformer tap settings; Lower and upper limits of the system variables, χ, are given by $\underline{\chi}$ and $\overline{\chi}$, respectively. The mapping $\mathbf{G}(\chi) : \Re^q \rightarrow \Re$ is the function that is being minimized and can include, for example, total losses in the system and generator costs. Once formulated, the problem can be solved using Interior Point (IP) methods [32, 45], Sequential Linear Programming (SLP) or Sequential Quadratic Programming (SQP) [44, 46, 47]. SLP and SQP formulations can be solved using well developed Linear and Quadratic Interior Point methods [44, 46]. When applying SLP and SQP methods, convergence has been shown to be dependent on a number of factors, such as good initial conditions and step size control [47]. For the problems considered in this thesis, a direct nonlinear Interior Point method is used.

The algorithm presented and used for solving the NLP is based primarily on the method presented in [31, 32, 41].

2.3 Logarithmic-Barrier Interior Point Method

NLP has experienced major developments over the past decade, largely due to the advancements in Interior Point methods [35]. In this section, a formulation for the Logarithmic-barrier IP method for a NLP with equality and inequality constraints is presented. A detailed analysis of the method can be found in many references including [31, 41]. For simplicity, the bounds $\underline{\chi} \leq \chi \leq \overline{\chi}$ in (2.1) are assumed to have been incorporated in $\underline{\mathbf{H}} \leq \mathbf{H}(\chi) \leq \overline{\mathbf{H}}$.

2.3.1 Associated Problem and Optimality Conditions

The first step in solving (2.1) using the Logarithmic-Barrier IP method (which will then be extended to the Predictor Corrector approach) is to transform the existing inequality constraints into equality constraints by introducing strictly positive slack variables $\mathbf{s}_1, \mathbf{s}_2 \in \Re^p$. Thus, the original problem can be re-written as

$$\begin{aligned} & \min \quad \mathbf{G}(\chi) \\ \text{s.t. :} \quad & \mathbf{F}(\chi) = \mathbf{0} \\ & \mathbf{H}(\chi) - \mathbf{s}_1 = \underline{\mathbf{H}} \\ & \mathbf{H}(\chi) + \mathbf{s}_2 = \overline{\mathbf{H}} \\ & \mathbf{s}_1, \mathbf{s}_2 > \mathbf{0} \end{aligned} \tag{2.2}$$

From (2.2) an associated problem is formed by introducing a logarithmic barrier term to the objective function to enforce the strict positivity constraints on $\mathbf{s}_1$ and $\mathbf{s}_2$.

$$
\begin{aligned}
\min \quad & \mathbf{G}(\chi) - \mu^k \sum_{i=1}^{p} \left(\log s_1(i) + \log s_2(i) \right) && (2.3)\\
\text{s.t. :} \quad & \mathbf{F}(\chi) = \mathbf{0} \\
& \mathbf{H}(\chi) - \mathbf{s}_1 = \underline{\mathbf{H}} \\
& \mathbf{H}(\chi) + \mathbf{s}_2 = \overline{\mathbf{H}} \\
& \mathbf{s}_1, \mathbf{s}_2 > \mathbf{0}
\end{aligned}
$$

where μ^k represents the positive barrier parameter at the k^{th} iteration. This parameter is monotonically decreased to zero as the iteration number, k, increases. Equation (2.3) can then be re-written to reduce the number of nonlinear terms as follows:

$$
\begin{aligned}
\min \quad & \mathbf{G}(\chi) - \mu^k \sum_{i=1}^{p} \left(\log \mathbf{s}_1 + \log \mathbf{s}_2 \right) && (2.4)\\
\text{s.t. :} \quad & \mathbf{F}(\chi) = \mathbf{0} \\
& -\mathbf{s}_1 - \mathbf{s}_2 - \underline{\mathbf{H}} + \overline{\mathbf{H}} = \mathbf{0} \\
& -\mathbf{H}(\chi) - \mathbf{s}_2 + \overline{\mathbf{H}} = \mathbf{0} \\
& \mathbf{s}_1, \mathbf{s}_2 > \mathbf{0}
\end{aligned}
$$

In order to optimally solve (2.4) for a fixed μ^k, the Lagrangian function $L_\mu(\boldsymbol{\upsilon})$ is first defined as

$$
\begin{aligned}
L_\mu(\boldsymbol{\upsilon}) = \quad & \mathbf{G}(\chi) - \mu^k \sum_{i=1}^{p} (\log \mathbf{s}_1 + \log \mathbf{s}_2) && (2.5)\\
& -\boldsymbol{\gamma}^T \mathbf{F}(\chi) - \boldsymbol{\nu}_1^T (-\mathbf{s}_1 - \mathbf{s}_2 - \underline{\mathbf{H}} + \overline{\mathbf{H}}) \\
& -\boldsymbol{\nu}_2^T (-\mathbf{H}(\chi) - \mathbf{s}_2 + \overline{\mathbf{H}})
\end{aligned}
$$

where $\boldsymbol{\upsilon} := [\chi; \mathbf{s}_1; \mathbf{s}_2; \boldsymbol{\gamma}; \boldsymbol{\nu}_1; \boldsymbol{\nu}_2]$ is introduced for ease of presentation, and $\boldsymbol{\gamma} \in \Re^m$ and $\boldsymbol{\nu}_1, \boldsymbol{\nu}_2 \in \Re^p$ are Lagrangian multipliers vectors, often called the dual variables [41].

The first-order Karush-Kuhn-Tucker (KKT) optimality conditions [35] define the minimum of (2.5) with the following necessary conditions [32, 35]:

$$\nabla_v L_\mu(\boldsymbol{v}) = \begin{bmatrix} \mathbf{D}_\chi \mathbf{G}(\chi) - \mathbf{J}_\mathbf{F}(\chi)^T\gamma + \mathbf{J}_\mathbf{H}(\chi)^T\nu_2 \\ -\mu^k \mathbf{S}_1^{-1}\mathbb{1} + \nu_1 \\ -\mu^k \mathbf{S}_2^{-1}\mathbb{1} + (\nu_1 + \nu_2) \\ -\mathbf{F}(\chi) \\ \mathbf{s}_1 + \mathbf{s}_2 + \underline{\mathbf{H}} - \overline{\mathbf{H}} \\ \mathbf{H}(\chi) + \mathbf{s}_2 - \overline{\mathbf{H}} \end{bmatrix} = \mathbf{0} \tag{2.6}$$

where $\mathbb{1} := (1, 1, 1, ...1)^T$ is a vector of ones of appropriate size, and $\mathbf{S}_1 = diag(\mathbf{s}_1)$ and $\mathbf{S}_2 = diag(\mathbf{s}_2)$. The function $diag(\mathbf{s}) : \Re^p \rightarrow \Re^{p \times p}$ forms a diagonal matrix with the i^{th} diagonal term equal to the i^{th} element in the vector $\mathbf{s}$, and $\mathbf{J}_\mathbf{F}(\chi) \in \Re^{m \times q}$ and $\mathbf{J}_\mathbf{H}(\chi) \in \Re^{p \times q}$ are the Jacobians of $\mathbf{F}(\chi)$ and $\mathbf{H}(\chi)$, respectively, i.e, $\mathbf{J}_\mathbf{F}(\chi) = \mathbf{D}_\chi \mathbf{F}(\chi)$ and $\mathbf{J}_\mathbf{H}(\chi) = \mathbf{D}_\chi \mathbf{H}(\chi)$. To reduce the number of nonlinear components, the second term is scaled by $\mathbf{S}_1$ and the third by $\mathbf{S}_2$, yielding

$$\nabla_v L_\mu(\boldsymbol{v}) = \begin{bmatrix} \mathbf{D}_\chi \mathbf{G}(\chi) - \mathbf{J}_\mathbf{F}(\chi)^T\gamma + \mathbf{J}_\mathbf{H}(\chi)^T\nu_2 \\ -\mu^k \mathbb{1} + \mathbf{S}_1\nu_1 \\ -\mu^k \mathbb{1} + \mathbf{S}_2(\nu_1 + \nu_2) \\ -\mathbf{F}(\chi) \\ \mathbf{s}_1 + \mathbf{s}_2 + \underline{\mathbf{H}} - \overline{\mathbf{H}} \\ \mathbf{H}(\chi) + \mathbf{s}_2 - \overline{\mathbf{H}} \end{bmatrix} = \mathbf{0} \tag{2.7}$$

This system has the following interpretation: The first term, along with $(\nu_1, \nu_1 + \nu_2) > \mathbf{0}$, ensures dual feasibility; the second and third terms are the μ-complementarity conditions; and the fourth through sixth terms, along with $(\mathbf{s}_1, \mathbf{s}_2) > \mathbf{0}$, ensure primal feasibility.

The steps to solve the nonlinear system defined by (2.7) are as follows: For a set of μ^k, one step of the Newton direction is taken, then the step length in the Newton direction is

calculated and the variables are updated. The algorithm terminates when the primal, dual and the complementarity conditions [32] fall below predetermined tolerances; otherwise, k is incremented, the barrier parameter μ^k is decreased, and a new Newton direction is determined. Different schemes exist for reducing μ and scaling the Newton step depending on the type of problem. In the implementation written, the barrier parameter was reduced based on an estimate of the decrease in the complementarity gap [31].

2.4 Higher Order Primal-Dual Interior Point Algorithms

Although the Interior Point method reviewed in the previous section can solve large problems [31], numerical difficulties due to nonlinearities and long running times [5] led to the implementation of a Predictor-Corrector Interior Point method.

The main concept behind the Predictor-Corrector method is to incorporate higher order information to improve the accuracy that the Newton Step takes to solve the KKT conditions. A brief overview of the Predictor-Corrector method developed to solve the nonlinear optimization problems proposed in this thesis follows. More details can be found in [31, 32].

2.4.1 Predictor-Corrector Interior Point Methods

The derivation of the Predictor-Corrector method follows the same steps as the Primal-Dual method up to the KKT conditions written in equation (2.7). Instead of applying one Newton step to (2.7) to estimate an approximate solution from the current point $\upsilon = [\chi; \mathbf{s}_1; \mathbf{s}_2; \gamma; \nu_1; \nu_2]$, a new point

$$\upsilon + \Delta\upsilon = [\chi + \Delta\chi; \mathbf{s}_1 + \Delta\mathbf{s}_1; \mathbf{s}_2 + \Delta\mathbf{s}_2; \gamma + \Delta\gamma; \nu_1 + \Delta\nu_1; \nu_2 + \Delta\nu_2] \tag{2.8}$$

is defined as being on the central path, i.e., the exact solution to equation (2.7) for μ^k. The equations defining this point on the central path, determined by substituting $(\boldsymbol{v} + \Delta\boldsymbol{v})$ in place of $\boldsymbol{v}$ in (2.7), is written as

$$\begin{bmatrix} \mathbf{J_H}(\chi)^T\Delta\boldsymbol{\nu}_2 + \nabla^2_{\boldsymbol{\chi}} L_\mu(\chi)\Delta\chi - \mathbf{J_F}(\chi)^T\Delta\gamma \\ \boldsymbol{\Upsilon}_1\Delta\mathbf{s}_1 + \mathbf{S}_1\Delta\boldsymbol{\nu}_1 \\ \mathbf{S}_2(\Delta\boldsymbol{\nu}_1 + \Delta\boldsymbol{\nu}_2) + (\boldsymbol{\Upsilon}_1 + \boldsymbol{\Upsilon}_2)\Delta\mathbf{s}_2 \\ -\mathbf{J_F}(\chi)\Delta\chi \\ \Delta\mathbf{s}_1 + \Delta\mathbf{s}_2 \\ \Delta\mathbf{s}_2 + \mathbf{J}_H(\chi)\Delta\chi \end{bmatrix}$$

$$= -\begin{bmatrix} \nabla_{\boldsymbol{\chi}} L_\mu(\chi) \\ \mathbf{S}_1\boldsymbol{\nu}_1 \\ \mathbf{S}_2(\boldsymbol{\nu}_1 + \boldsymbol{\nu}_2) \\ -\mathbf{F}(\chi) \\ \mathbf{s}_1 + \mathbf{s}_2 + \underline{\mathbf{H}} - \overline{\mathbf{H}} \\ \mathbf{H}(\chi) + \mathbf{s}_2 - \overline{\mathbf{H}} \end{bmatrix} + \begin{bmatrix} \mathbf{0} \\ \mu^k\mathbb{1} \\ \mu^k\mathbb{1} \\ \mathbf{0} \\ \mathbf{0} \\ \mathbf{0} \end{bmatrix} - \begin{bmatrix} -\mathbf{J_F}(\Delta\chi)^T\Delta\gamma + \mathbf{J_H}(\Delta\chi)^T\Delta\boldsymbol{\nu}_2 \\ \Delta\mathbf{S}_1\Delta\boldsymbol{\nu}_1 \\ \Delta\mathbf{S}_2(\Delta\boldsymbol{\nu}_1 + \Delta\boldsymbol{\nu}_2) \\ -\mathbf{F}^L(\Delta\chi) \\ \mathbf{0} \\ \mathbf{H}^L(\Delta\chi) \end{bmatrix} \tag{2.9}$$

where $\nabla_{\boldsymbol{\chi}} L_\mu(\chi) = \mathbf{D}_{\boldsymbol{\chi}}\mathbf{G}(\chi) - \mathbf{J_F}(\chi)^T\gamma + \mathbf{J_H}(\chi)^T\boldsymbol{\nu}_2$; $\boldsymbol{\Upsilon}_1 := diag(\boldsymbol{\nu}_1)$, and $\boldsymbol{\Upsilon}_2 := diag(\boldsymbol{\nu}_2)$ and $\mathbf{F}^L(\cdot) \in \Re^m$ and $\mathbf{H}^L(\cdot) \in \Re^p$ represent the quadratic terms of $\mathbf{F}(\cdot)$ and $\mathbf{H}(\cdot)$, respectively. Finally, $\nabla^2_{\boldsymbol{\chi}} L_\mu(\chi) \in \Re^q$ represents the Hessian of $L_\mu(\boldsymbol{v})$ with respect to χ. The second order terms $\mathbf{F}^L(\Delta\chi)$, $\mathbf{J_F}(\chi)$, $\mathbf{H}^L(\Delta\chi)$, and $\mathbf{J}_H(\chi)$ are only included if $\mathbf{F}(\chi)$ and $\mathbf{H}(\chi)$ are quadratic [31].

The full step $\Delta\boldsymbol{v}$ obtained from (2.9) consists of three components, generally expressed as [31]

$$\Delta\boldsymbol{v} = \Delta\boldsymbol{v}_{aff} + \Delta\boldsymbol{v}_{cen} + \Delta\boldsymbol{v}_{cor}. \tag{2.10}$$

where the $\Delta\boldsymbol{v}_{aff}$, $\Delta\boldsymbol{v}_{cen}$, and $\Delta\boldsymbol{v}_{cor}$ are defined by the first, second, and third right-hand side vectors of (2.9), respectively. The first component, the affine-scaling direction, $\Delta\boldsymbol{v}_{aff}$, is a pure Newton direction (for $\mu_k = 0$), and is responsible for reduction in the objective

function. The second component, $\Delta \boldsymbol{v}_{cen}$, is a centering direction and is used to keep the solution away from the boundary of the feasible region. Finally, the third component, $\Delta \boldsymbol{v}_{cor}$, is a corrector direction that it used to compensate for some of the nonlinear terms in the affine-scaling direction.

A good approximate solution to (2.9) is obtained by first calculating the predictor step when dropping the μ terms and the Δ terms from the right-hand side of (2.9), i.e., $\Delta \boldsymbol{v} = \Delta \boldsymbol{v}_{aff}$. The full step, $\Delta \boldsymbol{v} = \Delta \boldsymbol{v}_{aff} + \Delta \boldsymbol{v}_{cen} + \Delta \boldsymbol{v}_{cor}$, is then approximately solved using the target value for the barrier parameter and the solution obtained from the predictor step to approximate the nonlinear Δ terms in the right-hand side of (2.9). The variables are then updated and the solution is tested for convergence.

2.5 Summary

In this chapter, an introduction to the OPF problem is presented. This is followed by a derivation of two IP methods used to solve non-linear problems like the OPF problem. Both IP methods use a logarithmic function to move the solution obtained at each iteration towards the optimal solution while enforcing inequality constraints. The second method, the Predictor-Corrector IP method, incorporates higher order information to improve the accuracy of the method. Since, the OPF formulations proposed in this thesis are highly non-linear, the Predictor-Corrector method was implemented to solve all OPF problems in this thesis. The implementation uses a combination of MAPLE and MATLAB programming.

Chapter 3

Voltage Stability

3.1 Introduction

Several voltage collapse events throughout the world show that power systems are being operated close to their stability limits (e.g., [1]). This problem can only be exacerbated by the application of open market principles to the operation of power systems, as stability margins are being reduced even further to respond to market pressures. Since the overall stability limit can be closely associated with the voltage stability of the network, this chapter presents an overview of voltage stability and some analysis techniques.

A review of bifurcation analysis is presented first, focusing on some of the basic concepts and terminology. Characteristics of saddle-node bifurcations are then presented, along with an overview of limit induced bifurcations and their effect on system stability. Two traditional tools used to analyze and determine the location of bifurcations are discussed, and a review of some of the existing work in the application of optimization techniques to voltage stability analysis is presented.

3.2 Bifurcation Analysis

Nonlinear phenomena, especially bifurcations, have been shown to be responsible for a variety of stability problems in power systems (e.g., [48]). In particular, the lack of post contingency equilibrium points, typically associated with saddle-node and limit-induced bifurcations, have been shown to be one of the main reasons for voltage collapse problems

in power systems [3].

In general, bifurcation points can be basically defined as equilibrium points where changes in the "quantity" and/or "quality" of the equilibria associated with a nonlinear set of dynamic equations occur with respect to slow varying parameters in the system [18]. Since power systems are modeled by sets of nonlinear differential equations, various types of bifurcations are generically encountered as certain system parameters vary.

A typical power system model used for stability studies can be represented by a set of differential-algebraic equations (DAEs). These models are linearized at equilibrium points to determine their steady state stability using eigenvalue analysis. Of interest is where the system goes from being stable to unstable, from being unstable to stable, or where the number of equilibrium points change with respect to a bifurcation parameter. These bifurcations are mathematically characterized by one of the system eigenvalues becoming zero (saddle-node, transcritical and pitchfork bifurcation), by a pair of complex conjugate eigenvalues crossing the imaginary axis (Hopf bifurcation) or by eigenvalues changing when control limits are reached (limit-induced bifurcation).

The differential-algebraic equations used to model the power system are typically of the form:

$$\dot{\mathbf{z}} = \mathbf{f}_d(\mathbf{z}, \mathbf{y}, \lambda) \tag{3.1}$$

$$\mathbf{0} = \mathbf{f}_a(\mathbf{z}, \mathbf{y}, \lambda) \tag{3.2}$$

where $\mathbf{z} \in \Re^N$ is a vector of the differential variables, $\mathbf{y} \in \Re^M$ is a vector of algebraic variables, and $\lambda \in \Re^+$ is any parameter in the system that changes slowly, moving the system from one equilibrium point to another. Equilibrium points are the values $\mathbf{z}_0$, $\mathbf{y}_0$ and λ_0 where the rate of change of each state variable is zero, i.e.,

$$\mathbf{0} = \mathbf{f}_d(\mathbf{z}_0, \mathbf{y}_0, \lambda_0) \tag{3.3}$$

$$\mathbf{0} = \mathbf{f}_a(\mathbf{z}_0, \mathbf{y}_0, \lambda_0)$$

Equilibrium implies the system is at "rest" but does not imply stability.

When the Jacobian $\mathbf{D_y f}_a(\cdot)$ of the algebraic constraints in (3.2) is non-singular along system trajectories, the system model can be reformulated as [29]:

$$\mathbf{y} \equiv \mathbf{h}(\mathbf{z}, \lambda) \tag{3.4}$$

$$\mathbf{s}(\mathbf{z}, \lambda) \equiv \mathbf{f}_d(\mathbf{z}, \mathbf{h}(\mathbf{z}, \lambda), \lambda) \tag{3.5}$$

$$\dot{\mathbf{z}} = \mathbf{s}(\mathbf{z}, \lambda) \tag{3.6}$$

where $\mathbf{h}(\cdot)$ may be formed symbolically or numerically from $\mathbf{f}_a(\cdot)$. If the Jacobian of the algebraic constraints becomes singular, then the model used to describe the system becomes invalid. In this case, the original model can be modified to consider dynamics ignored in the original model, resulting in the transformation of some algebraic constraints into differential equations [29, 49].

Two paths to instability are considered in this research. The first, saddle-node bifurcations, is characterized by local equilibrium disappearing for further increases in the bifurcation parameter. The second, limit-induced bifurcations, is characterized by equilibria disappearing due to changing system models when system limits are encountered. Both forms of bifurcations are described below, with illustrative examples.

3.3 Saddle-node Bifurcations

Saddle-node bifurcations are characterized by two equilibrium points, typically one stable and one unstable, merging for a parameter value $\lambda = \lambda_*$; the resulting equilibrium point has a simple and unique zero eigenvalue of $\mathbf{D_z s}|_0$ [18, 29, 50]. If the two merging equilibria co-exist for $\lambda < \lambda_*$, the two equilibrium points locally disappear for $\lambda > \lambda_*$, or vice versa; hence, these are local bifurcations. The following conditions hold for saddle-node bifurcations [18]:

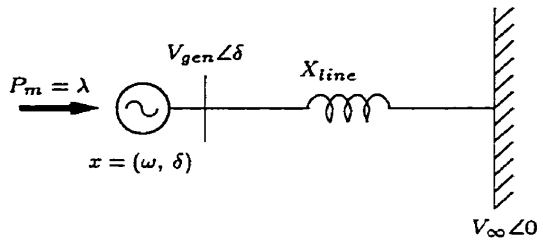


Figure 3.1: Generator-infinite bus system.

1. The point is an equilibrium point, i.e., $\mathbf{s}(\mathbf{z}, \lambda) = \mathbf{0}$.

2. The Jacobian of the function $\mathbf{s}(\mathbf{z}, \lambda)$ with respect to $\mathbf{z}$ at the bifurcation point $(\mathbf{z}_*,\lambda_*)$, has a unique zero eigenvalue.

3. At the saddle-node point, two branches of equilibria intersect and "disappear" beyond the saddle-node.

Saddle-node bifurcations are mathematically defined using transversality conditions [18, 28, 29, 48]. If the transversality conditions are met, then the system is at a saddle-node bifurcation. These conditions for a saddle-node bifurcation are

$$\mathbf{D}_\mathbf{z}\mathbf{s}|_*\mathbf{v} = \mathbf{D}_\mathbf{z}^T\mathbf{s}|_*\mathbf{w} = 0 \tag{3.7}$$

$$\mathbf{w}^T\mathbf{D}_\lambda\mathbf{s}|_* \neq 0 \tag{3.8}$$

$$\mathbf{w}^T[\mathbf{D}_\mathbf{z}^2\mathbf{s}|_*\mathbf{v}]\mathbf{v} \neq 0 \tag{3.9}$$

where $\mathbf{w}$ and $\mathbf{v} \in \Re^N$ are normalized right and left eigenvectors of the Jacobian of $\mathbf{s}(\mathbf{z}, \lambda)$, $\mathbf{D}_\mathbf{z}\mathbf{s}|_*$. The subscript $*$ is used to denote a bifurcation point. The first condition, implies the Jacobian matrix is singular, the second and third conditions ensure that there is no equilibria near (z_*,λ_*) for $\lambda > \lambda_*$ or $\lambda < \lambda_*$, depending on their sign, and a "quadratic" shape.

Example:

The two-bus lossless system shown in Figure 3.1 is used here to illustrate saddle-node bifurcations. Using the classical second order dynamic model for the generator [25], the

system equations are

$$\begin{aligned} \dot{\delta} &= \omega \\ \dot{\omega} &= \frac{1}{M_{inertia}}(P_m - P_{elec} - D\omega) \end{aligned} \tag{3.10}$$

where $M_{inertia}$ is the machine inertia, D is the machine damping, ω is the angular frequency of the generator, and δ is the generator bus voltage angle with respect to the infinite bus. By definition, the infinite bus will have a constant voltage regardless of the power delivered to it, or absorbed from it. The mechanical power P_m is used as the bifurcation parameter, i.e., $\lambda = P_m$, and the electrical power transmitted through the transmission line P_{elec} is defined as

$$P_{elec} = \frac{|V_{gen}||V_\infty|}{X_{line}} \sin\delta \tag{3.11}$$

Letting $z_1 = \delta$, $z_2 = \omega$, $M_{inertia} = 0.1$, $D = 0.1$, $X_{line} = 0.5$, $|V_{gen}| = 1$, and $|V_\infty| = 1$, then equations (3.10) can be re-written as

$$\begin{bmatrix} \dot{z_1} \\ \dot{z_2} \end{bmatrix} = \begin{bmatrix} z_2 \\ 10\,\lambda - 20\,\sin z_1 - z_2 \end{bmatrix} \tag{3.12}$$

The Jacobian of (3.12) with respect to $\mathbf{z} = [z_1\ z_2]^T$ is

$$\mathbf{D_z}s = \begin{bmatrix} 0 & 1 \\ -20\,\cos z_1 & -1 \end{bmatrix} \tag{3.13}$$

Figure 3.2 illustrates equilibrium values of δ for different values of λ. As can be seen for $\lambda = 2.0$, the lower and upper curves of equilibrium points merge, and no equilibrium exist for values of $\lambda > 2.0$. The upper branch of equilibrium corresponds to *stable* equilibria and the bottom branch corresponds to *unstable* equilibria. The point $\delta = \pi/2$ corresponds to a singular system Jacobian (3.13). The normalized right and left eigenvectors at this point are given by

$$\mathbf{w} = \begin{bmatrix} \frac{1}{\sqrt{2}} \\ \frac{1}{\sqrt{2}} \end{bmatrix}, \quad \mathbf{v} = \begin{bmatrix} 1 \\ 0 \end{bmatrix} \tag{3.14}$$

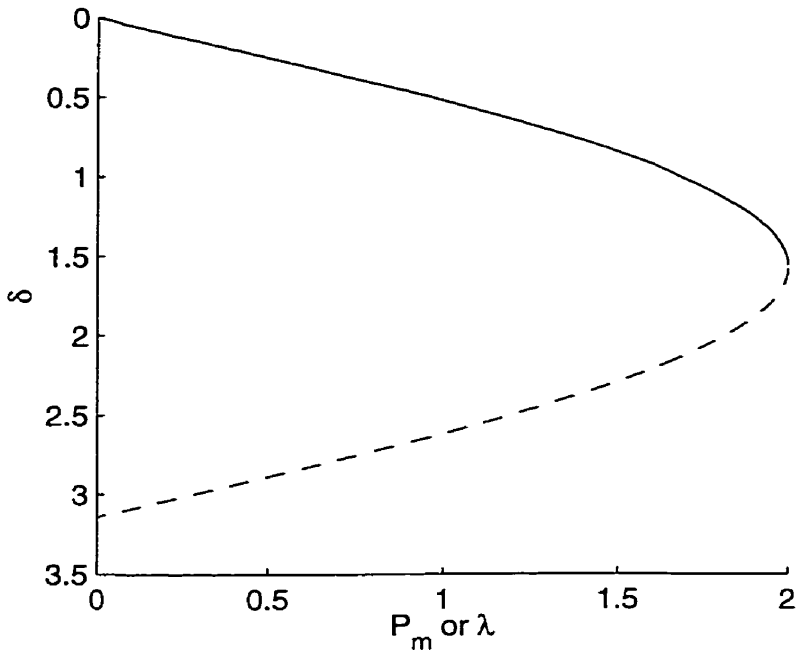


Figure 3.2: Bifurcation diagram for generator-infinite bus example.

The three transversality conditions for a saddle-node bifurcation (3.7-3.9) are met, i.e.,

$$\begin{bmatrix} 0 & 1 \\ 0 & -1 \end{bmatrix} \begin{bmatrix} 1 \\ 0 \end{bmatrix} = \begin{bmatrix} 0 & 0 \\ 1 & -1 \end{bmatrix} \begin{bmatrix} \frac{1}{\sqrt{2}} \\ \frac{1}{\sqrt{2}} \end{bmatrix} = \begin{bmatrix} 0 \\ 0 \end{bmatrix} \tag{3.15}$$

$$\begin{bmatrix} \frac{1}{\sqrt{2}} & \frac{1}{\sqrt{2}} \end{bmatrix} \begin{bmatrix} 0 \\ 10 \end{bmatrix} = 5\sqrt{2} \neq 0 \tag{3.16}$$

$$\begin{bmatrix} \frac{1}{\sqrt{2}} & \frac{1}{\sqrt{2}} \end{bmatrix} \begin{bmatrix} 0 & 0 \\ 20 & 0 \end{bmatrix} \begin{bmatrix} 1 \\ 1 \end{bmatrix} = 10\sqrt{2} \neq 0 \tag{3.17}$$

Saddle-node bifurcations are generally considered generic, that is, they are "expected" to occur in nonlinear systems that do not present a "special" structure [28, 48]. For example, if loading changes of a power system are used to represent the bifurcation parameter λ, saddle-node bifurcations would be expected for certain values of λ.

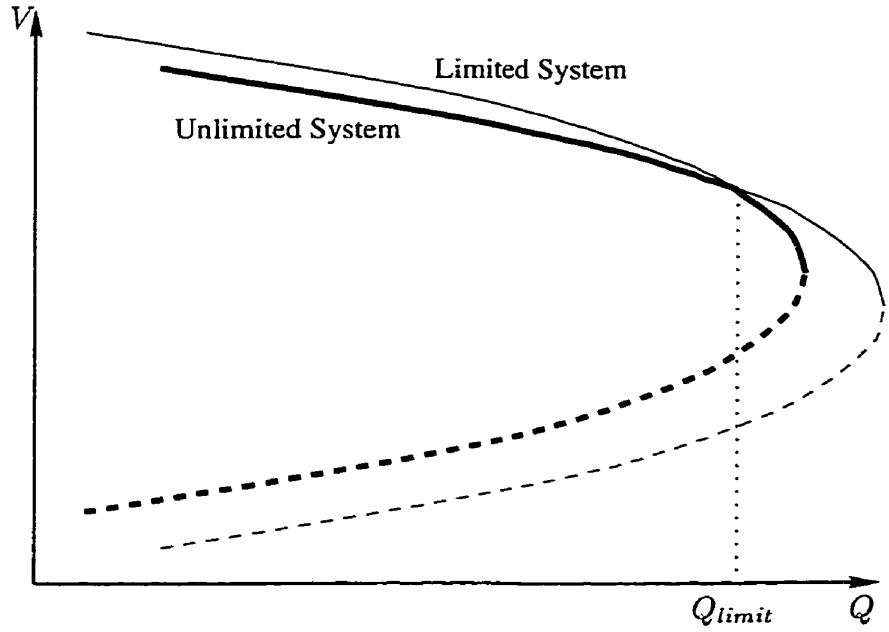
In the following section, the effect of limits restricting the space of feasible solutions and hence leading to limit-induced bifurcations is considered.

3.4 Limit-Induced Bifurcations

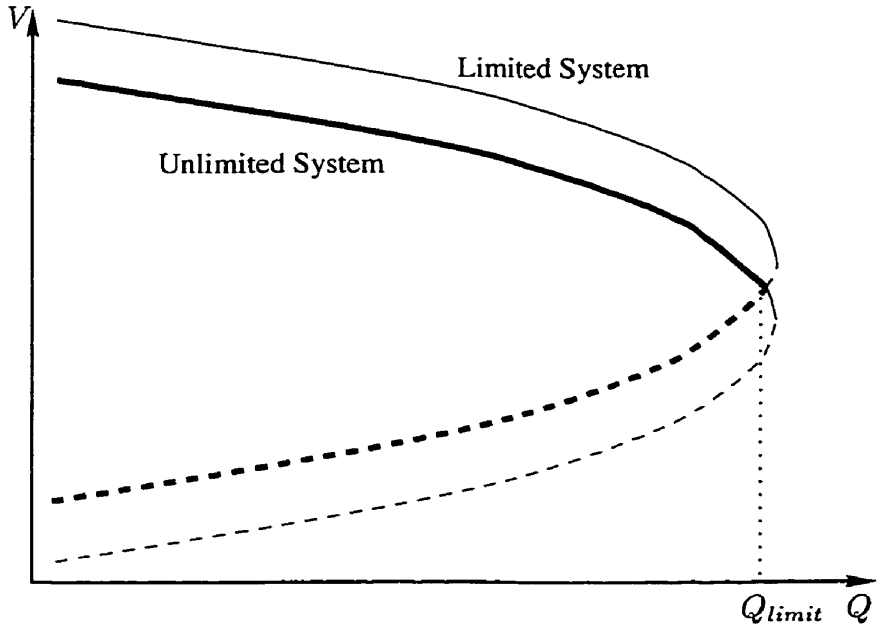
Although saddle-node bifurcations can be shown to be generic in power systems, limits, especially generator reactive power limits, may restrict the space of feasible solutions and thereby voltage collapse may be induced by limits as opposed to a saddle-node bifurcation [51, 52]. This has a major effect on "measuring" the distance to voltage collapse since the voltage collapse may occur not by a saddle-node but rather by reactive power limits, i.e., limit-induced bifurcations.

Limit induced bifurcations as analyzed in [51], occur in power flow equations when generator models are changed from constant voltage and active power models, to constant active and reactive power models on encountering reactive power limits. The change in models corresponds to a different set of equations; and it is found, in some cases, that the new equations are unstable at the current operating point. Both the original model and the "limit induced" model have the same equilibrium point when the limit is encountered but have different bifurcation diagrams. In the case where the system becomes unstable at the limit, the equilibrium point is on the unstable portion of the "limit induced" bifurcation diagram. It is also possible that the system remains stable when the limit is encountered since the equilibrium point may be on the stable portion of the "limit induced" model's bifurcation diagram. Figure 3.3 illustrates these two possibilities.

When the generator voltage control used in practice, which is the reason for this "switching", is considered fully, only the equilibrium branches in bold in Figure 3.3 exist. The higher voltage conditions on the limited system branch in Figure 3.3(a) are not feasible since the control would recover from its reactive power limits and would therefore "switch" back to the original system model. If the condition in Figure 3.3(b) is encountered, the system looses voltage control and collapses. The latter is very similar to a saddle-node bifurcation condition, although the system Jacobian is not singular in this case. This phenomena is not considered in [51].



(a) Stable Limit Point



(b) Unstable Limit Point

Figure 3.3: Illustration of limit induced instability.

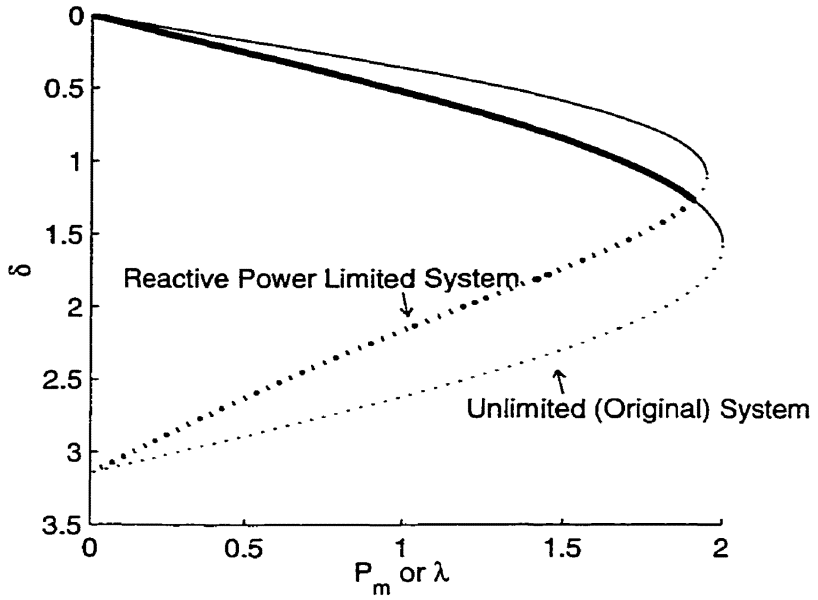


Figure 3.4: Bifurcation diagram for generator-infinite bus example.

Example:

The two-bus lossless system shown in Figure 3.1 is used to illustrate limit-induced bifurcations by adding a reactive power limit. In Figure 3.4, two bifurcation diagrams have been drawn. The "unlimited system" diagram is the same as in Figure 3.2 and corresponds to the original system with the generator modeled as a constant voltage source. The "limited system" diagram corresponds to the set of equilibrium points obtained when the generator is modeled as a constant reactive power source, i.e., the generator terminal voltage is "free" to change.

The "limited system" model is formed by combining the differential equations (3.10) and the load flow equation describing the reactive power supplied by the generator:

$$Q_{gen} = \frac{|V_{gen}|^2}{X_{line}} - \frac{|V_{gen}||V_\infty|}{X_{line}} \cos\delta \tag{3.18}$$

where $Q_{gen} = Q_{limit}$ is set to 1.4 p.u. Equilibrium points of the "limited system" are defined using (3.10), with $\dot{\delta}$ and $\dot{\omega}$ equal to zero, and the algebraic equation (3.18). The system has two differential variables (δ and ω) and one algebraic variable (V_{gen}).

With the reactive power limit, the maximum loading point of the system corresponds to a limit-induced bifurcation of the kind depicted in Figure 3.3(b).

3.5 Bifurcation Analysis Methods

Two traditional methods to analyze bifurcations are the continuation and direct methods [18, 52]. Continuation methods systematically increase the loading level or bifurcation parameter, until a bifurcation is detected. Therefore, not only is the bifurcation or point of collapse determined, but also the set of equilibrium points the system goes through to arrive at the bifurcation point. The continuation method can be used to detect any type of bifurcation without great difficulties [48, 52, 53, 54]. Direct methods, on the other hand, solve the set of algebraic equations used to define the bifurcation point, directly solving for the point at which the system collapses. Direct methods have been successfully applied to determine the exact location of saddle-node in power systems [52, 55]. However, these methods present serious difficulties when used to locate other types of bifurcations [48]. For both methods, it is assumed that the bifurcation parameter is a scalar, which typically corresponds to a given direction of load increases in power system models.

3.5.1 Continuation Methods

Continuation methods are iterative numerical techniques used to detect bifurcations by tracing the bifurcation diagram and indirectly detecting any bifurcations. Since these methods have been extensively studied (e.g., [18, 52, 53, 54, 56]), only a brief review is presented here.

In power systems, continuation methods typically trace the voltage profile of the system up to the maximum loading point of the system. These methods have the advantage that more information is obtained about the system behavior, but they may be computationally expensive, especially in large systems [3].

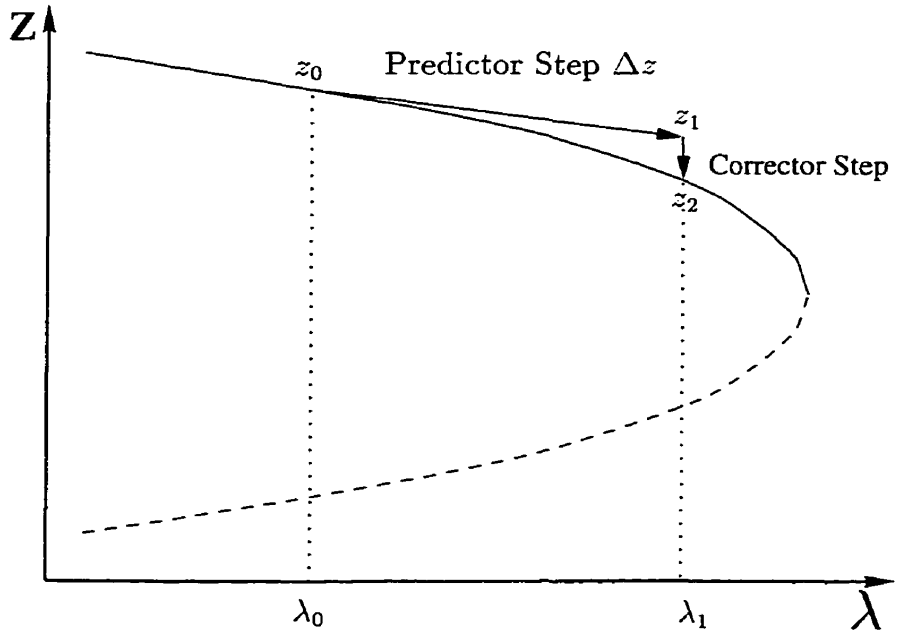


Figure 3.5: Illustration of continuation algorithm.

Continuation methods are generally composed of two or three steps. The first part is a predictor step, the second is a corrector step and the third is a parameterization step. The last step can be omitted in some algorithms. The predictor and corrector steps are illustrated in Figure 3.5. From an initial solution $(\mathbf{z}_0, \lambda_0)$, a step $\Delta\mathbf{z}$, and change $\Delta\lambda$ of the parameter are first determined. From the new point, $\mathbf{z}_1 = \mathbf{z}_0 + \Delta\mathbf{z}$, the new equilibrium point, $\mathbf{z}_2$, is calculated. A parameterization is used to ensure that the Jacobian used in the continuation method does not become singular at a saddle-node bifurcation.

There are several techniques to implement the predictor, corrector and parameterization steps (e.g., [18, 26, 56]). A brief description of one implementation of the three steps, based on [18, 56], follows:

Predictor and Parameterization

Given an initial operating point, the predictor step can be determined by computing the tangent vector to the bifurcation manifold at this point, as follows:

$$\mathbf{D}_z\mathbf{s}(\mathbf{z}_0,\lambda)\frac{d\mathbf{z}}{d\lambda}\bigg|_0 = -\frac{\partial \mathbf{s}}{\partial \lambda}\bigg|_0 \tag{3.19}$$

$$\Delta\lambda = \frac{l}{\| \, d\mathbf{z}/d\lambda \, \|_0} \tag{3.20}$$

$$\Delta\mathbf{z} = \Delta\lambda\frac{d\mathbf{z}}{d\lambda}\bigg|_0 \tag{3.21}$$

where $\frac{\partial \mathbf{s}}{\partial \lambda}|_0$ is the partial derivative of the system equations with respect to the parameter λ, and $\mathbf{D}_z\mathbf{s}(\mathbf{z}_0,\lambda_0)$ is the system Jacobian calculated at the initial point. The constant l is used to control the step "size". The new vector $\mathbf{z}_1$ and parameter value λ_1 are calculated as

$$\mathbf{z}_1 = \mathbf{z}_0 + \Delta\mathbf{z} \tag{3.22}$$

$$\lambda_1 = \lambda_0 + \Delta\lambda \tag{3.23}$$

The tangent predictor method has the disadvantage that near the collapse point, the Jacobian $\mathbf{D}_z\mathbf{s}(\mathbf{z}_0,\lambda_0)$ becomes ill-conditioned. To avoid this problem, a parameterization step can be applied, where the parameter λ is exchanged with the variable in $\mathbf{z}$ that presents the largest value in $\Delta\mathbf{z}$.

Because of the highly nonlinear behavior of the Jacobian's eigenvalues in power system problems, parameterization is not generally required to obtain good results, when step cutting is incorporated into the corrector step [52, 56]. Observe that once the continuation algorithm moves past a saddle-node or limit-induced bifurcation, the sign of $\Delta\lambda$ in equation (3.20) must be changed to trace to lower portion of the bifurcation diagram.

Alternative predictor steps include the arc-length method and the secant methods [3, 18, 54]. The arc-length method is based on representing $\mathbf{z}$ and λ at the equilibrium points as a function of the arc-length of the bifurcation manifold. The secant method,

on the other hand, approximates the tangent vector $d\mathbf{z}/d\lambda$ using two or more previously determined points on the bifurcation manifold.

Corrector Step

Using the new vector and parameter value found in the previous step, a corrector step is used to find a new point that is on the bifurcation manifold. This is found by solving the following set of equations:

$$\begin{aligned} \mathbf{s}(\mathbf{z}, \lambda) &= 0 \\ c(\mathbf{z}, \lambda) &= 0 \end{aligned} \tag{3.24}$$

where $c(\mathbf{z}, \lambda)$ is a scalar equation. The first equation in (3.24) insures that the new solution is an equilibrium point. Since $\mathbf{s}(\mathbf{z}, \lambda)$ has a singular Jacobian at a saddle-node bifurcation, the second scalar equation represents a phase condition that guarantees a non-singular Jacobian of the corrector equations [3]. One possible condition is to define a perpendicular vector to $\Delta\mathbf{z}$ as follows [52, 57]:

$$c(\mathbf{z}, \lambda) = \Delta\lambda(\lambda - \lambda_0 - \Delta\lambda) + \Delta\mathbf{z}^T(\mathbf{z} - \mathbf{z}_0 - \Delta\mathbf{z}) \tag{3.25}$$

where $\Delta\lambda$ and $\Delta\mathbf{z}$ are the solutions of the predictor step. Initial guesses for $\mathbf{z}$ and λ are $\mathbf{z}_1$ and λ_1, respectively, which usually result in good convergence characteristics [56].

3.5.2 Direct Methods

Since saddle-node bifurcations are considered generic, it is possible to consider only a subset of the transversality conditions to compute them. Therefore, saddle-node bifurcations can be directly determined using the following set of equations [52, 55]:

$$\begin{aligned} \mathbf{s}(\mathbf{z}_*, \lambda_*) &= 0 \\ \mathbf{D}_{\mathbf{z}}^T s|_* \mathbf{w} &= 0 \\ \|\mathbf{w}\|_\infty &= 1 \end{aligned} \tag{3.26}$$

where $\mathbf{w}$ is a normalized right eigenvector. Since these methods are formulated to determine saddle-node bifurcations, they cannot be used to determine a limit-induced bifurcation, as the singularity condition is not met in this case.

3.6 Optimization Based Voltage Stability Analysis

Recently, optimization-based techniques have been introduced to analyze voltage stability and determine system settings to maximize the distance to voltage collapse. These techniques are based on traditional bifurcation analysis methods and optimization techniques.

In this section, a review of previously proposed optimization techniques for voltage stability studies is presented. First, a generic explanation of the system model used in optimization based analysis is provided, followed by a discussion on how independent variables (control variables) effect bifurcation diagrams (stability limits). The optimization formulation corresponding to the Direct Method is given with an extension for maximum loadability analysis. Finally, the Maximum Distance to Saddle-node Bifurcation problem is discussed.

3.6.1 System Model

For this thesis, a static model for the power system of the form

$$0 = \mathbf{F}(\mathbf{x}, \boldsymbol{\rho}, \lambda) \tag{3.27}$$

is used, where the vector $\mathbf{x} \in \Re^n$ represents the system's dependent variables, normally non-generator bus voltage magnitudes and angles, reactive power levels of generators when using PV generator models, and real and reactive power levels of the slack bus generator. The vector $\boldsymbol{\rho} \in \Re^m$ represents the independent variables in the system; in a simple model, this would include generator active power settings and terminal voltage levels. The parameter $\lambda \in \Re^+$ represents the loading factor in the system, generally

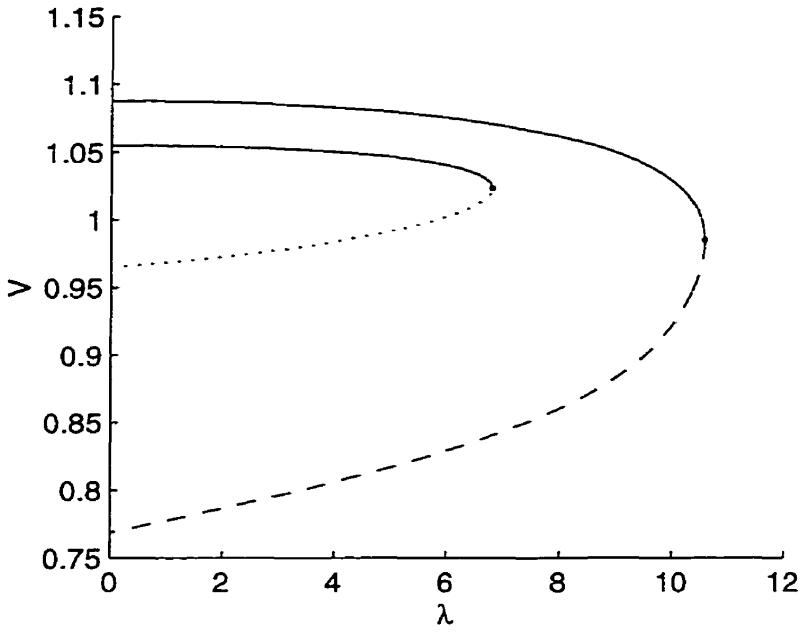


Figure 3.6: Bifurcation diagram for the IEEE 14-bus system. Bus 11 voltage level versus loading level, (λ), for two settings of the independent variables.

referred to as the bifurcation parameter [48]. Typically, the loading factor is used to model the direction of load increase in the system.

In Section 3.3, saddle-node bifurcations are defined using differential and algebraic equations used to model a system. Equation (3.27) is assumed to correspond to the steady state equations of this model.

3.6.2 Effects of Control Parameters on Bifurcation Diagrams

In this section, the effect of changing independent variables (control variables) on the operation of power systems from the point of view of voltage stability is presented. As independent variables are varied, the system effectively moves from one bifurcation diagram to another. This is shown in Figure 3.6 using the 14-bus system whose corresponding single line diagram shown in Figure 3.7.

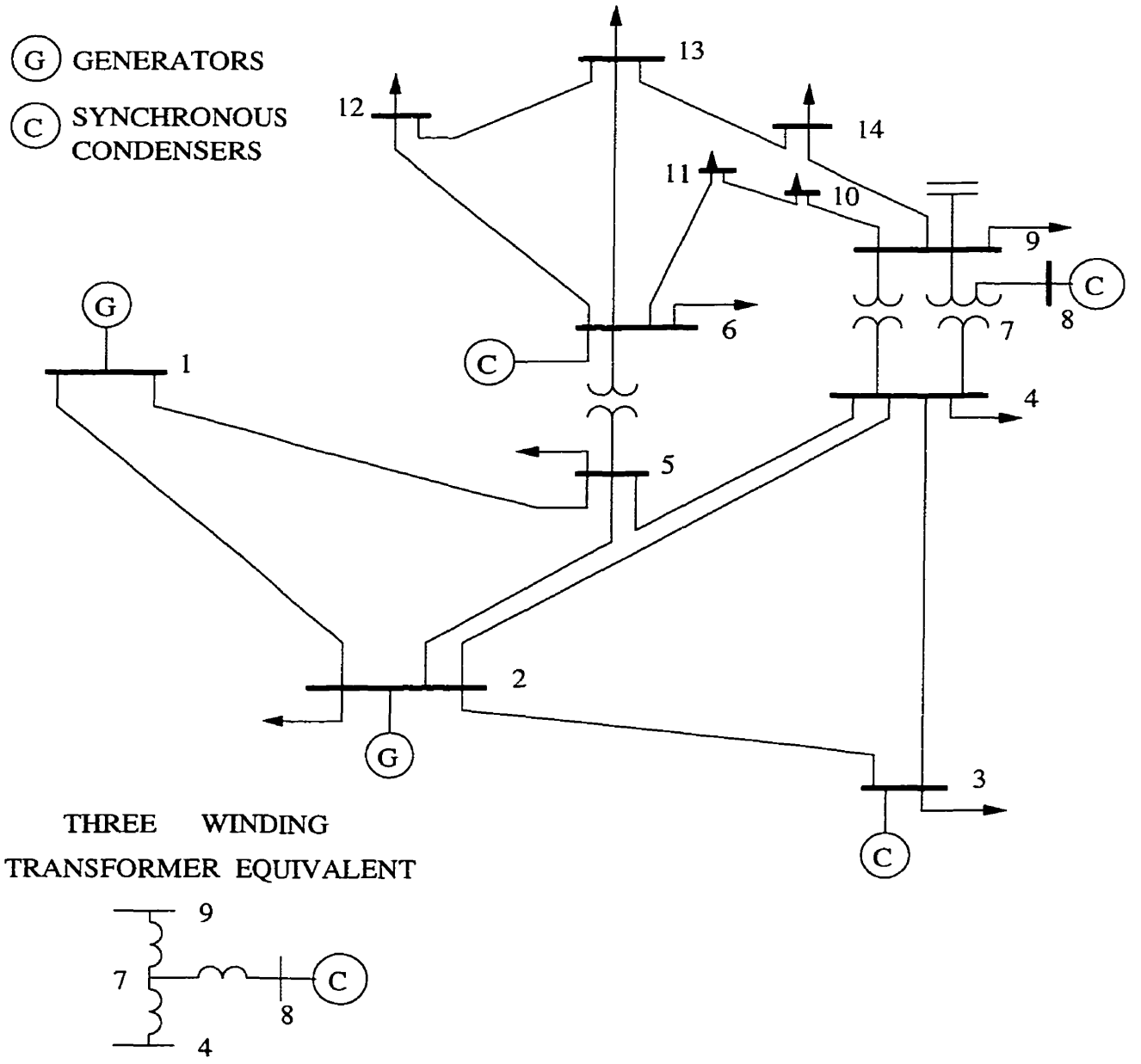


Figure 3.7: Single line diagram of the IEEE 14-bus system.

In Figure 3.6, the per unit voltage level at Bus 11 is plotted versus the loading level λ for two different settings of the independent variables. The maximum loading point of the system is increased by changing the power output of the non-slack bus generators and raising generator voltage settings, resulting in a different bifurcation diagram. Figure 3.6 also shows that setting independent variables to maximize the distance to collapse results in different operating points for all loading levels (i.e., all other values of λ_p). Therefore, when applying techniques to maximize the distance to collapse, the effect of the control variables at the current operating point should be considered.

Bifurcation diagrams can also be varied by changing other parameters in the system, such as shunt capacitance levels and transformer tap settings.

3.6.3 Optimization Based Direct Method

Similar equations and solutions for bifurcation studies can be obtained as the traditional Direct Method (3.26) by using an optimization formulation [11, 15, 58]. For example, by stating the problem as:

$$\begin{aligned} \min \quad & -\lambda_* \\ \text{s.t.:} \quad & \mathbf{F}(\mathbf{x}_*, \boldsymbol{\rho}, \lambda_*) = 0 \end{aligned} \tag{3.28}$$

where λ_* is the value of the loading parameter (bifurcation parameter) at the maximum loading point. For a given value of $\boldsymbol{\rho}$, the solution can be found using the Lagrangian of (3.28):

$$\mathbf{L}(\mathbf{x}_*, \lambda_*, \boldsymbol{\gamma}) = -\lambda_* + \boldsymbol{\gamma}^T \mathbf{F}(\mathbf{x}_*, \boldsymbol{\rho}, \lambda_*) \tag{3.29}$$

where $\boldsymbol{\gamma}$ corresponds to the Lagrangian multipliers, called the dual variables. The local optimal solution of (3.28) is found by satisfying the first order necessary KKT optimality

conditions [35]:

$$\begin{aligned} \mathbf{D}_{\gamma}\mathbf{L} = & \quad \mathbf{F}(\mathbf{x}_*, \boldsymbol{\rho}, \lambda_*) = 0 \\ \mathbf{D}_{\mathbf{x}}\mathbf{L} = & \quad \mathbf{D}_{\mathbf{x}}^T\mathbf{F}(\mathbf{x}_*, \boldsymbol{\rho}, \lambda_*)\gamma = 0 \\ \frac{\partial \mathbf{L}}{\partial \lambda} = & \gamma^T \frac{\partial}{\partial \lambda}\mathbf{F}(\mathbf{x}_*, \boldsymbol{\rho}, \lambda_*) - 1 = 0 \end{aligned} \tag{3.30}$$

where the above equations have the same form as the Direct Method equations (3.26). Therefore, well defined optimization routines can be utilized to obtain the bifurcation point, by stating the problem as an optimization problem.

3.6.4 Maximum Distance to Collapse Problem

The optimization-based Direct Method can be modified to determine the values of the independent variables (control variables) that maximize the distance to voltage collapse. Thus, let us consider the maximum distance to collapse problem:

$$\begin{aligned} \min \quad & -\lambda_* \\ \text{s.t.:} \quad & \mathbf{F}(\mathbf{x}_*, \boldsymbol{\rho}, \lambda_*) = 0 \\ & \underline{\boldsymbol{\rho}} \leq \boldsymbol{\rho} \leq \overline{\boldsymbol{\rho}} \end{aligned} \tag{3.31}$$

Limits on $\mathbf{x}_*$ have been excluded to simplify the problem, and lower and upper limits on the independent variables $\boldsymbol{\rho}$ are given by the vectors $\underline{\boldsymbol{\rho}}$ and $\overline{\boldsymbol{\rho}}$, respectively. The inequality constraints may be incorporated into the objective function using a logarithmic barrier term as follows:

$$\begin{aligned} \min \quad & -\lambda_* - \mu \textstyle\sum_{i=1}^{m} log\,(\boldsymbol{\rho}_* - \underline{\boldsymbol{\rho}_*}) - \mu \sum_{i=1}^{m} log\,(\overline{\boldsymbol{\rho}_*} - \boldsymbol{\rho}_*) \\ \text{s.t. :} \quad & \mathbf{F}(\mathbf{x}_*, \boldsymbol{\rho}_*, \lambda_*) = 0 \end{aligned} \tag{3.32}$$

The solution can then be determined using the related Lagrangian function

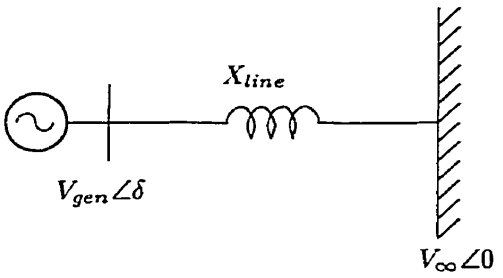


Figure 3.8: Generator-infinite bus single line diagram.

$$\mathbf{L}(\mathbf{x}_*, \boldsymbol{\rho}, \lambda_*, \boldsymbol{\gamma}) = -\lambda_* - \mu \sum_{i=1}^{m} log\,(\boldsymbol{\rho} - \underline{\boldsymbol{\rho}}) - \mu \sum_{i=1}^{m} log\,(\overline{\boldsymbol{\rho}} - \boldsymbol{\rho}) + \boldsymbol{\gamma}^T \mathbf{F}(\mathbf{x}, \boldsymbol{\rho}, \lambda_*) \qquad (3.33)$$

where $\boldsymbol{\gamma}$ corresponds to the Lagrangian multipliers, called the dual variables. The optimal solution is defined by the KKT first-order optimality conditions [35]:

$$\begin{aligned}
\mathbf{D}_{\mathbf{x}}\mathbf{L} = & \quad \mathbf{D}_{\mathbf{x}}^T \mathbf{F}(\mathbf{x}_*, \boldsymbol{\rho}, \lambda_*)\boldsymbol{\gamma} = 0 \qquad (3.34)\\
\mathbf{D}_{\boldsymbol{\rho}}\mathbf{L} = & \mathbf{D}_{\boldsymbol{\rho}}^T \mathbf{F}(\mathbf{x}_*, \boldsymbol{\rho}, \lambda_*)\boldsymbol{\gamma} - \mu\, diag(\boldsymbol{\rho} - \underline{\boldsymbol{\rho}})^{-1}\mathbb{1} - \mu\, diag(\overline{\boldsymbol{\rho}} - \boldsymbol{\rho})^{-1}\mathbb{1} = 0\\
\frac{\partial \mathbf{L}}{\partial \lambda} = & \quad \boldsymbol{\gamma}^T \frac{\partial}{\partial \lambda}\mathbf{F}(\mathbf{x}_*, \boldsymbol{\rho}, \lambda_*) - 1 = 0\\
\mathbf{D}_{\boldsymbol{\gamma}}\mathbf{L} = & \quad \mathbf{F}(\mathbf{x}_*, \boldsymbol{\rho}, \lambda_*) \quad = 0
\end{aligned}$$

where $\mathbb{1} = [1,\ 1,\ 1, ...,\ 1]^T$ of appropriate size. These equations are very similar to the equations used in the Direct Method as outlined in Section 3.5. Specifically, the fourth equation in (3.34) guarantees an equilibrium point, whereas the first equation guarantees a singular Jacobian of the power system model. Therefore, the proposed variation will determine a point of collapse and the value of independent variables that will maximize λ_*.

Example:

The difference between the original Direct Method and the optimization-based method is illustrated with the following example: Consider a single generator connected through a

lossless transmission line to a network modeled as an infinite bus as shown in Figure 3.8. The generator terminal voltage V_{gen} is the only independent variable (control variable) ρ, and is initially set to unity. It is assumed in this example that the generator terminal voltage will be constant for all loading conditions. The value of X_{line} is set to 0.1 p.u., and the value of V_{gen} can be set to 1.0 ± 0.1 p.u. Finally, the generator power output P_{gen} is used as the bifurcation parameter λ, with the dependent variables of the system being the generator voltage angle and reactive power (δ, Q_{gen}). The system of equations governing the operation of this system are:

$$\begin{aligned} P_{gen} &= \frac{|V_{gen}||V_{\infty}|}{X_{line}} \sin\delta \\ Q_{gen} &= \frac{|V_{gen}|^2}{X_{line}} - \frac{|V_{gen}||V_{\infty}|}{X_{line}} \cos\delta \end{aligned} \tag{3.35}$$

where X_{line} is the transmission line impedance, and V_{∞} is the voltage magnitude of the infinite bus. Since the first equation is independent of Q_{gen} and no limits are considered for Q_{gen}, only the first equation in (3.35) is needed to find the maximum loading point.

Using the Direct Method, discussed in Section 3.5, the maximum value of P_{gen} is found to be 10 p.u., with the original terminal voltage setting of $V_{gen} = 1.0$ p.u. Using the optimization formulation given by (3.31), the maximum value of P_{gen} is found to be 11 p.u., with a corresponding terminal voltage setting of 1.1 p.u. Both problems found a point of collapse, but formulation (3.31) is such that it also maximizes the value of the loading parameter at the bifurcation.

3.6.5 Maximum Distance to Saddle-node Bifurcation

Based on bifurcation theory and optimization techniques, two formulations are presented in this section that determine the optimal control to maximize the distance to a saddle-node bifurcation. Several different algorithms have been proposed in the literature based on the saddle-node bifurcation transversality conditions (e.g., [4, 5, 10]). The objective of

the problem is to increase the value of the loading parameter λ_* at the bifurcation, thus, increasing the distance from the current operating point to this critical value.

One form of the Maximum Distance to Saddle-node Bifurcation problem can be stated as an optimization problem as follows:

$$\begin{aligned} \min \quad & -\tfrac{1}{2}(\lambda_p - \lambda_*)^2 \\ \text{s.t. :} \quad & \mathbf{F}(\mathbf{x}_*, \boldsymbol{\rho}, \lambda_*) = 0 \\ & \mathbf{D}_x^T \mathbf{F}(\mathbf{x}_*, \boldsymbol{\rho}, \lambda_*)\mathbf{w} = 0 \end{aligned} \tag{3.36}$$

where $\mathbf{w}$ is the left eigenvector and is assumed to be a properly normalized nonzero vector. The current value of the bifurcation parameter is given by λ_p and its value at the saddle-node bifurcation is denoted as λ_*. The second equality constraint is used to explicitly define the maximum loading point as a saddle-node bifurcation. This formulation, including the quadratic objective function, was used in [5, 10].

The next step is to incorporate feasibility of the current operating point. This has the advantage that, as independent variables (control variables) are changed to maximize the distance to collapse, bounds can be incorporated into the present operating point. Therefore, the modified Maximum Distance to Saddle-node Bifurcation problem may be written as:

$$\begin{aligned} \min \quad & -\tfrac{1}{2}(\lambda_p - \lambda_*)^2 \\ \text{s.t. :} \quad & \mathbf{F}(\mathbf{x}_p, \boldsymbol{\rho}, \lambda_p) = 0 \\ & \mathbf{F}(\mathbf{x}_*, \boldsymbol{\rho}_*, \lambda_*) = 0 \\ & \mathbf{D}_{\mathbf{x}}^T \mathbf{F}(\mathbf{x}_*, \boldsymbol{\rho}_*, \lambda_*)\mathbf{w} = 0 \\ & \underline{\mathbf{x}}_p \le \mathbf{x}_p \le \overline{\mathbf{x}}_p \\ & \underline{\mathbf{x}}_* \le \mathbf{x}_* \le \overline{\mathbf{x}}_* \\ & \underline{\boldsymbol{\rho}} \le \boldsymbol{\rho} \le \overline{\boldsymbol{\rho}} \end{aligned} \tag{3.37}$$

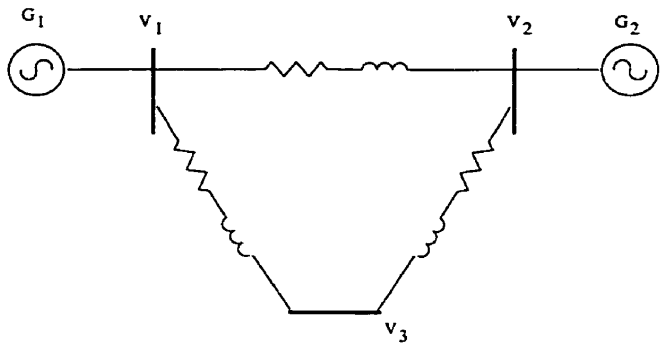


Figure 3.9: 3-bus system single line diagram.

where $\boldsymbol{\rho}_* \supset \boldsymbol{\rho}$ is used to map the control variables $\boldsymbol{\rho}$, at the current operating point, into the collapse point to account for certain system changes (e.g., generation changes modeled using a distributed slack bus), and the subscripts p denotes the present or current loading level. Since $\mathbf{x}_p$ is now introduced in the nonlinear programming problem, minimum and maximum constraints can be placed on all system variables. Observe that this formulation fails if the system collapses due to a limit-induced bifurcation.

Example:

The above two problems are applied to the three bus system shown in Figure 3.9. Applying the maximum distance to saddle-node bifurcation formulation, a maximum loading $\lambda_* = 8.5$ is found. Adding constraints on the current operating point (modified maximum distance to saddle-node bifurcation formulation) results in an optimal $\lambda_* = 7.4$. The difference in the two results is attributed to the fact that incorporating constraints on the current operating point reduces the space of feasible solutions. In both cases, the maximum loading point corresponded to a saddle-node bifurcation.

3.7 Summary

In this chapter, an introduction to voltage stability and bifurcation analysis is presented. Traditional methods used to determine bifurcations are given and extended to optimiza-

tion based approaches. The problems are then reformulated, from finding the maximum loading point for a given set of control variables, to maximizing the distance to collapse. Finally, the concept of considering both the current loading point and the collapse point in the problem is briefly introduced.

Chapter 4

Voltage Stability Constrained Optimal Power Flow

4.1 Introduction

Voltage stability problems in power systems may occur for a variety of reasons, from voltage control problems with Automatic Voltage Regulators (AVR) and Under-Load Tap-Changer (ULTC) transformers, to instabilities created by different types of bifurcations. Several conference proceedings (e.g., [59, 60, 61]) summarize many of the voltage stability problems, and discuss techniques and models proposed by researchers relating to the area of bifurcation theory. As loading levels in a system increase, the stability margin decreases. Generally, control actions can be taken to increase the available transfer capability of the system, but this may result in increased costs. These increased costs may be considered as the operational cost of enforcing a voltage stability constraint.

This chapter presents a numerical analysis of applying optimization techniques to proposed voltage stability constrained Optimal Power Flow problems. Numerical analysis using the IEEE 57-bus and 118-bus systems are presented to highlight the characteristics of these problems. The single line diagrams for the 57-bus and 118-bus system are shown in Figures 4.1 and 4.2, respectively; the data for these systems was based on data provided in [62]. Emphasis is given to change in generator cost when including voltage stability criteria in the OPF.

This chapter is structured as follows: First, a general formulation to combine OPF and voltage stability is given. A modification to the Maximum Distance to Collapse problem that includes constraints and feasibility of the current operating point is presented. In

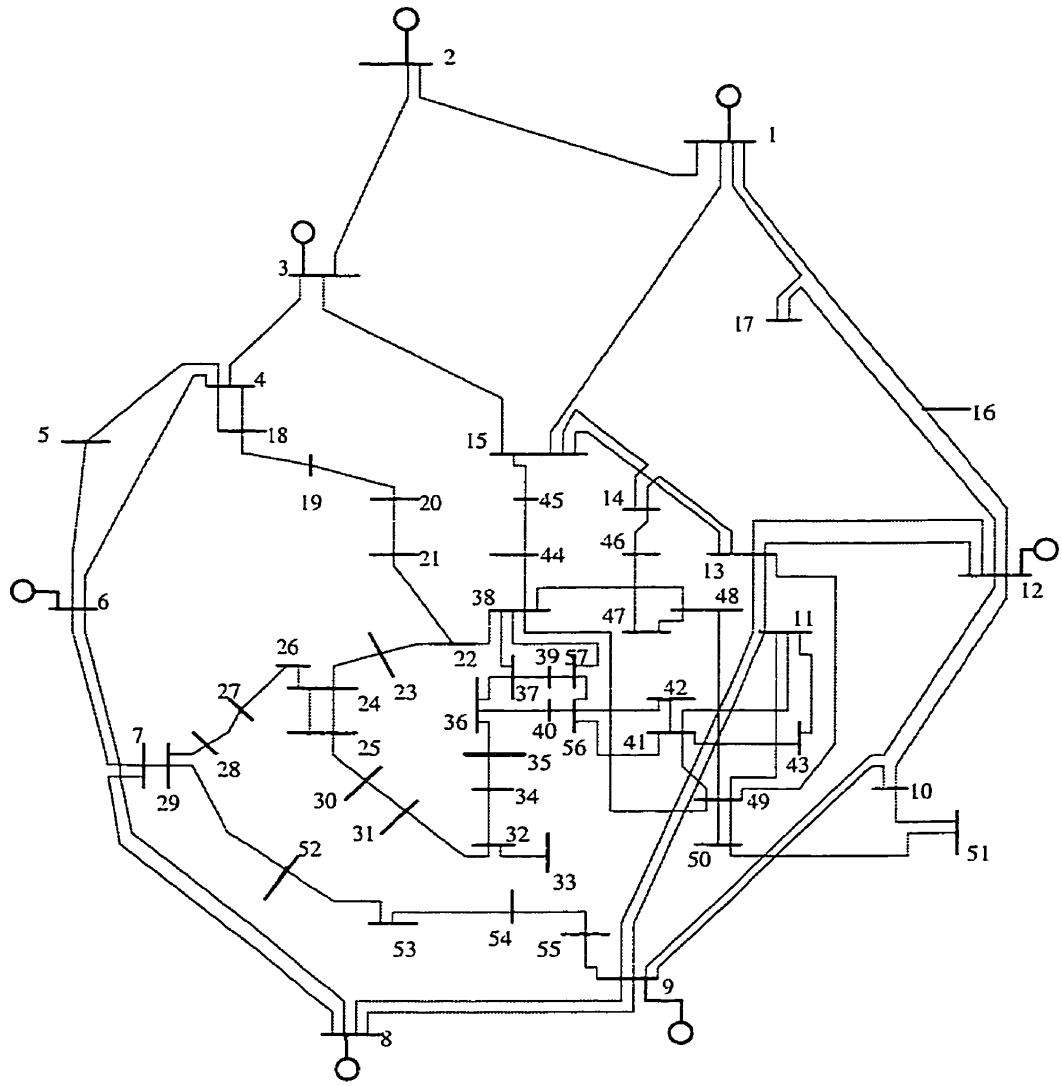


Figure 4.1: Single line diagram of the 57-bus system.

addition, several Voltage Stability Constrained-Optimal Power Flow (VSC-OPF) formulations are presented, followed by an analysis of the results obtained from applying the formulations to the two test systems. Finally, a summary of the main results presented in this chapter is given.

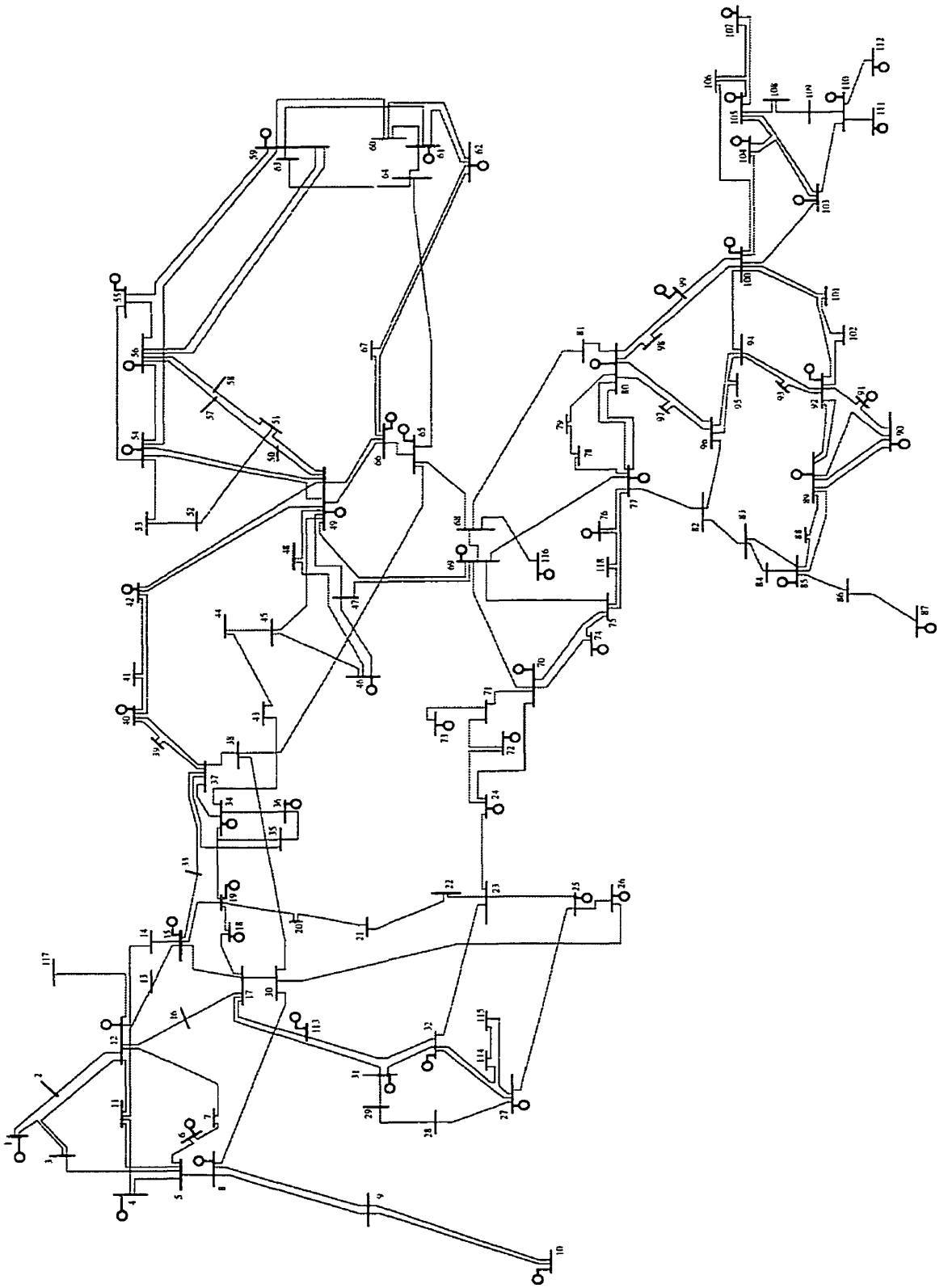


Figure 4.2: Single line diagram of the 118-bus system.

4.1.1 OPF and Voltage Stability Criteria

A general OPF problem that incorporates voltage stability criteria can be written as

$$\begin{aligned} \min \quad & \mathbf{G}(\mathbf{x}_p, \boldsymbol{\rho}, \lambda_p, \lambda_*) \\ \text{s.t. :} \quad & \mathbf{F}(\mathbf{x}_p, \boldsymbol{\rho}, \lambda_p) = 0 \\ & \mathbf{F}(\mathbf{x}_*, \boldsymbol{\rho}_*, \lambda_*) = 0 \\ & \underline{\mathbf{H}_p} \leq \mathbf{H}(\mathbf{x}_p) \leq \overline{\mathbf{H}_p} \\ & \underline{\mathbf{H}_*} \leq \mathbf{H}(\mathbf{x}_*) \leq \overline{\mathbf{H}_*} \\ & \underline{\mathbf{x}_p} \leq \mathbf{x}_p \leq \overline{\mathbf{x}_p} \\ & \underline{\mathbf{x}_*} \leq \mathbf{x}_* \leq \overline{\mathbf{x}_*} \\ & \underline{\boldsymbol{\rho}} \leq \boldsymbol{\rho} \leq \overline{\boldsymbol{\rho}} \end{aligned} \tag{4.1}$$

where the subscripts p and $*$ indicate the current and collapse points, respectively. The function $\mathbf{G}(\mathbf{x}_p, \boldsymbol{\rho}, \lambda_p, \lambda_*)$, is the objective function to be minimized, which includes an OPF component, such as production costs or losses, and a voltage stability component. The OPF component may be dependent on ($\mathbf{x}_p$,$\boldsymbol{\rho}$,λ_p), whereas the voltage stability component is generally a function of λ_* and possibly of λ_p. It is assumed that the inequality constraints can be separated into constraints at the current and collapse points. The lower and upper limits on the power system independent or control variables $\boldsymbol{\rho}$ are given by $\underline{\boldsymbol{\rho}}$ and $\overline{\boldsymbol{\rho}}$, respectively. Finally, $\boldsymbol{\rho}_* \supset \boldsymbol{\rho}$ is used to map the control variables at the current operating point, defined by $\boldsymbol{\rho}$, into the collapse point to account for certain system changes (e.g., generation changes modeled using a distributed slack bus).

It is important to highlight the fact that in (4.1), λ stands for only one parameter instead of several, contrary to what is proposed in [13], i.e., the optimization is done in a particular direction of load change. This is not a problem, given that the optimization would be typically done several times a day during the operation of the system, as in the case of any other OPF procedure. This assumption simplifies the numerical solution process of the optimization problem, which is already a difficult numerical problem, given the highly nonlinear behavior of the system constraints and the effect of limits associated

with the inclusion of the collapse conditions.

Depending on the definition of the objective function $\mathbf{G}(\cdot)$ in (4.1), one can pursue different optimization strategies and hence obtain solutions to a variety of distinct problems.

4.1.2 Limit-induced Versus Saddle-node Bifurcations

Using a Logarithmic Barrier approach [32], the first order KKT optimality conditions to problem (4.1) is given to demonstrate when the maximum loading point is defined by a limit-induced bifurcation or a saddle-node bifurcation. Using slack variables, problem (4.1) can be rewritten as

$$\begin{aligned}
\min \quad & \mathbf{G}(\mathbf{x}_p, \boldsymbol{\rho}, \lambda_p, \lambda_*) \\
\text{s.t. :} \quad & \mathbf{F}(\mathbf{x}_p, \boldsymbol{\rho}, \lambda_p) = 0 \\
& \mathbf{F}(\mathbf{x}_*, \boldsymbol{\rho}_*, \lambda_*) = 0 \\
& \mathbf{H}(\mathbf{x}_p) - \underline{\mathbf{H}_p} - \mathbf{s}_1 = 0 \\
& \overline{\mathbf{H}_p} - \mathbf{H}(\mathbf{x}_p) - \mathbf{s}_2 = 0 \\
& \mathbf{H}(\mathbf{x}_*) - \underline{\mathbf{H}_*} - \mathbf{s}_3 = 0 \\
& \overline{\mathbf{H}_*} - \mathbf{H}(\mathbf{x}_*) - \mathbf{s}_4 = 0 \\
& \boldsymbol{\rho} - \underline{\boldsymbol{\rho}} - \mathbf{s}_5 = 0 \\
& \overline{\boldsymbol{\rho}} - \boldsymbol{\rho} - \mathbf{s}_6 = 0 \\
& \mathbf{s}_1, \mathbf{s}_2, \mathbf{s}_3, \mathbf{s}_4, \mathbf{s}_5, \mathbf{s}_6 \geq 0
\end{aligned} \tag{4.2}$$

where $\mathbf{s}_1, \mathbf{s}_2, \mathbf{s}_3, \mathbf{s}_4 \in \Re^p$ and $\mathbf{s}_5, \mathbf{s}_6 \in \Re^m$ are the primal non-negative slack variables used to transform the inequality constraints to equalities. The non-negativity constraints are

incorporated into the objective function using a logarithmic barrier terms as follows:

$$\begin{aligned} \min\ & \mathbf{G}(\mathbf{x}_p, \boldsymbol{\rho}, \lambda_p, \lambda_*) - \mu \sum_{i=1}^{m} (log\ \mathbf{s}_5[i] + log\ \mathbf{s}_6[i]) \\ & - \mu \sum_{i=1}^{p} (log\ \mathbf{s}_1[i] + log\ \mathbf{s}_2[i] + log\ \mathbf{s}_3[i] + log\ \mathbf{s}_4[i]) \end{aligned} \tag{4.3}$$

$$\begin{aligned} \text{s.t. :} \qquad \mathbf{F}(\mathbf{x}_p, \boldsymbol{\rho}, \lambda_p) &= 0 \\ \mathbf{F}(\mathbf{x}_*, \boldsymbol{\rho}_*, \lambda_*) &= 0 \\ \mathbf{H}(\mathbf{x}_p) - \underline{\mathbf{H}_p} - \mathbf{s}_1 &= 0 \\ \overline{\mathbf{H}_p} - \mathbf{H}(\mathbf{x}_p) - \mathbf{s}_2 &= 0 \\ \mathbf{H}(\mathbf{x}_*) - \underline{\mathbf{H}_*} - \mathbf{s}_3 &= 0 \\ \overline{\mathbf{H}_*} - \mathbf{H}(\mathbf{x}_*) - \mathbf{s}_4 &= 0 \\ \boldsymbol{\rho} - \underline{\boldsymbol{\rho}} - \mathbf{s}_5 &= 0 \\ \overline{\boldsymbol{\rho}} - \boldsymbol{\rho} - \mathbf{s}_6 &= 0 \end{aligned}$$

where μ is the barrier parameter and $\mathbf{s}[i]$ represents the i^{th} element of the vector $\mathbf{s}$. The Lagrangian function of the modified barrier problem (4.3) is then defined as

$$\begin{aligned} L \;=\; & \mathbf{G}(\mathbf{x}_p, \boldsymbol{\rho}, \lambda_p, \lambda_*) - \mu \sum_{i=1}^{m} (log\ \mathbf{s}_1[i] + log\ \mathbf{s}_2[i]) \\ & - \mu \sum_{i=1}^{p} (log\ \mathbf{s}_3[i] + log\ \mathbf{s}_4[i] + log\ \mathbf{s}_5[i] + log\ \mathbf{s}_6[i]) \\ & - \boldsymbol{\gamma}_1^T (\mathbf{F}(\mathbf{x}_p, \boldsymbol{\rho}, \lambda_p)) - \boldsymbol{\gamma}_2^T (\mathbf{F}(\mathbf{x}_*, \boldsymbol{\rho}_*, \lambda_*)) \\ & - \boldsymbol{\nu}_1^T (\mathbf{H}(\mathbf{x}_p) - \underline{\mathbf{H}_p} - \mathbf{s}_1) - \boldsymbol{\nu}_2^T (\overline{\mathbf{H}_p} - \mathbf{H}(\mathbf{x}_p) - \mathbf{s}_2) \\ & - \boldsymbol{\nu}_3^T (\mathbf{H}(\mathbf{x}_*) - \underline{\mathbf{H}_*} - \mathbf{s}_3) - \boldsymbol{\nu}_4^T (\overline{\mathbf{H}_*} - \mathbf{H}(\mathbf{x}_*) - \mathbf{s}_4) \\ & - \boldsymbol{\zeta}_1^T (\boldsymbol{\rho} - \underline{\boldsymbol{\rho}} - \mathbf{s}_5) - \boldsymbol{\zeta}_2^T (\overline{\boldsymbol{\rho}} - \boldsymbol{\rho} - \mathbf{s}_6) \end{aligned} \tag{4.4}$$

where $\boldsymbol{\gamma}_1, \boldsymbol{\gamma}_2 \in \Re^n$; $\boldsymbol{\nu}_1, \boldsymbol{\nu}_2, \boldsymbol{\nu}_3, \boldsymbol{\nu}_4 \in \Re^p$ and $\boldsymbol{\zeta}_1, \boldsymbol{\zeta}_2 \in \Re^m$ are the Lagrange multipliers. The vector $\mathbf{y} = (\mathbf{x}_*, \mathbf{x}_p, \lambda_*, \boldsymbol{\rho}, \mathbf{s}_1, \mathbf{s}_2, \mathbf{s}_3, \mathbf{s}_4, \mathbf{s}_5, \mathbf{s}_6, \boldsymbol{\gamma}_1, \boldsymbol{\gamma}_2, \boldsymbol{\nu}_1, \boldsymbol{\nu}_2, \boldsymbol{\nu}_3, \boldsymbol{\nu}_4, \boldsymbol{\zeta}_1, \boldsymbol{\zeta}_2)$ is introduced to simplify the expression. The Karush-Kuhn-Tucker (KKT) first-order necessary conditions are used

to define the local minimum of equation (4.3),

$$\nabla_{\mathbf{y}} L = \begin{bmatrix} \nabla_{\mathbf{x}_*} L \\ \nabla_{\mathbf{x}_p} L \\ \nabla_{\lambda_*} L \\ \nabla_{\boldsymbol{\rho}} L \\ -\mu \mathbb{1} + \mathbf{S}_1 \boldsymbol{\nu}_1 \\ -\mu \mathbb{1} + \mathbf{S}_2 \boldsymbol{\nu}_2 \\ -\mu \mathbb{1} + \mathbf{S}_3 \boldsymbol{\nu}_3 \\ -\mu \mathbb{1} + \mathbf{S}_4 \boldsymbol{\nu}_4 \\ -\mu \mathbb{1} + \mathbf{S}_5 \boldsymbol{\zeta}_1 \\ -\mu \mathbb{1} + \mathbf{S}_6 \boldsymbol{\zeta}_2 \\ \mathbf{F}(\mathbf{x}_p, \boldsymbol{\rho}, \lambda_p) \\ \mathbf{F}(\mathbf{x}_*, \boldsymbol{\rho}_*, \lambda_*) \\ \mathbf{H}(\mathbf{x}_p) - \underline{\mathbf{H}_p} - \mathbf{s}_1 \\ \overline{\mathbf{H}_p} - \mathbf{H}(\mathbf{x}_p) - \mathbf{s}_2 \\ \mathbf{H}(\mathbf{x}_*) - \underline{\mathbf{H}_*} - \mathbf{s}_3 \\ \overline{\mathbf{H}_*} - \mathbf{H}(\mathbf{x}_*) - \mathbf{s}_4 \\ \boldsymbol{\rho} - \underline{\boldsymbol{\rho}} - \mathbf{s}_5 \\ \overline{\boldsymbol{\rho}} - \boldsymbol{\rho} - \mathbf{s}_6 \end{bmatrix} = 0 \tag{4.5}$$

where $\mathbf{S}_1$ through $\mathbf{S}_6$ are diagonal matrices with elements of the corresponding vector $\mathbf{s}_1$ through $\mathbf{s}_6$ on the diagonal; $\mathbb{1} \in \Re^p$ is a vectors of ones; and

$$\begin{aligned}
\nabla_{\mathbf{x}_*} L &= \boldsymbol{\gamma}_2^T \mathbf{D}_{\mathbf{x}_*} \mathbf{F}(\mathbf{x}_*, \boldsymbol{\rho}_*, \lambda_*) - (\boldsymbol{\nu}_3^T + \boldsymbol{\nu}_4^T) \mathbf{D}_{\mathbf{x}_*} \mathbf{H}(\mathbf{x}_*) \\
\nabla_{\mathbf{x}_p} L &= \mathbf{D}_{\mathbf{x}_p} \mathbf{G}(\mathbf{x}_p, \boldsymbol{\rho}, \lambda_p, \lambda_*) + \boldsymbol{\gamma}_1^T \mathbf{D}_{\mathbf{x}_p} \mathbf{F}(\mathbf{x}_p, \boldsymbol{\rho}, \lambda_p) \\
&\quad -(\boldsymbol{\nu}_1^T + \boldsymbol{\nu}_2^T) \mathbf{D}_{\mathbf{x}_p} \mathbf{H}(\mathbf{x}_p) \\
\nabla_{\lambda_*} L &= \mathbf{D}_{\lambda_*} \mathbf{G}(\mathbf{x}_p, \boldsymbol{\rho}, \lambda_p, \lambda_*) - \boldsymbol{\gamma}_2^T \mathbf{D}_{\lambda_*} \mathbf{F}(\mathbf{x}_*, \boldsymbol{\rho}_*, \lambda_*) \\
\nabla_{\boldsymbol{\rho}} L &= \mathbf{G}(\mathbf{x}_p, \boldsymbol{\rho}, \lambda_p, \lambda_*) - \boldsymbol{\gamma}_1^T \mathbf{D}_{\boldsymbol{\rho}} \mathbf{F}(\mathbf{x}_p, \boldsymbol{\rho}, \lambda_p) \\
&\quad -\boldsymbol{\gamma}_2^T \mathbf{D}_{\boldsymbol{\rho}} \mathbf{F}(\mathbf{x}_*, \boldsymbol{\rho}_*, \lambda_*) - \boldsymbol{\zeta}_1 + \boldsymbol{\zeta}_2
\end{aligned}$$

The issue of collapse due to limit-induced bifurcation versus saddle-node bifurcation can now be explained as follows: The first condition in (4.5), $\nabla_{\mathbf{x}_*} L$, includes the Jacobian of the system model at the maximum loading point multiplied by γ_2, which can be considered to be equivalent to an eigenvector of a Jacobian. Therefore, the first condition corresponds to a singular Jacobian if $(\nu_3^T + \nu_4^T)\mathbf{D}_{\mathbf{x}_*}\mathbf{H}(\mathbf{x}_*) = 0$; this would imply that, if one assumes that $\mathbf{D}_{\mathbf{x}_*}\mathbf{H}(\mathbf{x}_*)$ is non-singular (which is typically the case when limits directly on $\mathbf{x}$ are being enforced, i.e. $\mathbf{D}_{\mathbf{x}_*}\mathbf{H}(\mathbf{x}_*)$ is an identity matrix), the dependent variables are not at their limits, since ν_3 and ν_4 are zero when their corresponding limits are not active. If dependent variables of the critical point are at their limits, then ν_3 and ν_4 may become non-negative, i.e., the load flow Jacobian may be non-singular. If ν_3 and ν_4 are non-negative, which implies that locally the objective function could be improved if the limits are not enforced, the system has reached a limit-induced bifurcation point. If limits are reached and ν_3 and ν_4 remain zero, this implies that the limits are not locally limiting an improvement to the objective function and hence the system has reached a saddle-node bifurcation point.

The above derivation demonstrates when the inequality constraints can be separated based on the dependent and independent variables of the load flow model, the maximum loading point may be a limit-induced point only when constraints based on the dependent variables become active. The independent variables $\boldsymbol{\rho}$ being at their limits, do not directly affect the type of bifurcation. Furthermore, if the system collapses through a saddle-node bifurcation and limits on dependent variables are active, (4.5) implies that the Lagrangian multipliers associated with this limit are zero. Therefore, for the particular bifurcation, removing the limit that is active will not affect the bifurcation.

4.1.3 Modified Maximum Distance to Collapse

The Maximum Distance to Collapse problem with constraints incorporated on the current and critical loading point [5, 6] is a particular example using optimization techniques to

enhance voltage stability. This problem can be written as

$$\begin{aligned} \min \quad & -(\lambda_* - \lambda_p) \\ \text{s.t.} : \quad & \mathbf{F}(\mathbf{x}_p, \boldsymbol{\rho}, \lambda_p) = 0 \\ & \mathbf{F}(\mathbf{x}_*, \boldsymbol{\rho}_*, \lambda_*) = 0 \\ & \underline{\mathbf{H}_p} \leq \mathbf{H}(\mathbf{x}_p) \leq \overline{\mathbf{H}_p} \\ & \underline{\mathbf{H}_*} \leq \mathbf{H}(\mathbf{x}_*) \leq \overline{\mathbf{H}_*} \\ & \underline{\boldsymbol{\rho}} \leq \boldsymbol{\rho} \leq \overline{\boldsymbol{\rho}} \end{aligned} \tag{4.6}$$

This OPF maximizes the distance to a saddle-node or limit-induced bifurcation. Including the current loading point into the constraints ensures that, when independent variables are calculated to maximize the distance to voltage collapse, feasibility and inequality constraints at the current loading point are met [6]. For example, increasing generator voltage magnitude settings generally increases the distance to collapse but, under lighter loading conditions, the increased levels may lead to over-voltages. Incorporating the current operating point into the optimization problem can eliminate this problem; however, it also reduces the space of feasible solutions.

Example:

Reactive Power limits are added to the two-bus example from Section 3.6.4, illustrated in Figure 3.8, and modeled with equations (3.35) to demonstrate the ability of the maximum distance to bifurcation algorithm to converge to limit induced bifurcations. Again, the generator terminal voltage (independent variable) is restricted to 1.0 ± 0.1 per unit but Q_{gen} is now limited to the range $-4.0 \leq Q_{gen} \leq 4.0$ per unit. The dependent variables for the system are the generator voltage angle and reactive power (δ, Q_{gen}). Using the maximum distance to collapse formulation, with limits on Q_{gen}, the maximum loading point is found to be 8.06 per unit which is lower than the value of 11 per unit found when no reactive power limits where included. At the critical point, Q_{gen} is at the upper limit.

4.2 VSC-OPF Formulations

With the current loading point included into the optimization problem, it is possible to incorporate voltage stability criteria into an OPF formulation at the "current" operating point $\mathbf{x}_p$. As the operating point moves closer to a voltage collapse or bifurcation point, i.e., as $\mathbf{x}_p$ approaches $\mathbf{x}_*$, more emphasis must be placed on maximizing voltage stability as opposed to minimizing operating costs.

An initial approach to this problem consisted of introducing voltage stability indices in the objective function as indicators of the proximity to voltage collapse, as explained in [5]; However, since voltage stability indices present rather nonlinear characteristics, especially when limits are considered, this technique did not produce adequate results.

In order to incorporate voltage stability constraints into a traditional OPF formulation, the following five formulations are proposed:

- Hybrid VSC-OPF Formulation
- Linear Combination VSC-OPF Formulation
- Fixed Stability Margin VSC-OPF Formulation
- Goal Programming VSC-OPF Formulation
- VSC-OPF with Reactive Power Pricing Formulation

In each of the above formulations, the difference between λ_* and λ_p is used as an "exact" measure of the distance to collapse. For the first formulation, the $(\lambda_* - \lambda_p)$ measure is used to automatically shift the weighting between cost minimization and voltage stability security depending on the current system conditions p. This formulation tends to emphasize voltage stability when the system is closer to a collapse point, but there is no direct control on the relative weighting assigned to stability versus costs, so there is no way to guarantee that this will actually occur.

The second formulation uses a Linear Combination [35] approach to incorporate voltage stability criteria into a traditional OPF objective. This requires that all the objective functions be defined using some common unit; thus, since the original objective is to minimize the cost of the system, a "value" must be added to account for the level of stability of the system. At higher loading levels, more weight or value can be given to the stability portion, emphasizing the importance of stability. The disadvantage of this technique is in determining the "weights" of stability versus costs.

The motivation behind the third formulation, the Fixed Stability Margin formulation, is to introduce a fixed inequality constraint that prevents the stability margin of the system to be below a given value. The disadvantage of this approach is that at higher loading levels, the desired stability margin may be more than what the system can provide, yielding convergence problems.

In the fourth formulation, concepts from goal programming are used [35]. In traditional goal programming, a *goal* or *value* is assigned to each component in the objective function. The problem is then formulated to minimize the difference between the values of each of the components in the objective function and their goal or desired value. This technique works well for incorporating the voltage stability criteria, but does not incorporate minimization of cost appropriately. Therefore, the goal programming approach is only applied to the voltage stability component of the problem and the economic cost component is incorporated using a linear combination approach.

The final formulation incorporates a reactive power cost. Reactive power limits are often associated with voltage collapse and their inclusion into the OPF can be used to assign a value to reactive power support.

In the following sections, the above five formulations are discussed in greater detail.

4.2.1 Hybrid VSC-OPF Formulation

Since the maximum loading point of the system is a variable in the optimization problem, it is possible to accurately use a measure of the distance to collapse as an automatic way of shifting the weighting between cost minimization and the voltage collapse margin. The motivation behind this formulation is illustrated with the following example. Consider a problem with the objective function

$$\text{min: } \frac{\mathbb{K}(\cdot)}{\mathbb{L}(\cdot)} \tag{4.7}$$

where both $\mathbb{K}(\cdot)$ and $\mathbb{L}(\cdot)$ are strictly positive functions. The objective function can be minimized both by minimizing $\mathbb{K}(\cdot)$ or maximizing $\mathbb{L}(\cdot)$. Therefore, if $\mathbb{K}(\cdot)$ is replaced by generator operating costs and $\mathbb{L}(\cdot)$ is replaced by the stability margin, the solution to the problem would try to maximize the distance to collapse and minimize costs. The amount of emphasis placed on minimizing cost versus increasing the stability margin is automatic and problem dependent. Thus, the following formulation is proposed:

$$\min g(\mathbf{x}_p, \boldsymbol{\rho}, \lambda_p)\Phi \tag{4.8}$$

$$\begin{aligned}
\text{s.t. : } \quad \mathbf{F}(\mathbf{x}_p, \boldsymbol{\rho}, \lambda_p) &= 0 \\
\mathbf{F}(\mathbf{x}_*, \boldsymbol{\rho}_*, \lambda_*) &= 0 \\
\Phi(\lambda_* - \lambda_p) &= 1 \\
\underline{x}_p \leq \mathbf{x}_p \leq \overline{x}_p & \\
\underline{\boldsymbol{\rho}} \leq \boldsymbol{\rho} \leq \overline{\boldsymbol{\rho}} & \\
\underline{\boldsymbol{\rho}_*} \leq \boldsymbol{\rho}_* \leq \overline{\boldsymbol{\rho}_*} &
\end{aligned}$$

where $g(\cdot)$ represents a traditional OPF objective function. The scalar Φ is introduced to reduce some numerical problems as the function $\frac{g(\mathbf{x}_p,\boldsymbol{\rho},\lambda)}{\lambda_*-\lambda_p}$ tends to infinity as λ_p approaches λ_*. Nevertheless, if the current loading point λ_p is at the bifurcation point λ_*, the algorithm will fail since the inverse of $\lambda_* - \lambda_p$ is infinity. Although, it is unlikely that $\lambda_p = \lambda_*$,

some numerical problems may occur if they are "close". If the system is effectively at λ_*, then a strict maximum distance to voltage collapse algorithm should be utilized.

4.2.2 Linear Combination VSC-OPF Formulation

In this formulation, the distance to collapse is directly incorporated into the objective function, i.e.,

$$\min \omega_1 \, g(\mathbf{x}_p, \rho, \lambda_p) - \omega_2 \, (\lambda_* - \lambda_p) \tag{4.9}$$

$$\begin{aligned} \text{s.t. :} \quad & \omega_1 + \omega_2 = 1 \\ & \mathbf{F}(\mathbf{x}_p, \rho, \lambda_p) = 0 \\ & \mathbf{F}(\mathbf{x}_*, \rho_*, \lambda_*) = 0 \\ & \underline{\mathbf{H}_p} \leq \mathbf{H}(\mathbf{x}_p) \leq \overline{\mathbf{H}_p} \\ & \underline{\mathbf{H}_*} \leq \mathbf{H}(\mathbf{x}_*) \leq \overline{\mathbf{H}_*} \\ & \underline{\rho} \leq \rho \leq \overline{\rho} \end{aligned}$$

Observe that this requires the introduction of two weighting factors ω_1 and ω_2 to balance the emphasis placed on maximizing stability, i.e., $(\lambda_* - \lambda_p)$, versus minimizing costs, which are represented by $g(\mathbf{x}_p, \rho, \lambda_p)$ in (4.9). Generally, ω_2 must be significantly larger than ω_1, as the relative difference in the magnitudes of each term in the objective function is large, with $\omega_1 + \omega_2 = 1$ to normalize their values. Values obtained from previous OPF and Maximum Distance to Collapse analysis can be used to determine reasonable values of ω_1 and ω_2 at different loading conditions. A disadvantage of this formulation is that at higher loading levels, the stability margin $(\lambda_* - \lambda_p)$ decreases, resulting in less emphasis being placed on stability in the objective function. Furthermore, in the Linear Combination formulation, it is not possible to set a value for the voltage stability margin.

4.2.3 Fixed Stability Margin VSC-OPF

An alternative approach to assigning a cost to voltage stability is to include a voltage stability inequality constraint as follows:

$$\min\ g(\mathbf{x}_p, \boldsymbol{\rho}, \lambda_p) \tag{4.10}$$

$$\begin{aligned} \text{s.t. :} \quad & \lambda_* - \lambda_p \geq \Delta\lambda_{min} \\ & \mathbf{F}(\mathbf{x}_p, \boldsymbol{\rho}, \lambda_p) = 0 \\ & \mathbf{F}(\mathbf{x}_*, \boldsymbol{\rho}_*, \lambda_*) = 0 \\ & \underline{\mathbf{H}_p} \leq \mathbf{H}(\mathbf{x}_p) \leq \overline{\mathbf{H}_p} \\ & \underline{\mathbf{H}_*} \leq \mathbf{H}(\mathbf{x}_*) \leq \overline{\mathbf{H}_*} \\ & \underline{\boldsymbol{\rho}} \leq \boldsymbol{\rho} \leq \overline{\boldsymbol{\rho}} \end{aligned}$$

where $\Delta\lambda_{min}$ represents the minimum acceptable margin of stability for the system and is defined by the system operator. An advantage of the Fixed Stability Margin formulation versus the Linear Combination formulation is that choosing a value for $\Delta\lambda_{min}$ may be easier for the system operator than choosing appropriate weighting factors. This is because a minimum acceptable margin of stability has a more physical meaning.

A disadvantage of the Fixed Stability Margin formulation is that it may be possible to define a stability margin for which there is no solution to the optimization problem, as the stability margin may be greater than what the system can provide.

4.2.4 Goal Programming VSC-OPF Formulation

The limitations of the Linear Combination and Fixed Stability Margin formulations can be overcome using Goal Programming, where a desired "goal", $\Delta\lambda_g$, can be explicitly declared for the voltage stability margin. In this case, the formulation is defined as:

$$\min \boldsymbol{\omega}_1 \, \mathbf{g}(\mathbf{x}_p, \boldsymbol{\rho}, \lambda_p) + \boldsymbol{\omega}_2 \, \beta_1 + \boldsymbol{\omega}_3 \, \beta_2 \tag{4.11}$$

$$\begin{aligned}
\text{s.t. :} \quad & (\lambda_* - \lambda_p) - \Delta\lambda_g = \beta_1 - \beta_2 \\
& \mathbf{F}(\mathbf{x}_p, \boldsymbol{\rho}, \lambda_p) \quad = 0 \\
& \mathbf{F}(\mathbf{x}_*, \boldsymbol{\rho}_*, \lambda_*) \quad = 0 \\
& \underline{\mathbf{H}_p} \leq \mathbf{H}(\mathbf{x}_p) \leq \overline{\mathbf{H}_p} \\
& \underline{\mathbf{H}_*} \leq \mathbf{H}(\mathbf{x}_*) \leq \overline{\mathbf{H}_*} \\
& \underline{\boldsymbol{\rho}} \leq \boldsymbol{\rho} \leq \overline{\boldsymbol{\rho}} \\
& \underline{\boldsymbol{\rho}_*} \leq \boldsymbol{\rho}_* \leq \overline{\boldsymbol{\rho}_*} \\
& \beta_1, \, \beta_2 > 0
\end{aligned}$$

where the relative weights $\boldsymbol{\omega}_1$, $\boldsymbol{\omega}_2$ and $\boldsymbol{\omega}_3$ are used to vary the emphasis put on the desired stability margin, and the new variables $\beta_1, \beta_2 > 0$, which are minimized, depend on the stability margin. If β_1 and β_2 are equal to zero, then the stability margin equals the desired value $\Delta\lambda_g$.

In the above formulation, the stability margin $(\lambda_* - \lambda_p)$ can be less or greater than the desired margin $\Delta\lambda_g$, depending on the proximity of the system to collapse and the relative weights. A disadvantage of the Goal Programming formulation is determining appropriate values for the relative weights.

4.2.5 VSC-OPF with Reactive Power Pricing Formulation

The final formulation consists of modifying (4.11) to add reactive power pricing to the previous formulation based on a possible market environment (e.g., [63]). Here, it is assumed that generator companies are asked to operate at a given power factor, and if they deviate from it due to system conditions, additional costs must be paid by either the

company or the Market Operator; this is based on how some markets currently operate (e.g., Italy). Hence, goal programming is used to minimize the difference between the actual power factor of each generator and its desired power factor as follows:

$$\min \boldsymbol{\omega}_1\, g(\mathbf{x}_p, \boldsymbol{\rho}, \lambda_p) + \boldsymbol{\omega}_2\, \beta_1 + \boldsymbol{\omega}_3\, \beta_2 + \sum_{i=1}^{n_g} (\boldsymbol{\omega}_4 \beta_{3_i} + \boldsymbol{\omega}_5 \beta_{4_i}) \tag{4.12}$$

$$\begin{aligned}
\text{s.t. :} \quad & (\lambda_* - \lambda_p) - \Delta\lambda_g = \beta_1 - \beta_2 \\
& Q_{gen_i} - \tan(arccos(pf)) P_{g_i} = \beta_{3_i} - \beta_{4_i}\ \forall i = 1, \ldots, n_g \\
& \mathbf{F}(\mathbf{x}_p, \boldsymbol{\rho}, \lambda_p) \quad = 0 \\
& \mathbf{F}(\mathbf{x}_*, \boldsymbol{\rho}_*, \lambda_*) \quad = 0 \\
& \underline{\mathbf{H}_p} \leq \mathbf{H}(\mathbf{x}_p) \leq \overline{\mathbf{H}_p} \\
& \underline{\mathbf{H}_*} \leq \mathbf{H}(\mathbf{x}_*) \leq \overline{\mathbf{H}_*} \\
& \underline{\boldsymbol{\rho}} \leq \boldsymbol{\rho} \leq \overline{\boldsymbol{\rho}} \\
& \underline{\boldsymbol{\rho}_*} \leq \boldsymbol{\rho}_* \leq \overline{\boldsymbol{\rho}_*} \\
& \beta_1 > 0 \\
& \beta_2 > 0 \\
& \beta_{3_i} > 0 \qquad \forall i = 1, \ldots, n_g \\
& \beta_{4_i} > 0 \qquad \forall i = 1, \ldots, n_g
\end{aligned}$$

where the desired power factor is represented by pf; n_g represents the number of generators in the system; $\boldsymbol{\omega}_{1,2,3,4}$ are weights used for varying the relative emphasis on operating costs, stability margin and power factor (reactive power costs); and $\boldsymbol{\beta}_3$ and $\boldsymbol{\beta}_4$ are vectors used for measuring the difference between the actual and the desired power factors for each generator. The formulation is such that generators would try to operate close to the desired power factor; otherwise, a penalty cost is automatically assigned. A disadvantage of this formulation is determining appropriate values for the relative weights, especially for the reactive power support.

4.3 Numerical Analysis

The Maximum Distance to Collapse and Voltage Stability Constrained OPF (VSC-OPF) formulations presented in Section 4.2 are tested on two sample systems, the first based on the IEEE 57-bus system and the second based on the 118-bus test system [62, 64]. A number of simulations are performed to analyze how the current loading point and system limits influence the optimal solution. Based on the algorithm presented in Chapter 2, a nonlinear Predictor-Corrector Interior Point method written in MATLAB is used to perform the numerical analysis. Simulations are performed considering various operational limits at both the current operating point p and the collapse point $*$.

4.3.1 Modified Maximum Distance to Collapse Formulation

Including constraints on the current loading point p in the Maximum Distance to Collapse formulation resulted in different "optimum" solutions depending on the value of λ_p. The results of solving this optimization problem for the 57-bus and 118-bus system are depicted in Figures 4.3 and 4.4, respectively, where changes in λ_* versus λ_p are depicted. Observe that, as expected, the presence of operational limits reduces the maximum loading margin of the system ($*$ versus $\diamond$ in Figures 4.3 and 4.4), and that the generator limits dominate over voltage limits ($\diamond$ versus $\times$ in Figures 4.3 and 4.4). Figure 4.4 illustrates one of the principle disadvantages of considering both the current and critical loading point in one formulation (notice some points missing on the plots). For some loading points, no solution to the optimization problem could be found. This is attributed to the highly non-linear nature of the problem, especially when limits are considered at the critical loading point.

Enforcing operational limits at the collapse point $*$ results in a lower λ_*, as one would expect, since generator limits, particularly reactive power limits, are the main limiting factor ($\diamond$ versus $*$ in Figure 4.3); this is consistent with the type of results that one would typically obtain in voltage stability studies. At low values of λ_p, upper limits on

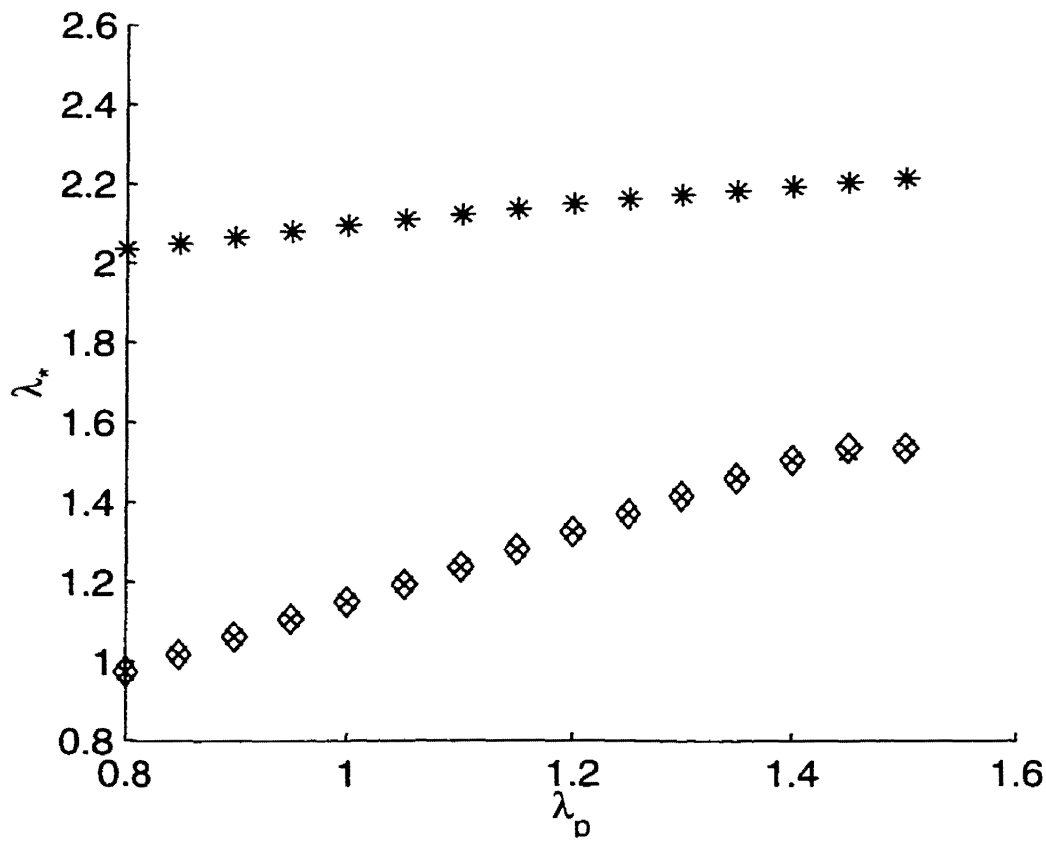


Figure 4.3: Maximum loading versus current operating point using the Maximum Distance to Collapse problem for the 57-bus test system. The symbols $*$, $\diamond$, and $\times$ correspond to solutions for the system with no limits, generator P and Q limits, and both bus voltage limits and generator P and Q limits, respectively, at the maximum loading point; operational limits are always enforced at the current operating point.

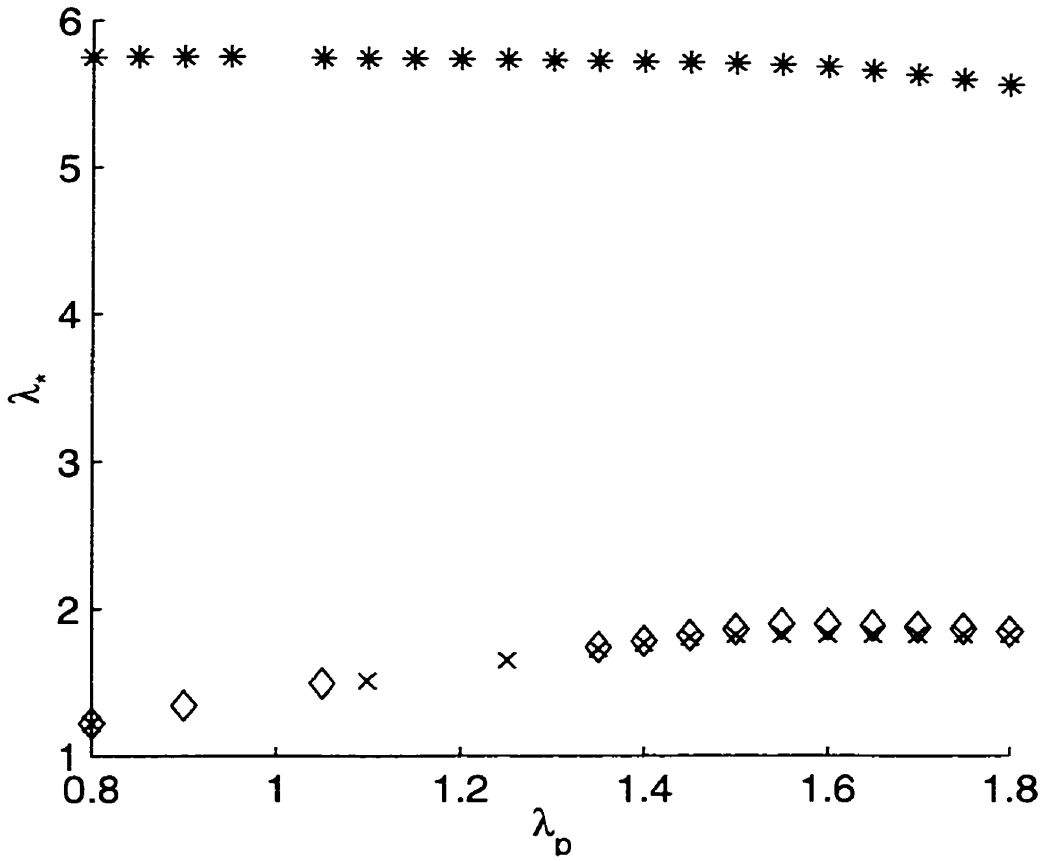


Figure 4.4: Maximum loading versus current operating point using the Maximum Distance to Collapse problem for the 118-bus test system. The symbols $*$, $\diamond$, and $\times$ correspond to solutions for the system with no limits, generator P and Q limits, and both bus voltage limits and generator P and Q limits, respectively, at the maximum loading point; operational limits are always enforced at the current operating point.

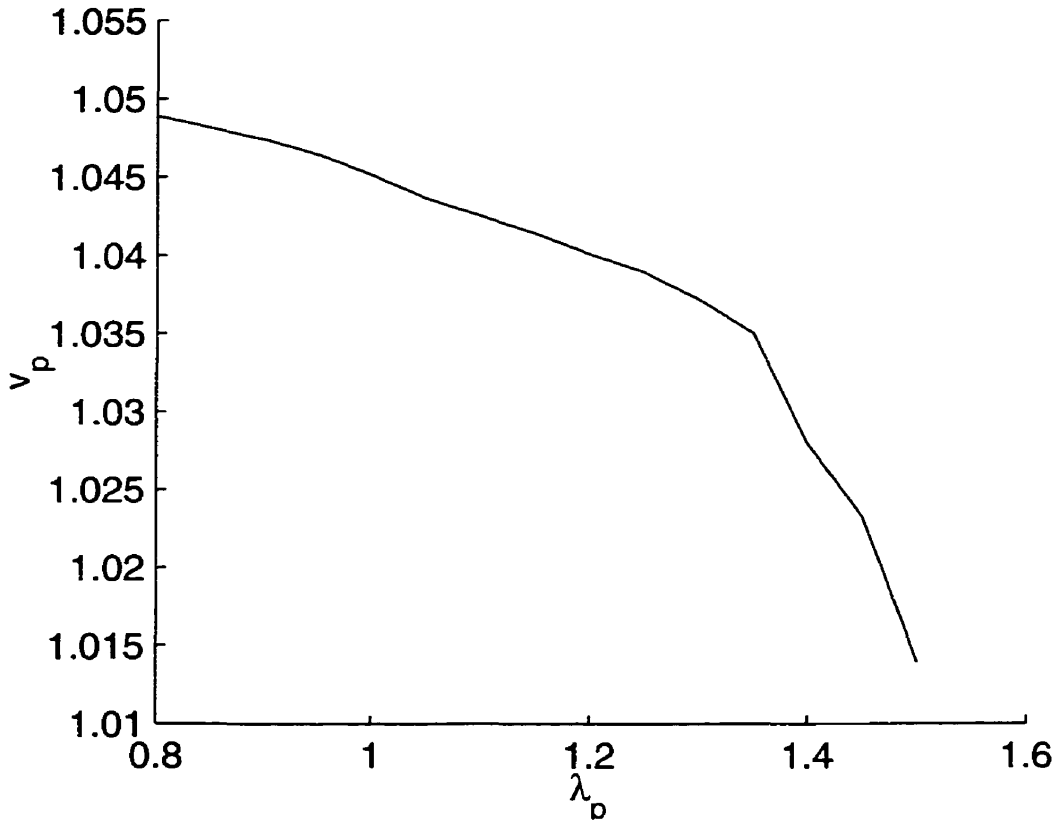


Figure 4.5: Change in voltage magnitude at Bus 30 versus λ_p for the 57-bus test system.

bus voltages become active, resulting in lower values of λ_*, with the opposite happening at higher values of λ_p. This phenomena is clearly illustrated on Figure 4.5, where the p.u. voltage magnitude at different loading levels is given for a non-generator bus (Bus 30) of the 57-bus system. At lower loading levels, the voltage tends to go to the upper limit, limiting the set points of generators nearby; at higher loading values, generator set points are raised, as upper voltage limits are not a problem.

If the reactive power limits on the generators become active the problem calculates maximum loading points that correspond to limit-induced bifurcations; the power flow Jacobian is not singular in this case, confirming the analysis presented in Section 4.1.2. For active and non-active reactive power limits, a comparison of generator reactive power levels is given in Table 4.1 (where $\lambda_p = 0.95$). In the case where no reactive power limits are enforced at the maximum loading point, the system collapses via a saddle-node

Table 4.1: Results of reactive power limits on various system variables for the 57-bus system (at λ_* for $\lambda_p = 0.95$)

Parameter	Without Reactive Power Limits (p.u.)	With Reactive Power Limits (p.u.)
Q_{gen_1}	1.2649	1.5975
Q_{gen_2}	0.8993	0.5000*
Q_{gen_3}	1.4826	0.6000*
Q_{gen_4}	0.4298	0.2500*
Q_{gen_5}	0.6528	2.0000*
Q_{gen_6}	1.5783	0.0900*
Q_{gen_7}	3.0348	−0.2828

* indicates the parameter is at its limit

bifurcation, on the other hand, when reactive power limits are enforced, several generators reach reactive power limits at the maximum loading point, and in this case, the maximum loading point corresponds to a limit-induced bifurcation.

4.3.2 Hybrid VSC-OPF Formulation

The Hybrid formulation was applied to both test systems. A plot of the generation costs versus the current loading point for the 57-bus system is shown in Figure 4.6. Furthermore, Figure 4.7 is a plot of the maximum loading point versus the current loading point for the 57-bus system. The solution for the Hybrid VSC-OPF problem when applied to the 57-bus system shows some similar characteristics as the Modified Maximum Distance to Collapse problem. Upper limits, on non-generator bus voltages, at the current loading point limit the maximum distance to collapse, but these limits are relaxed as the current loading point increases, allowing for an increased stability margin.

To get a better idea of how the added voltage security criteria affects the generation costs, and thus be able to give a "dollar value" to voltage security, the costs obtained

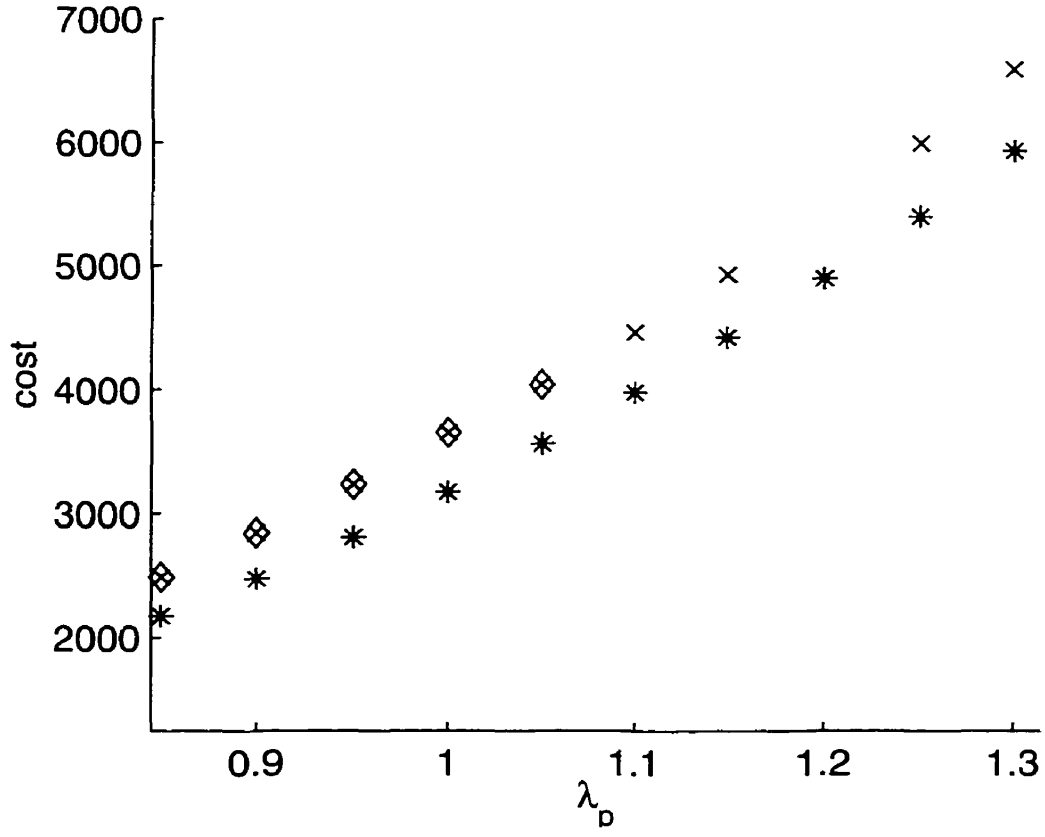


Figure 4.6: Generation costs versus current operating point applying the Hybrid VSC-OPF problem for the 57-bus test system. The symbols $*$, $\diamond$, and $\times$ correspond to solutions for the system with no limits, generator P and Q limits, and both bus voltage limits and generator P and Q limits, respectively, on the maximum loading point; operational limits are always active on the current operating point.

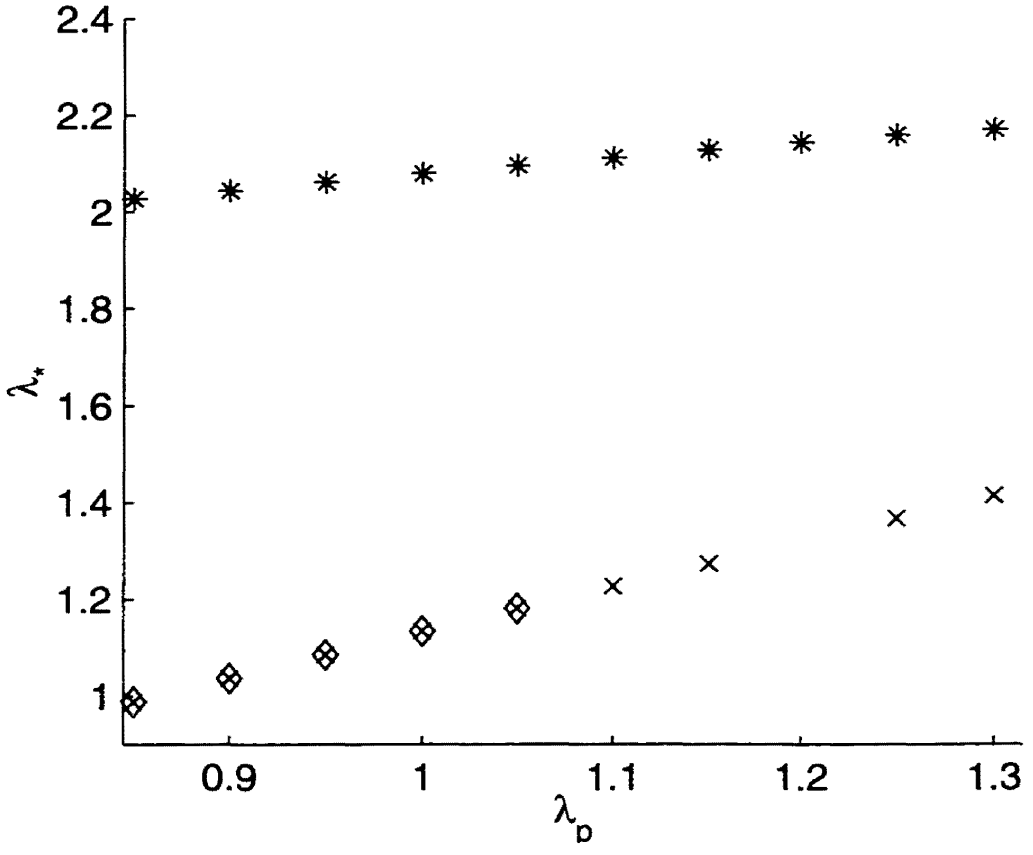


Figure 4.7: Maximum loading point versus current operating point applying the Hybrid VSC-OPF problem for the 57-bus test system. The symbols $*$, $\diamond$, and $\times$ correspond to solutions for the system with no limits, generator P and Q limits, and both bus voltage limits and generator P and Q limits, respectively, on the maximum loading point; operational limits are always active on the current operating point.

with the Hybrid VSC-OPF formulation are compared to those obtained by using the Maximum Distance to Collapse procedure and the standard OPF for the 57-bus system in Figure 4.8. The Maximum Distance to Collapse problem resulted in the highest costs at each loading level, followed by the OPF with Voltage Stability, with the traditional OPF giving the lowest operating costs, as one would expect. Observe that the proposed OPF with Voltage Stability tends to automatically shift the optimization importance from costs to maximum distance to collapse as the loading level increases. Hence, the "cost" of voltage security would be simply given by the difference between the minimum OPF costs and those produced by the proposed optimization technique. At higher loading levels, the difference between the three sets of solutions decreases as the feasible space of solutions is also decreased due to system and stability limits.

To better understand how the automatic shift on the proposed OPF with Voltage Stability technique affects the system security, a comparison of the values of λ_* at different loading levels for all optimization problems considered is plotted in Figure 4.9 for the 57-bus system. The Maximum Distance to Collapse formulation consistently calculated a larger λ_* for all cases. The "small" differences in λ_* are due to the fact that active power limits of generators basically define this value, as discussed in the previous section; furthermore, the corresponding "large" differences in costs indicate that this system is rather sensitive to its generation patterns. The maximum loading point for the solutions obtained using the traditional OPF formulation were calculated using the continuation method in the software package UWPFLOW [65].

One disadvantage of the Hybrid VSC-OPF problem, is that there is no direct way to control the amount of emphasis placed on stability versus cost minimization. The "lack" of direct control on the emphasis placed on stability enhancement versus cost minimization is illustrated by examining the maximum loading point versus the current loading point for the 57-bus system when applying the Modified Maximum Distance to Collapse problem and the Hybrid VSC-OPF problem shown in Figure 4.9. For most loading levels there is little difference in the maximum loading point for the two methods. But this difference

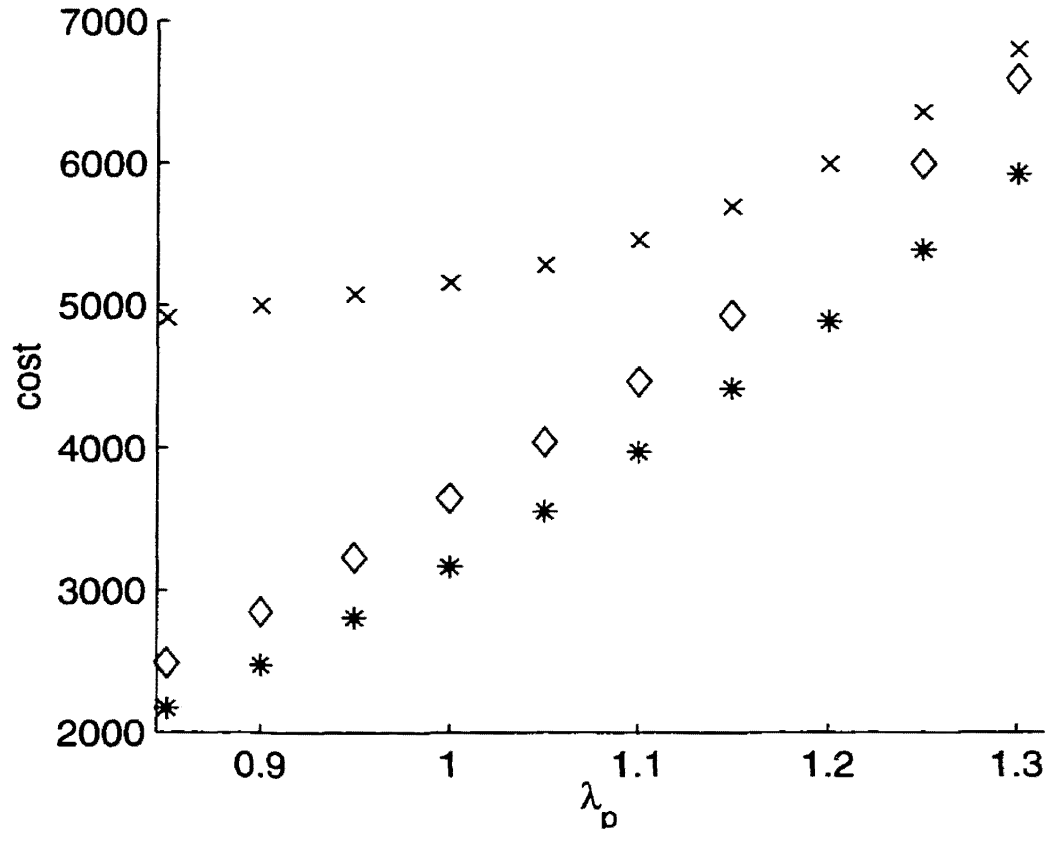


Figure 4.8: Generator cost versus current operating point for the 57-bus test system with operational limits on both the current and maximum loading point. The symbols $*$, $\diamond$, and $\times$ correspond to solutions for the system solved using the traditional OPF problem, Hybrid VSC-OPF problem and Modified Maximum Distance to Collapse problem, respectively.

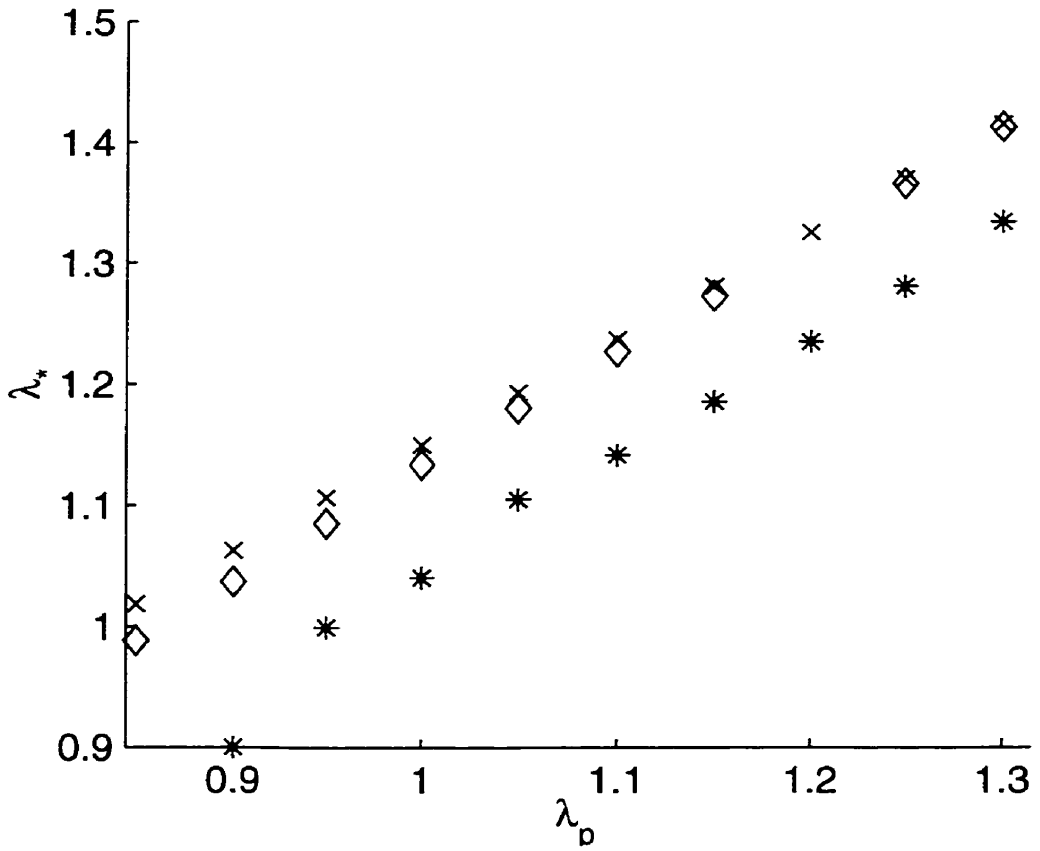


Figure 4.9: Maximum loading point versus current operating point for the 57-bus test system with operational limits on both the current and maximum loading point. The symbols $*$, $\diamond$, and $\times$ correspond to solutions for the system solved using the traditional OPF problem, Hybrid VSC-OPF problem and Modified Maximum Distance to Collapse problem, respectively.

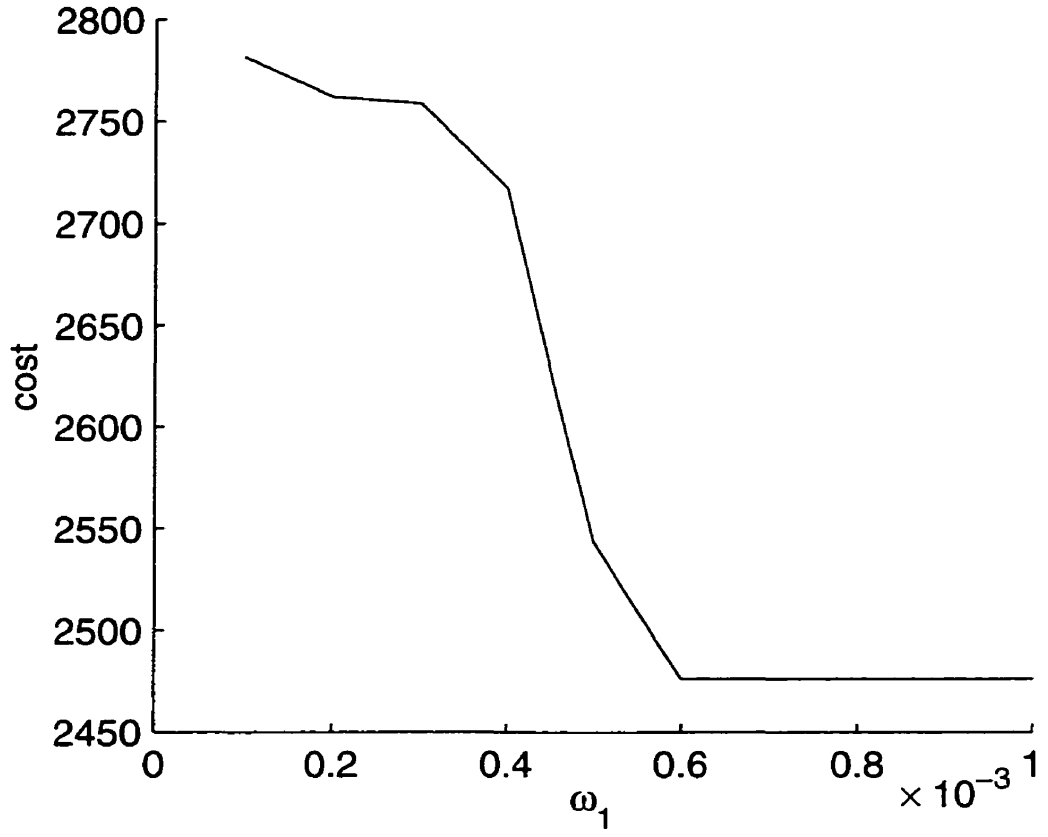


Figure 4.10: Operating costs versus weighting factor ω_1 for the Linear Combination formulation applied to the 57-bus test system for $\lambda_p = 0.9$.

does result in significant cost differences. If the system operator wanted a solution with more emphasis on cost minimization, the Hybrid VSC-OPF would not be the appropriate tool.

4.3.3 Linear Combinations VSC-OPF

The multi-objective Linear Combination formulation was applied to both test systems. The effect on cost and stability margin for different values of one of the weighting factors at a given value of λ_p for the 57-bus system are shown in Figures 4.10 and 4.11. As the factor ω_1 is increased, more emphasis is placed on operating costs and less on stability margin, as expected.

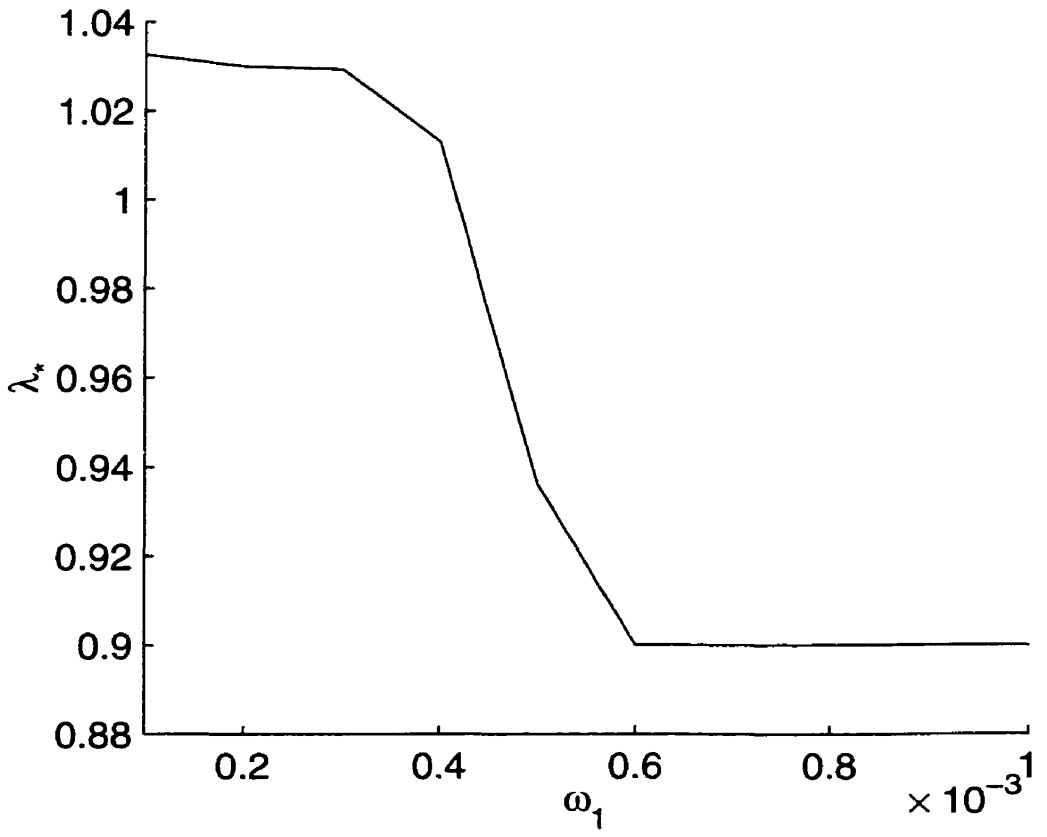


Figure 4.11: Maximum loading versus weighting factor ω_1 for the Linear Combination formulation applied to the 57-bus test system for $\lambda_p = 0.9$.

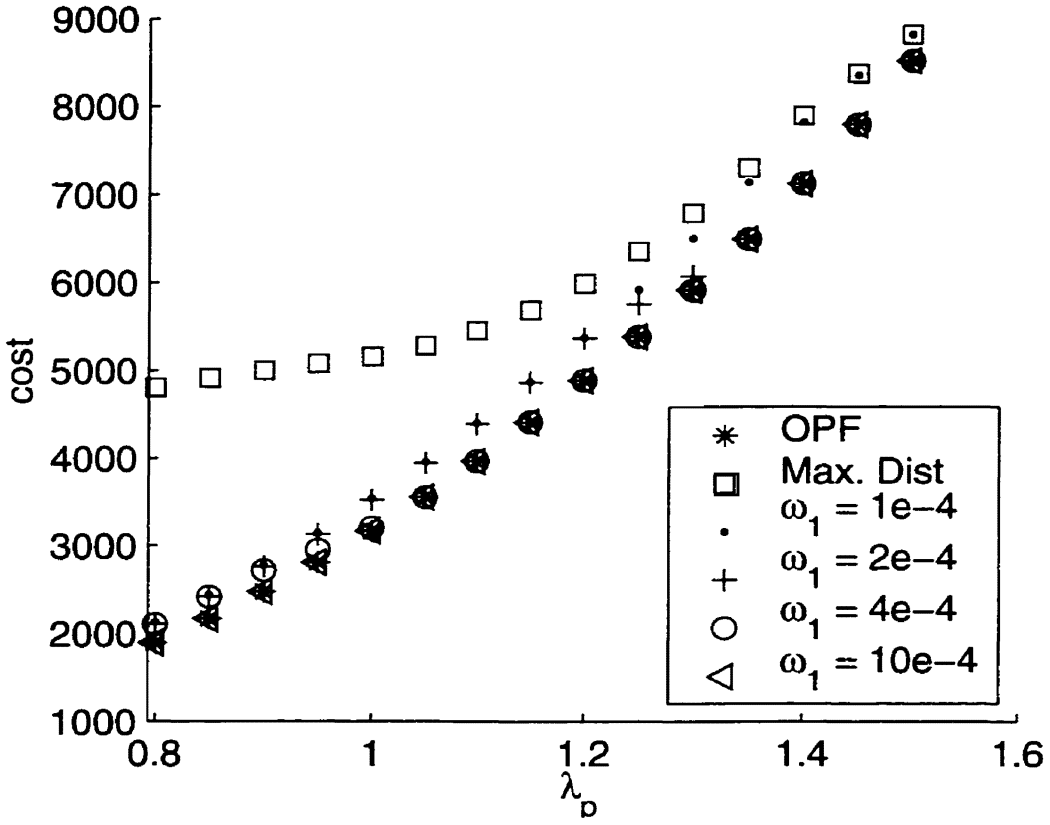


Figure 4.12: Operating costs versus current operating point for the Linear Combinations formulation, Maximum Distance to Collapse and traditional OPF for the 57-bus test system.

Figures 4.12 and 4.13 depict the results obtained from applying the Linear Combination formulation, the Maximum Distance to Collapse and the traditional OPF to the 57-bus system. As expected, the solutions obtained from the Linear Combinations formulation are *bounded* by the solutions obtained from the Maximum Distance to Collapse and normal OPF. At lower values of ω_1, the Linear Combination solutions tend to go to the Maximum Distance to Collapse solutions, whereas at higher values of ω_1 these solutions approach the OPF solutions. As illustrated in Figure 4.14, the 118-bus system exhibited similar characteristics as the 57-bus system.

The disadvantage of the Linear Combinations formulation is illustrated in Figure 4.13. Observe that there is a loading point, which varies with the values of the weighting factors, where the algorithm solution basically switches over from maximizing stability margins

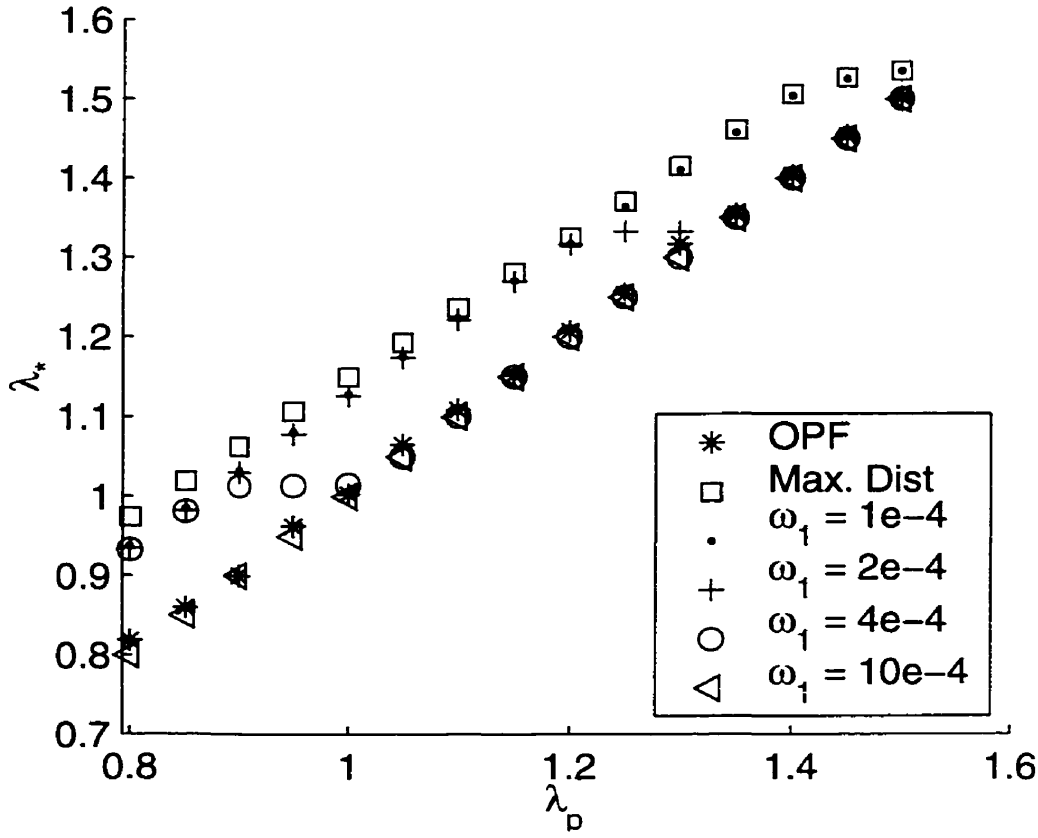


Figure 4.13: Maximum loading point versus current operating point for the Linear Combinations and Maximum Distance to Collapse formulations for the 57-bus test system.

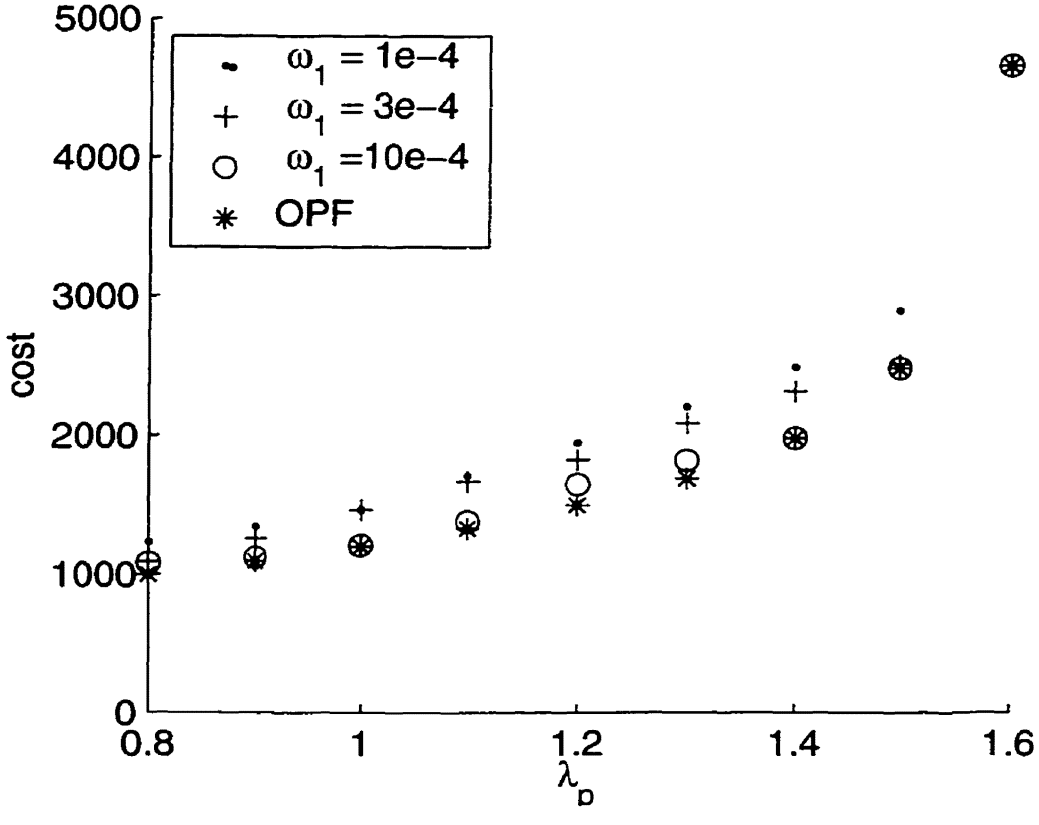


Figure 4.14: Operating costs versus current operating point for the Linear Combination and traditional OPF formulations for the 118-bus test system.

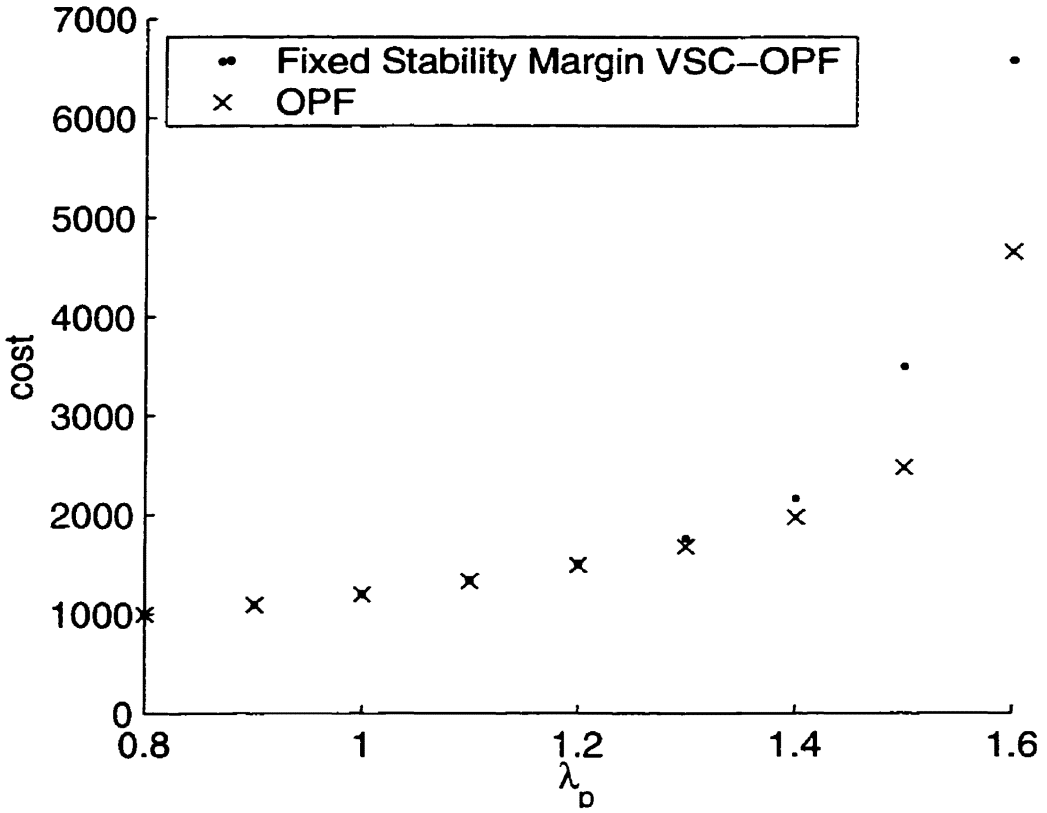


Figure 4.15: Cost versus current operating point for the Fixed Stability Margin and traditional OPF formulations for the 118-bus test system.

to minimizing costs. This is partly related to the difference between λ_* and λ_p becoming smaller at higher loading levels; therefore, the emphasis of this term in the objective function decreases.

4.3.4 Fixed Stability Margin VSC-OPF

The third set of numerical analysis involves applying the Fixed Stability Margin formulation to both test systems. Recall that this method is basically an OPF where a minimum stability margin is ensured.

For both test systems, a minimum stability margin $\Delta\lambda_{min} = 0.1$ p.u. is used. In general, the algorithm found a solution that ensured this constraint; however, this resulted

in higher operating costs. A comparison of the operating costs of the 118-bus system versus current loading point for the Fixed Stability Margin and traditional OPF formulations is shown in Figure 4.15. Observe that the difference in the total operating costs increases as the loading increases, due to the fact that a minimum stability margin is being enforced, which becomes a dominant constraint as the system gets closer to collapse.

4.3.5 Goal Programming VSC-OPF

The next set of numerical analysis involves applying the Goal Programming formulation to both test systems. Recall that the idea is to define a stability margin that is not a binding constraint, but that if violated, increases the objective function cost. As illustrated in Figure 4.16, the Goal Programming formulation shifted the importance of cost as ω_1 increased. As the loading level is increased, the cost of maintaining the desired minimum stability margin increases, and, eventually, for constant values of all weighting factors ω the minimum stability margin is reduced to zero. When less weight is placed on cost and greater weight is placed on stability, i.e., for smaller values of ω_1, the minimum stability margin is maintained, as shown in Figure 4.17. It is found in the numerical analysis that ω_2 does not greatly effect the solution of the problem, which is to be expected, since there is no benefit in having a stability margin greater than the desired value (this tends to also result in greater operating costs).

Similar results were obtained for the 118-bus system.

4.3.6 VSC-OPF with Reactive Power Pricing

The final set of numerical analysis involves applying the Goal Programming formulation, which is probably the best compromise for a VSC-OPF, considering reactive power costs to both test systems. In this case, the idea is to add a penalty to the objective function if generators are not operated at the desired power factor. Figures 4.18 and 4.19 depict the results obtained for operating cost and maximum loading point, and are somewhat

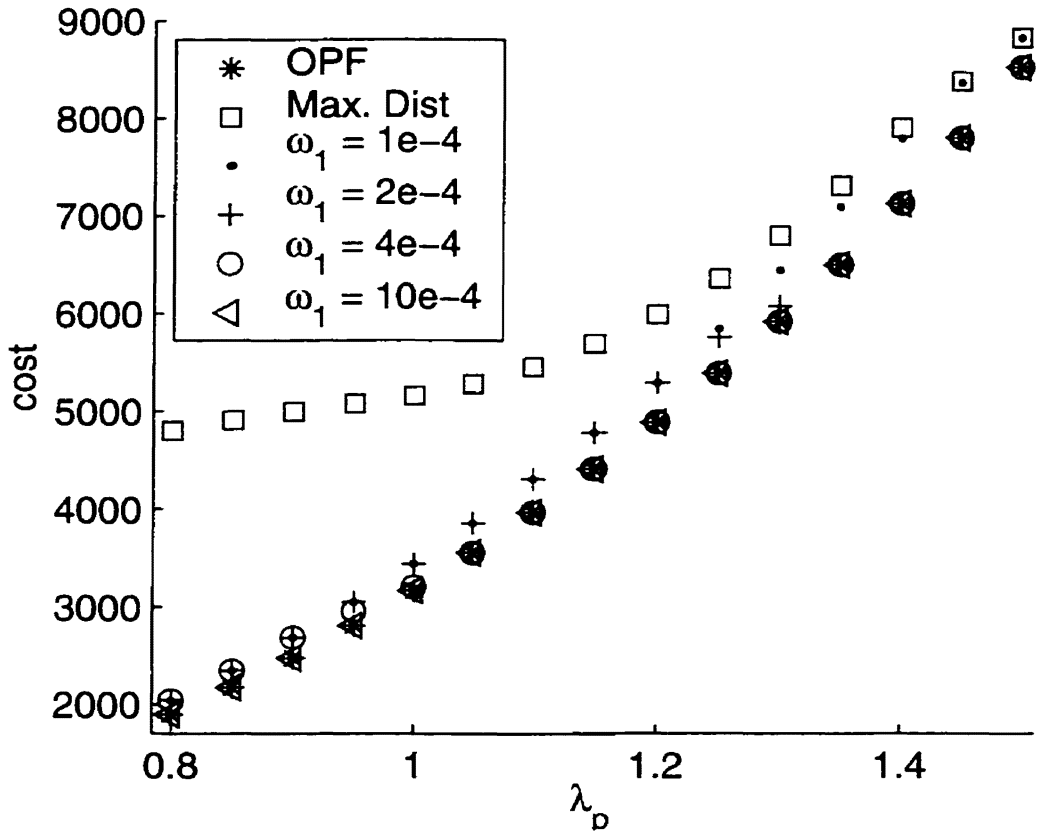


Figure 4.16: Cost versus current operating point for the Goal Programming ($\omega_2 = 0.001$, $\omega_3 = 1 - \omega_1$) and traditional OPF formulations for the 57-bus test system.

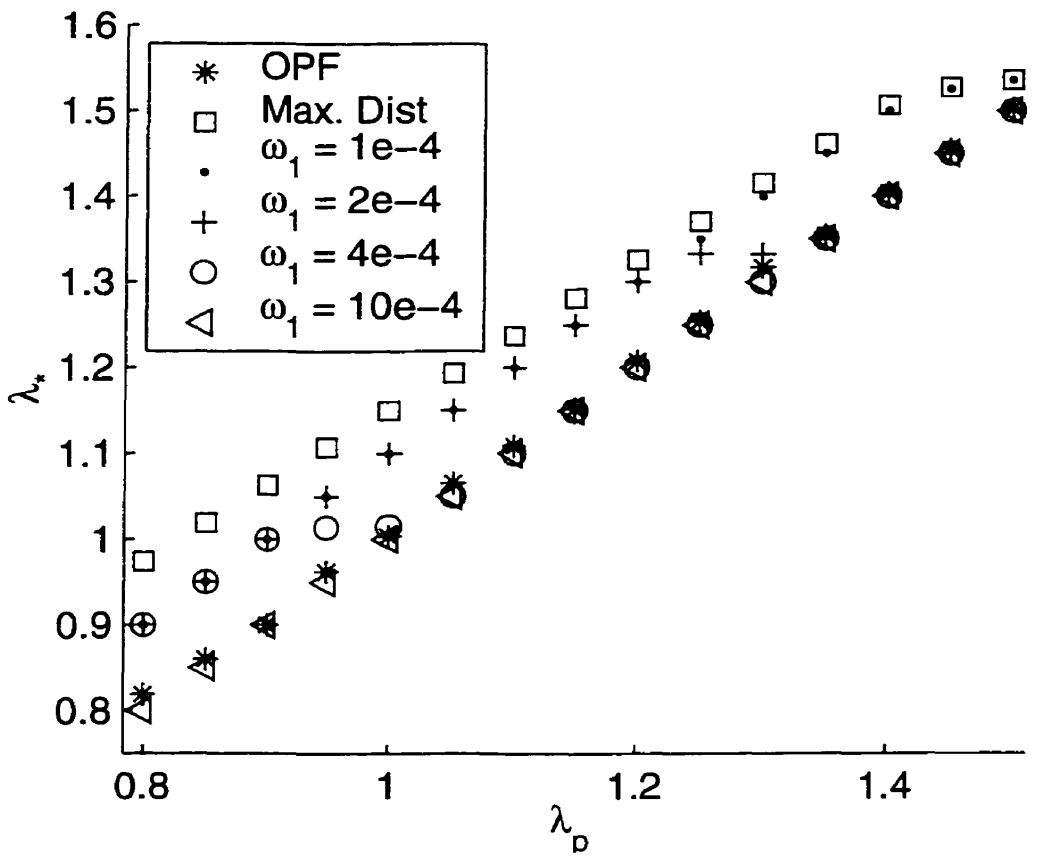


Figure 4.17: Maximum loading point versus current operating point for the Goal Programming ($\omega_2 = 0.001$, $\omega_3 = 1 - \omega_1$), traditional OPF and Maximum Distance to Collapse formulations for the 57-bus test system.

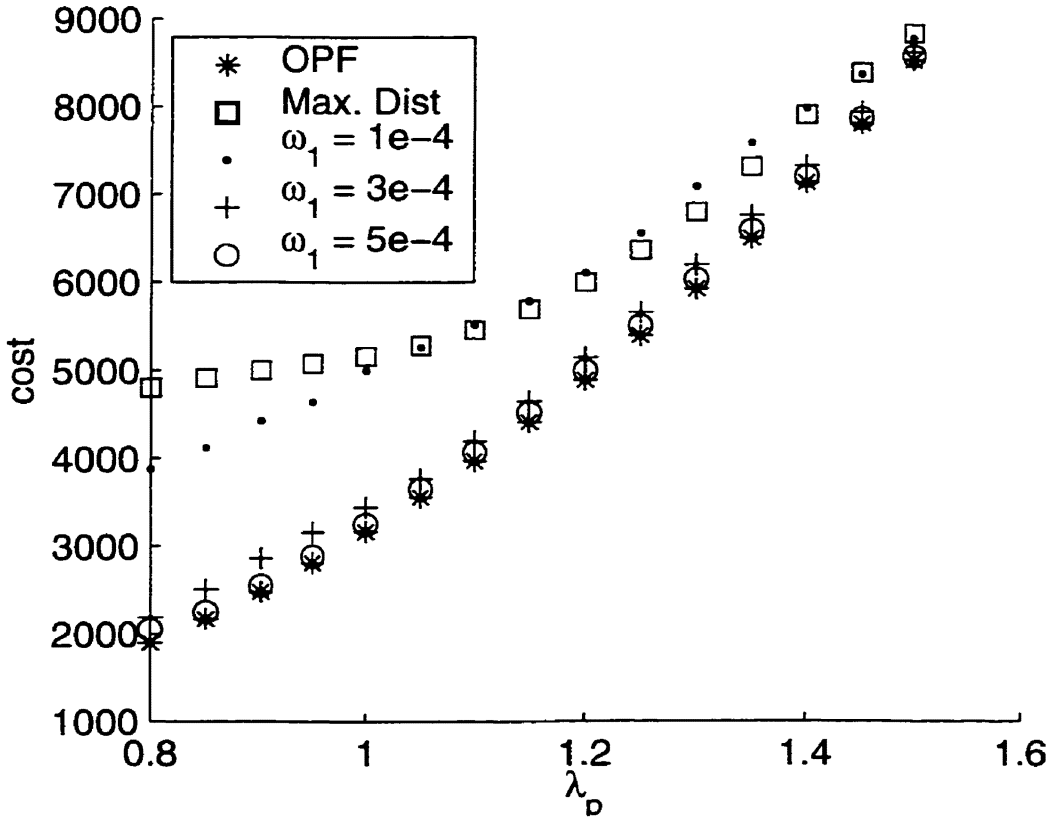


Figure 4.18: Cost versus current operating point for the Goal Programming formulation considering reactive power costs ($\omega_2 = 0.001$, $\omega_3 = 1 - \omega_1$, $\omega_4 = \omega_5 = 0.3$) and traditional OPF formulation for the 57-bus test system.

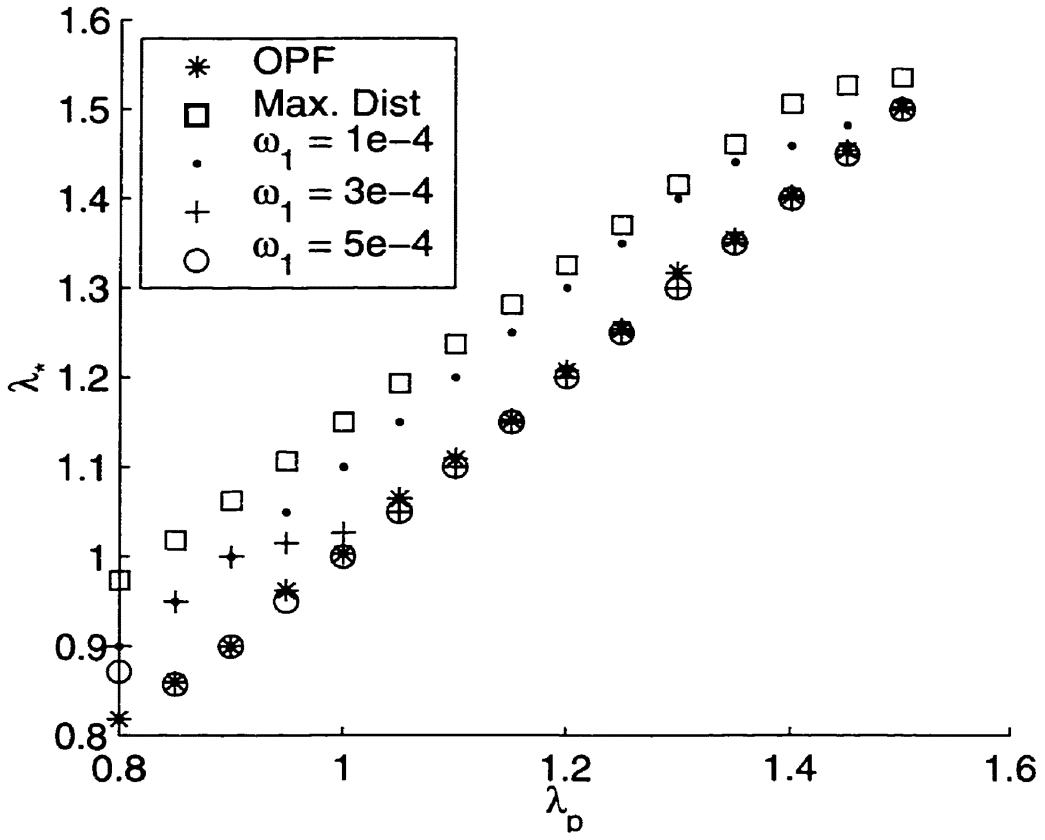


Figure 4.19: Maximum loading point versus current operating point for Goal Programming formulation considering reactive power costs ($\omega_2 = 0.001$, $\omega_3 = 1 - \omega_1$, $\omega_4 = \omega_5 = 0.3$), traditional OPF and Maximum Distance to Collapse formulations for the 57-bus test system.

similar to the results obtained when applying the Goal Programming formulation without including reactive power costs. Thus, costs increase with loading and larger weighting on the stability margin, and as the system is loaded, the formulation puts more emphasis on cost minimization than on maintaining a given stability margin, as enforcing this margin becomes more expensive. However, observe that when the reactive power costs become dominant with respect to the other two terms in the objective function, i.e., for smaller values of ω_1, it leads to higher operating costs.

4.4 Cost of Voltage Stability

From the results presented in the previous section, a dollar value can be assigned to the cost of incorporating voltage stability. For example, Figure 4.20 shows the change in operating cost for the 57-bus system when solving the Modified Maximum Distance to Collapse formulation versus the tradition OPF problem when enforcing full operating limits at the maximum loading point.

In this case, the cost of considering only stability is highest at lower loading levels, since the "space" of feasible solutions is larger in this case, allowing for the greatest difference between the two solutions. Figure 4.21 illustrates the percentage difference in operating costs and stability margin, for the same two formulations. From Figure 4.21, it can be seen that the large percentage increase in cost at lower loading points versus higher loading levels does not correspond to a significantly larger increase in stability margin. This is attributed to the sensitivity of the cost to changes in the active power settings of the generators.

A more appropriate approach to incorporating voltage stability would be to use one of the proposed VSC-OPF formulations. Figures 4.22 and 4.23 show the change in operating cost and percent change in operating cost when using the Fixed Stability Margin VSC-OPF formulation versus the traditional OPF. In this case, a fixed stability margin of 0.1 p.u. was used. As shown in the figures, the "cost" of incorporating this stability

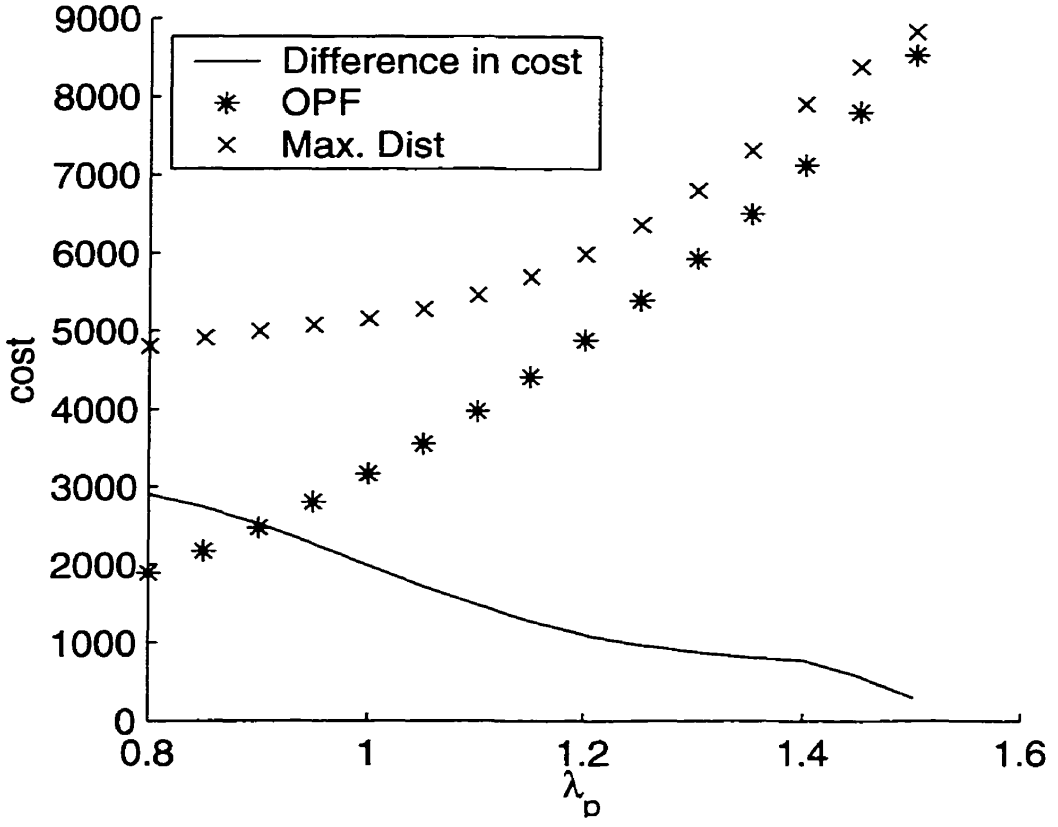


Figure 4.20: Difference in operating cost (solid line) when applying the Maximum Distance to Collapse formulation (×) versus a traditional OPF (∗) formulation for the 57-bus system.

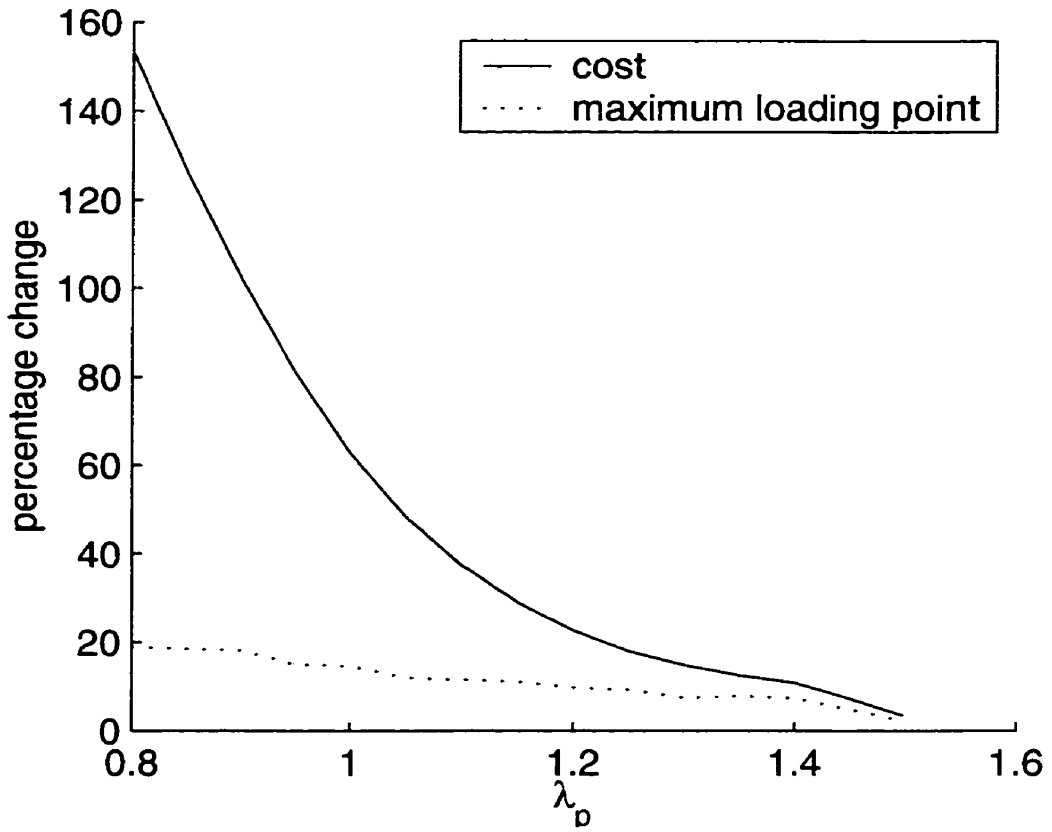


Figure 4.21: Percent change in operating costs (solid line) and stability margin (dashed line) when applying the Maximum Distance to Collapse formulation versus a traditional OPF formulation for the 57-bus system.

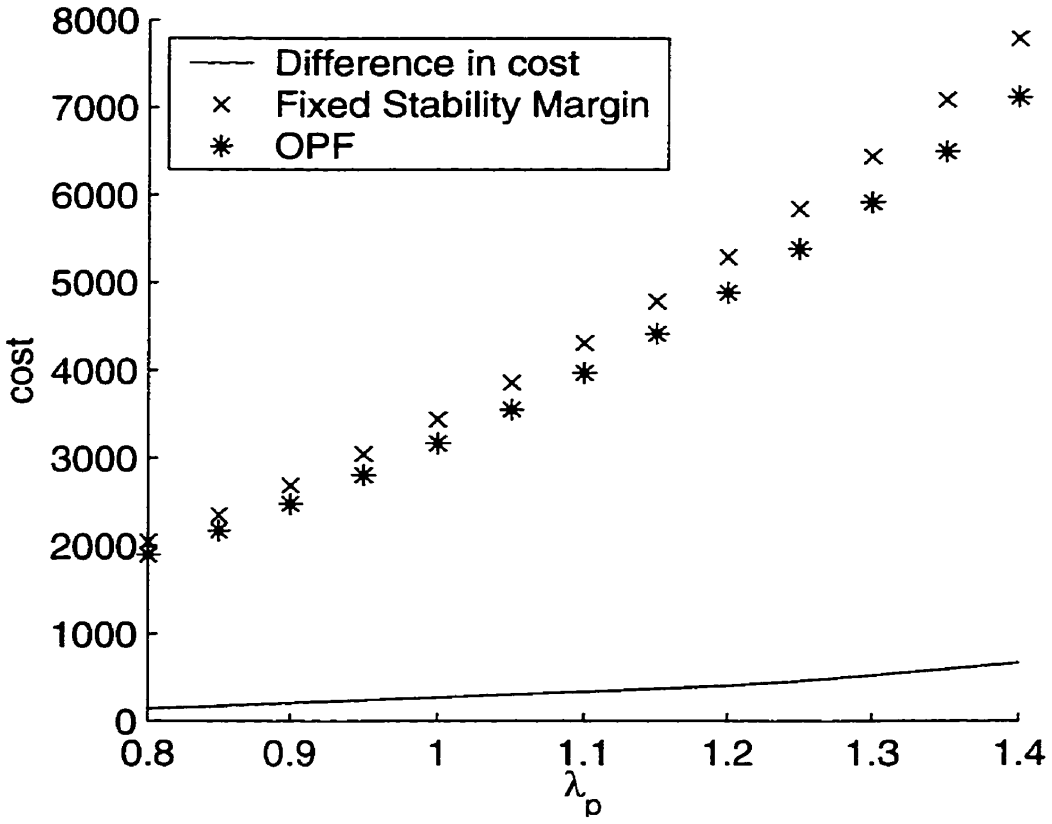


Figure 4.22: Difference in operating cost (solid line) when applying the Fixed Stability Margin VSC-OPF formulation (×) versus a traditional OPF (∗) formulation for the 57-bus system.

margin, is significantly less than the case where no economic cost was incorporated into the formulation.

4.5 Numerical Implementation

Several disadvantages were encountered with the implementation used in performing the numerical analysis presented in the previous section. The use of MAPLE to symbolically form the vectors and matrices required for the optimization method proved to be relatively slow. The execution of the "data files" was also slow because of the size of the matrices to be formed. But the implementation allowed for a flexible analysis of different models

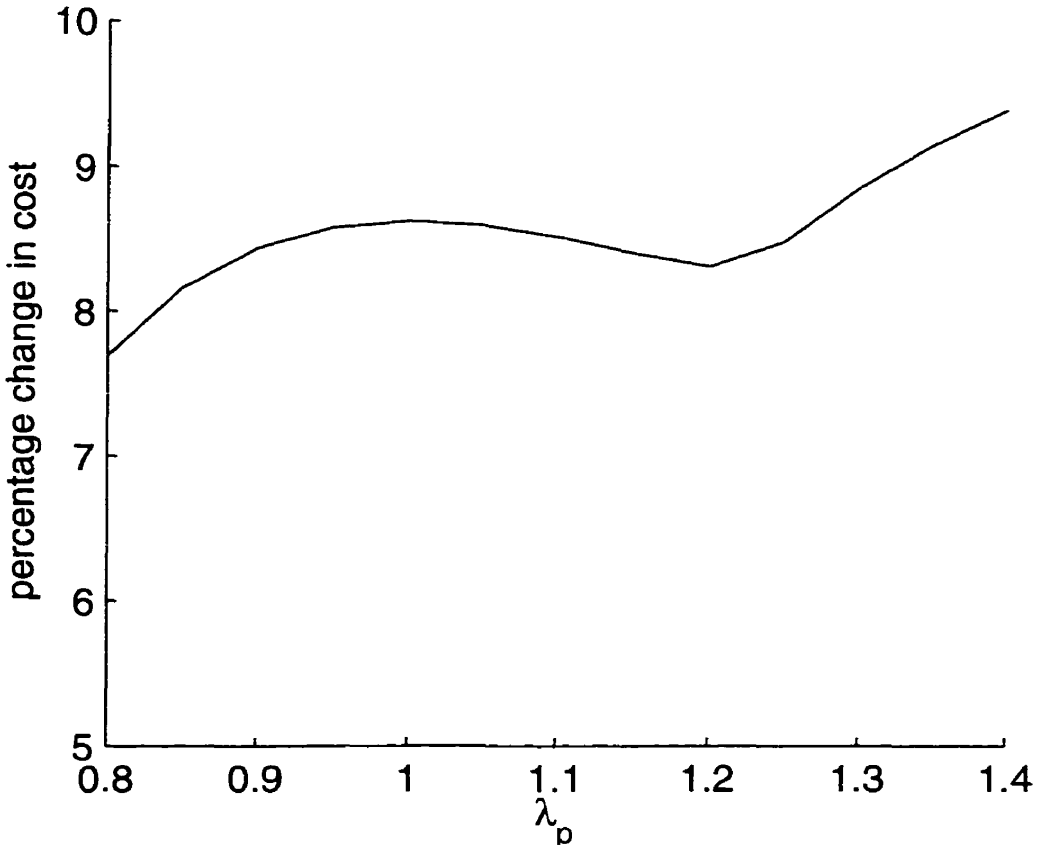


Figure 4.23: Percent change in operating costs when applying the Fixed Stability Margin VSC-OPF formulation versus a traditional OPF formulation for the 57-bus system.

and formulations. In order to improve the running time, the problems could be solved directly using sparse matrix methods with no symbolic calculations.

A second numerical problem encountered was the stability of the IP method. Because of the highly nonlinear coupling between the current point and maximum point, some convergence problems occurred, which were reflected in missing points in some of the figures presented in the chapter. Dynamically varying some of the parameters in the interior point method may leading to improvements in the convergence.

4.6 Summary of Results

This chapter demonstrates that voltage stability and OPF studies can be performed concurrently, proposing and comparing a variety of methodologies to allow operators to carry out this task in an electricity market environment. It is shown that incorporating voltage stability into a traditional OPF problem can result in higher operating costs, and hence the proposed OPF formulations can be used for "pricing" voltage security. The results show the importance of including the current loading point in optimization procedures used for voltage stability analysis, as limits on this point significantly influence these types of studies. Finally, the chapter proposes a feasible way to include reactive power costs in an OPF formulation, which could be a very useful tool in the operation of electricity markets.

As the proposed OPF formulations include stability constraints, a possible enhancement to these techniques would be to improve the steady state system models used, so that accuracy can be improved at higher loading conditions. Furthermore, since the proposed tools may have a direct application in the operation of electricity markets, other representations of active and reactive power "costs" could be analyzed.

CHAPTER 5

Power System Modeling

5.1 Introduction

As open access market principles are applied to power systems, an increased emphasis on using accurate OPF algorithms arises. Power systems will have to be operated under higher loading conditions as market influences demand greater attention to operating cost versus stability margin. It is shown in [21, 22, 66] that traditional power flow models may fail to accurately represent power systems in voltage stability studies. Hence, this chapter examines the effects of detailed generator models, exponential load models and Static-Var Compensators (SVC) in Voltage Stability Constrained Optimal Power Flow (VSC-OPF) problems. The various VSC-OPF problems considered are based on the problems presented in Chapter 4.

This chapter is structured as follows: In Sections 5.2, 5.3 and 5.4 the detailed generator, exponential load and SVC models are given. Numerical results of applying an Interior Point method to the several VSC-OPF problems are given in Section 5.5. The problems are the applied to the 57-bus, and 118-bus systems. Finally, Section 5.6 summarizes the main results presented in this chapter.

5.2 Generator Model

As loading levels in power systems increase, the effect of generator modeling in the results obtained in systems analysis increases. Simplified models seldom incorporate nonlinear

characteristics and device limits properly. The usual treatment of generators using constant power and fixed voltage (PV) buses with reactive power limits may lead to unreliable results in voltage stability analysis. Since limits on the armature current and field voltage accurately reflect the true limits of generators, their inclusion in the standard power flow equations will enhance the system model used in voltage stability studies.

The model of the synchronous generator used in this section is based on the detailed model presented in [67, 68]. It is assumed that the field current is proportional to the magnitude of the induced voltage and that saturation can be neglected. The following equations are used to describe the *dq-axis* generator model written in a reference frame using the rotor's angular velocity [67].

$$\begin{aligned} E_f - V_q &= R_a I_q - X_d I_d \\ -V_d &= R_a I_d + X_q I_q \\ V_{gen} &= \sqrt{V_d^2 + V_q^2} \\ I_a &= \sqrt{I_d^2 + I_q^2} \\ P_{gen} &= V_q I_q + V_d I_d \\ Q_{gen} &= V_q I_d - V_d I_q \end{aligned} \tag{5.1}$$

where E_f is the field voltage, I_d and I_q are the direct and quadrature components of the armature current I_a, V_d and V_q are the direct and quadrature components of the terminal voltage V_{gen} and R_a, X_d and X_q are the armature resistance and direct and quadrature synchronous reactances, respectively. The real and imaginary power injected into the transmission system by the generator is given by P_{gen} and Q_{gen} respectively.

5.2.1 Generator Limits

In this section, the relationship between traditional PV generator models and the proposed model for optimal power flow studies is considered. This is best done by examining the

limits of generators and how these limits affect the two models.

There are several basic limits of a synchronous generator that are expressed as ratings of the machine. Typical ratings include voltage magnitude, field current, apparent power, power factor, frequency, and speed. The frequency and speed ratings are not discussed here, since the models considered are steady state phasor models and assume that the machine is operating at synchronous frequency and speed. The relationship between the other ratings is briefly reviewed below to demonstrate the relationship between the proposed and traditional models and how limits for these models are selected. A more detailed explanation of the characteristics and ratings of generators can be found in several text books (e.g., [25, 69, 70]).

The terminal voltage rating of a machine is dependent on the system to which it is connected, and its winding insulation. Typically, the terminal voltage magnitude is set between 0.9 p.u. and 1.1 p.u.

The two main windings in the machine, the armature and field windings must be protected from overheating. The heating of the armature winding, which is mainly due to copper losses, is given in p.u. by $P_{heating} = |I_a|^2 R_a$, where R_a is the armature winding resistance. Therefore, the protection of the armature winding results in a limit on the armature current magnitude $|I_a|$. If the terminal voltage is considered constant, the armature current effectively sets the apparent power rating of the generator, i.e., $\tilde{S} = \tilde{V}_t \tilde{I}_a^*$ in p.u.

In the same manner, the maximum allowable heating of the field winding sets the maximum field current. Since the field voltage E_f is directly proportional to the field current, the field winding limit can be expressed as a limit on E_f.

Synchronous generator capability curves [25, 26, 69] can be used to graphically illustrate the limits and their relationship. These curves depict the reactive power versus the real power of the generator, assuming an unsaturated, round-rotor machine characterized by $X_d = X_q = X$. Figure 5.1 illustrates a capability curve, including various limits. A

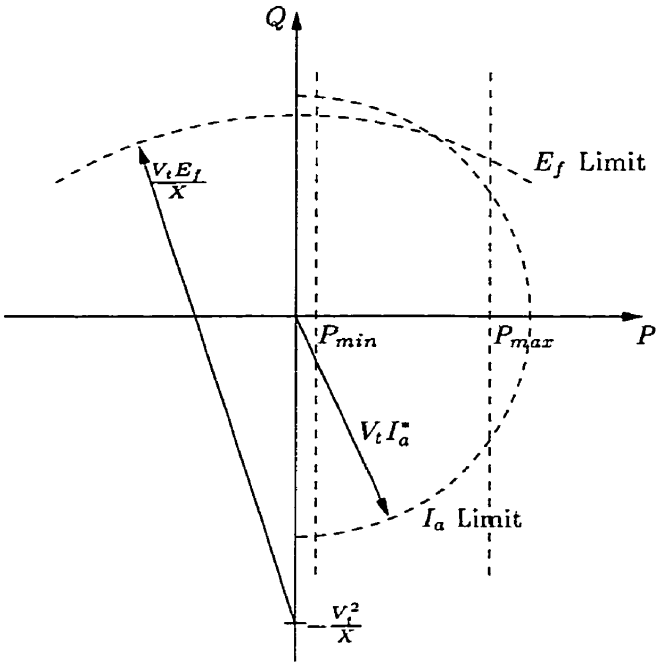


Figure 5.1: Capability curve for synchronous generator.

detailed discussion of the formulation of capability curves can be found in [25, 26].

The maximum and the minimum armature current and field voltage are defined according to

$$\begin{bmatrix} |I_{a\,max}| \\ |I_{a\,min}| \\ |E_{f\,max}| \\ |E_{f\,min}| \end{bmatrix} = \begin{bmatrix} \frac{1}{V_t}\sqrt{Q_{max}^2 + P_{max}^2} \\ 0.0 \\ \frac{1}{V_t}\sqrt{(Q_{max} + \frac{V_{t\,max}^2}{X_d})^2 + P_{max}^2} \\ 0.0 \end{bmatrix} \tag{5.2}$$

where the above limits are based on the modified capability curve shown in Figure 5.2. The terminal voltage V_t was set to the minimum voltage limit, for the generator bus, to insure that when the detailed model was used, both the maximum active and reactive power limit could be reached for all acceptable voltage settings. Since there is no one-to-one mapping between the limits for the proposed model and the traditional model for all loading levels, this approximation is adequate to demonstrate the differences in the two models.

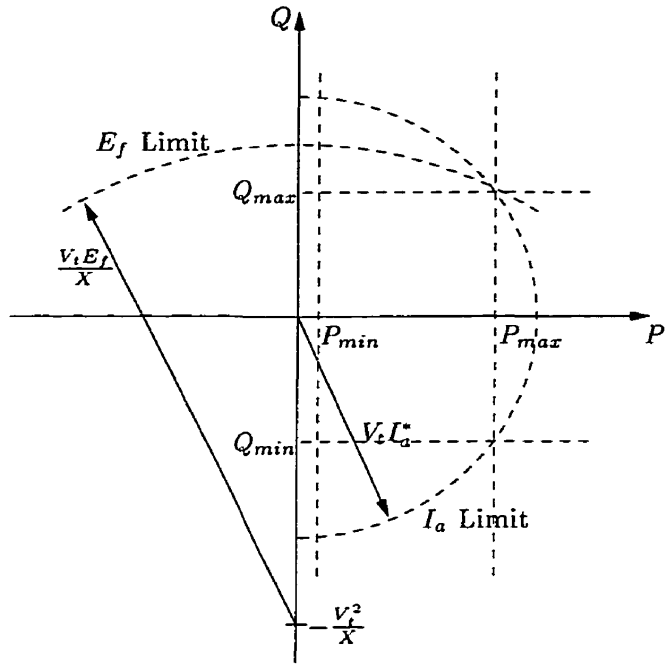


Figure 5.2: Implemented capability curve for synchronous generator.

5.3 Load Models

Because of the use of "aggregating" methods to determine load models, standard PQ (constant real and reactive power) models may not accurately reflect the characteristic of the system in all cases. In this section, different static load models that express the active and reactive powers of loads as a function of the voltage magnitude at the load bus are considered.

Several voltage dependent load models have been analyzed in voltage stability studies (e.g., [21, 26]). In this section, the exponential load model is presented for use in an OPF formulation. The exponential load model represents the power demand of the load to its terminal voltage using exponential equations, generally expressed as:

$$\begin{aligned} P_{load} &= P_0\left(\frac{V}{V_0}\right)^{\varrho_1} \\ Q_{load} &= Q_0\left(\frac{V}{V_0}\right)^{\varrho_2} \end{aligned} \tag{5.3}$$

where P_0 , Q_0 are the reference real and reactive powers consumed at a reference voltage V_0. The exponents ϱ_1 and ϱ_2 depend on the type of load that is being represented. The following standard static load representations are derived directly from equation (5.3) with the proper choices of ϱ_1 and ϱ_2.

- Constant impedance load model: The power varies directly with the square of the voltage magnitude ($\varrho_1 = \varrho_2 = 2$).
- Constant current load model: The power varies directly with the voltage magnitude ($\varrho_1 = \varrho_2 = 1$).
- Constant power load model: The power does not vary with changes in the voltage magnitude ($\varrho_1 = \varrho_2 = 0$).

5.4 Static Var Compensator (SVC)

Since the early eighties, advances in Flexible AC Transmission Systems (FACTS) controllers in power systems have led to their application in improving stability of power networks [23]. Several studies analyzing the application of FACTS controllers for voltage and angle stability have been reported in the literature (e.g., [24, 71]).

The effect of the Static Var Compensator (SVC) FACTS controller on the economic operation and voltage stability of the network is the principle motivation behind incorporating the SVC into the proposed OPF formulations. The fast response of SVCs make them ideal for not just voltage stability improvements but also for cost reduction. The steady state model proposed in [24] is used for incorporating the SVC into the various VSC-OPF problems, and is briefly reviewed here.

The basic steady state model of the SVC presented in this section is based on representing the controller as a variable impedance [24]. The Fixed Capacitor (FC) with a Thyristor Controlled Reactor (TCR) configuration of the SVC is used in this analysis.

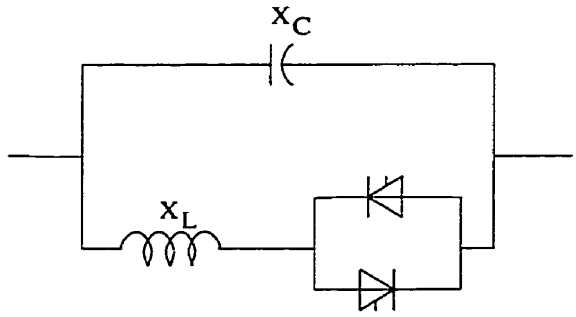


Figure 5.3: Common structure for SVC.

The structure of this configuration is illustrated in Figure 5.3. The controller is composed of a fixed capacitor, fixed reactor and a bi-directional thyristor valve, composed of two thyristors.

If it is assumed that the SVC bus voltage is sinusoidal, a Fourier analysis on the inductor current waveform can be used to demonstrate that the fixed reactor and bi-directional valve can be modeled as an equivalent variable inductance X_v [24]. The value of this impedance is a function of the thyristor firing angle of the TCR and is then given as

$$X_v = X_L \frac{\pi}{2(\pi - \alpha) + \sin 2\alpha} \tag{5.4}$$

where X_L is the fundamental frequency reactance of the inductor without thyristor control and α is the firing angle of the valves with respect to the positive zero crossing of the controller voltage. The total equivalent impedance of the controller X_e is given as

$$X_e = \frac{\pi X_L}{\sin 2\alpha - 2\alpha + \pi(2 - \frac{X_L}{X_C})} \tag{5.5}$$

where X_C is the impedance of the fixed capacitor. Equation (5.5) is found by taking the parallel combination of X_v and X_C. The model incorporated in this section is written in terms of the equivalent susceptance, $B_e = -1/X_e$, rather than the corresponding reactance equations, based on numerical performance as discussed in [24, 71].

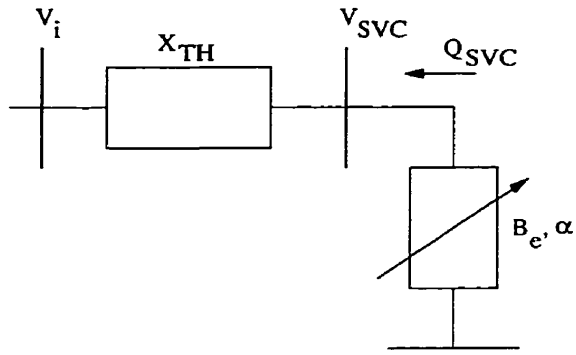


Figure 5.4: SVC steady state circuit representation.

The SVC is usually connected to the transmission system through a step-down transformer, which can be treated as other transformers in the system. A steady state circuit representation of the connection of the SVC through a step-down transformer is illustrated in Figure 5.4, where V_i is the magnitude of the voltage at the bus which the SVC controls, V_{SVC} is the voltage across the controller, X_{TH} is the impedance of the step-down transformer, and Q_{SVC} is the reactive power that the SVC injects into the power network. The magnitude of Q_{SVC} can be determined using the SVC voltage and the equivalent impedance,

$$Q_{SVC} = V_{SVC}^2 B_e \tag{5.6}$$

The typical steady state control of the SVC is depicted in Figure 5.5. This control law can be represented as

$$V_{SVC} = V_{REF} + X_{SL} I_{SVC} \tag{5.7}$$

where V_{REF} is a reference voltage for the controller, X_{SL} is the SVC control slope and α_{min} and α_{max} represent the lower and upper limits on the firing angle. The SVC current, I_{SVC}, can be expressed as

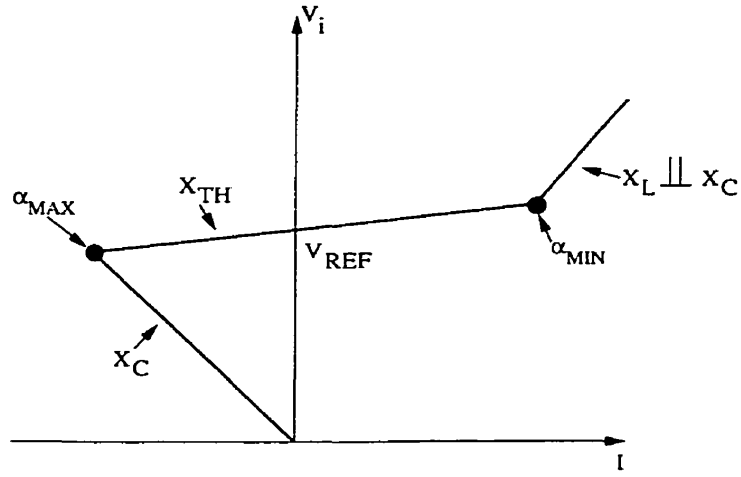


Figure 5.5: Typical steady state V-I characteristics of a SVC.

$$I_{SVC} = V_{SVC} B_e \tag{5.8}$$

Based on the model reviewed in this section, the SVC can be modeled in a power flow environment as

$$F(V_{REF}, I_{SVC}, Q_{SVC}, \alpha, B_e) = \begin{bmatrix} V_{SVC} - V_{REF} - X_{SL} I_{SVC} \\ I_{SVC} - V_{SVC} B_e \\ Q_{SVC} - V_{SVC}^2 B_e \\ \pi B_e X_L + \sin 2\alpha - 2\alpha + \pi(2 - \frac{X_L}{X_C}) \end{bmatrix} = 0 \tag{5.9}$$

In terms of Optimal Power Flow formulation, the set of equations (5.9) introduces four new dependent variables and one additional independent variable. The dependent variables are the current I_{SVC}, the reactive power Q_{SVC}, the firing angle α, and the equivalent conductance B_e. The independent variable is the voltage reference V_{REF}.

5.5 Numerical Analysis

The effect of incorporating the detailed generator model, static load models, and the SVC model into the VSC-OPF problems from Chapters 3 and 4 is analyzed by applying these problems to the 57-bus and 118-bus test systems. To determine both the general characteristics of the models and the effect of limits and loading conditions on the models, the analysis is done at several loading points, with and without limits on generation and bus voltage magnitudes.

The nonlinear Predictor-Corrector Interior Point method, presented in Chapter 2, is used to perform the numerical analysis.

5.5.1 Detailed Generator Model

The difference between the detailed generator model and the traditional (PV) model is first compared for a traditional OPF problem. A plot of the cost versus loading level when using the two models for the 57-bus system is shown in Figure 5.6. For all loading levels the costs for the two models are similar, but at higher loading levels, as reactive power limits for the PV generator model become active, the detailed generator model has a lower cost. This characteristic is shown in Figure 5.7, which is a plot of the percentage difference in operating costs when using the two generator models. This behavior corresponds to a better incorporation of machine limits directly into the system model. It is noted that the traditional model does provide a conservative estimate and that, in most cases, the generator set-points were similar. However, the difference in cost is very small when compared to the total operating costs.

The detailed generator model was incorporated into the formulations presented in Chapters 3 and 4. A summary showing the maximum loading value found by solving the Maximum Distance to Collapse formulation for the 57-bus system is given in Table 5.1. In each case, using the detailed generator model gave a higher maximum loading level, however, as generator active power limits tend to become active before voltage limits,

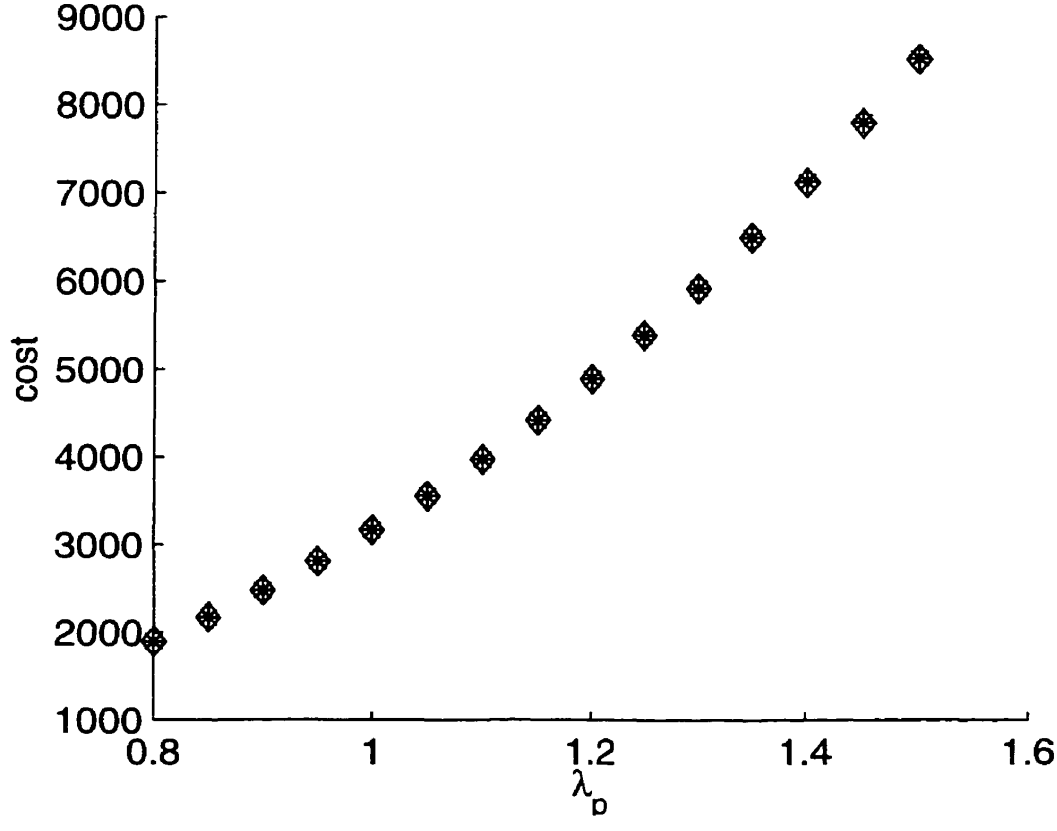


Figure 5.6: Cost versus current loading point for the 57-bus system when minimizing cost. The $*$ and $\Diamond$ symbols indicate the use of the PV model and the detailed generator model respectively.

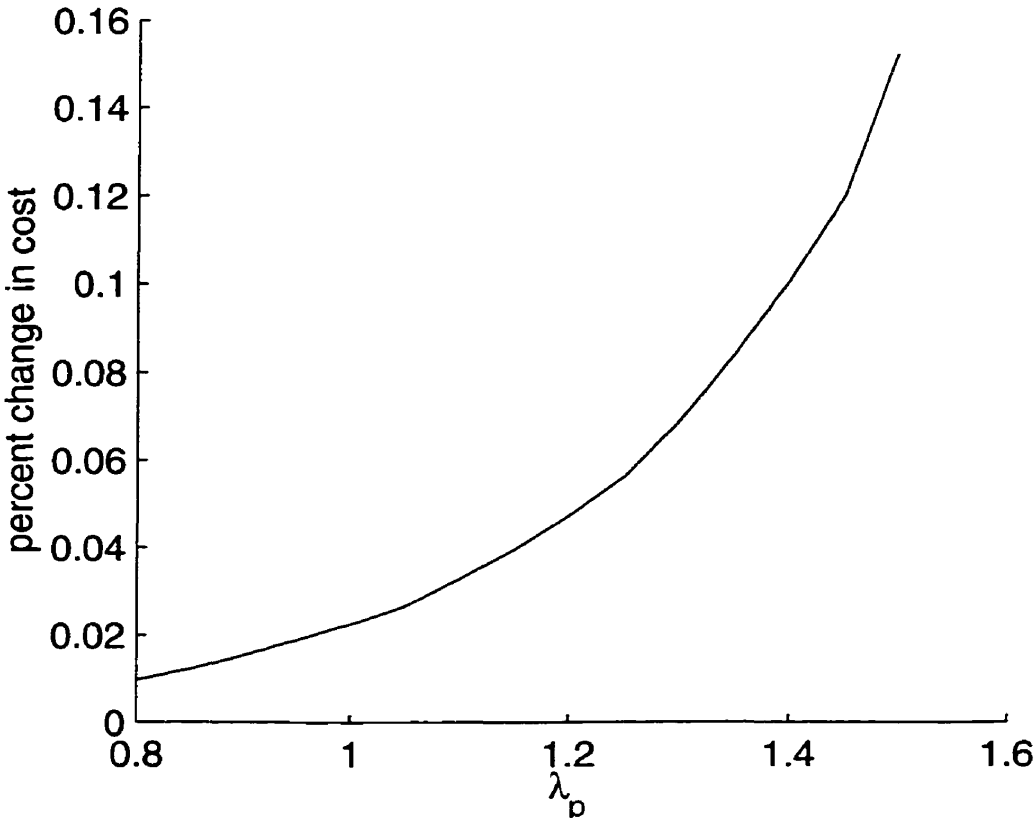


Figure 5.7: Difference in operating costs between the detailed generator model and the traditional PV generator model for the 57-bus system.

Table 5.1: Maximum Loading (λ_*) for the 57-bus system found by applying the Maximum Distance to Collapse formulation using the detailed generator model

Parameter	Detailed Generator Model	Constant PV Generator Model
Only Generator Limits	1.5371	1.5360
Operational Limits	1.5371	1.5360

including voltage limits in the problem did not affect the maximum loading point. The higher loading point for the detailed model is attributed to the relaxation of reactive limits due to limits on the armature current and field voltage. The maximum loading point for both models was limited by active power limits, which explains why both models have similar values of λ_*.

A plot of the maximum loading level (λ_*) versus the current operating point (λ_p) when applying the Modified Maximum Distance to Collapse formulation is shown in Figure 5.8. The Modified Maximum Distance to Collapse formulation (equation (4.6)) considers both the maximum and the current operating point, whereas the Maximum Distance to Collapse formulation only considers the maximum loading point. In general, for all loading levels, the PV and detailed generator model have similar characteristics, but using the detailed generator model resulted in a higher maximum loading level until a fixed upper limit of $\lambda_* = 1.537$. For both models, at lower loading levels, upper voltage limits for some non-generator buses at the current operating point limited raising generator voltage settings, which in turn reduced the maximum loading level. As the current loading level is increased, these bus voltages decrease, allowing the generator voltage settings to be increased which in turn results in a higher maximum loading level. For the PV generator models, reactive power limits also limit the maximum loading level. For both models,

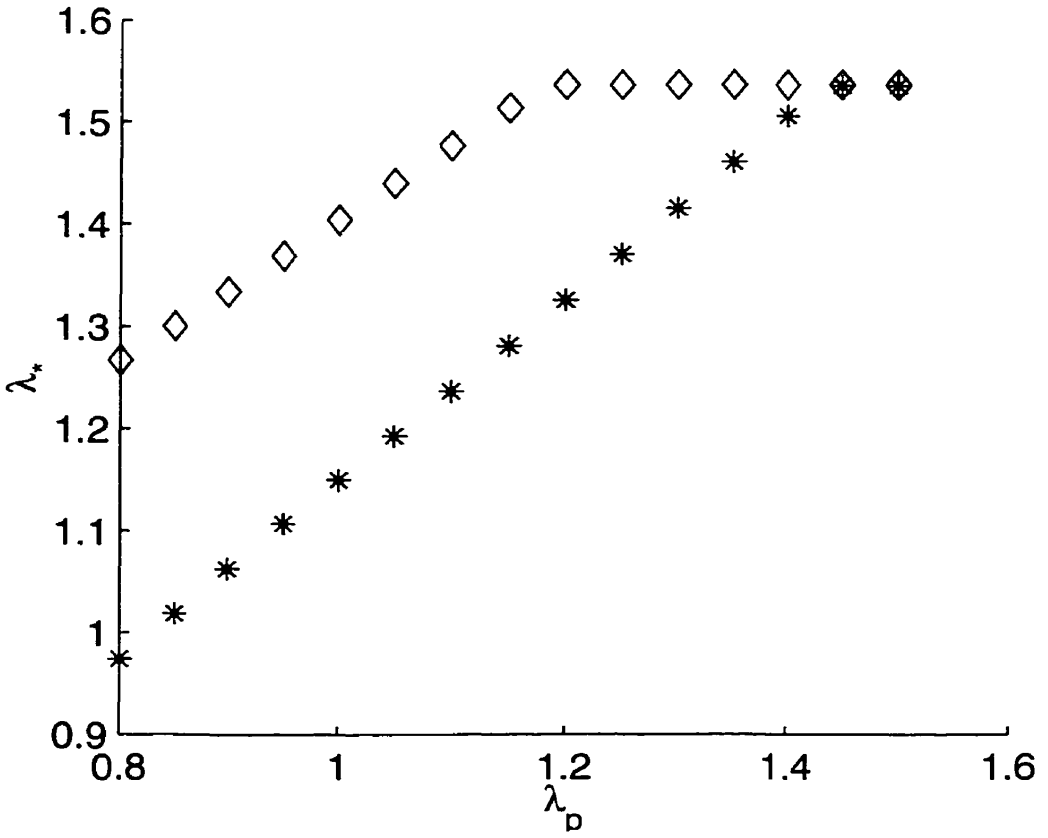


Figure 5.8: Maximum loading versus current loading point for the 57-bus system when solving the maximum distance to collapse formulation. The symbols $*$ and $\Diamond$ indicate the use of PV and the detailed generator models, respectively.

limits on active power eventually define a fixed upper limit on the maximum loading level, resulting in approximately the same maximum loading level (λ_*).

The effect of solving the other VSC-OPF formulations proposed in Chapter 4 using the detailed generator model, resulted in similar characteristics as was observed in Section 4.3, except that using the detailed generator model results, in general, in higher maximum loading levels, as expected.

5.5.2 Exponential Load Models

In traditional voltage stability analysis, constant impedance and current load models tend to have larger stability margins than constant power or current models. This is attributed to the fact that the actual power consumption of the load decreases as the bus voltage decreases for both constant current and impedance models, resulting in a less stressed system. For the analysis presented in this section, load increases for all loading models, are given as:

$$\begin{aligned} P &= \lambda P_{load} \\ Q &= \lambda Q_{load} \end{aligned} \tag{5.10}$$

where λ is the bifurcation or loading parameter and P_{load} and Q_{load} are defined from equations (5.3).

The different load models are first incorporated into a traditional OPF problem, i.e., voltage stability is not considered in this case. A plot of the cost versus loading level using the three load models for the 57-bus system is shown in Figure 5.9. For all loading levels the constant impedance model results in the lowest cost, followed by the constant current model, and finally the constant power model. Generator voltage settings for the constant current/impedance models tend to be set low, to reduce the amount of power absorbed by the loads. With the constant power load model, the generator voltage levels

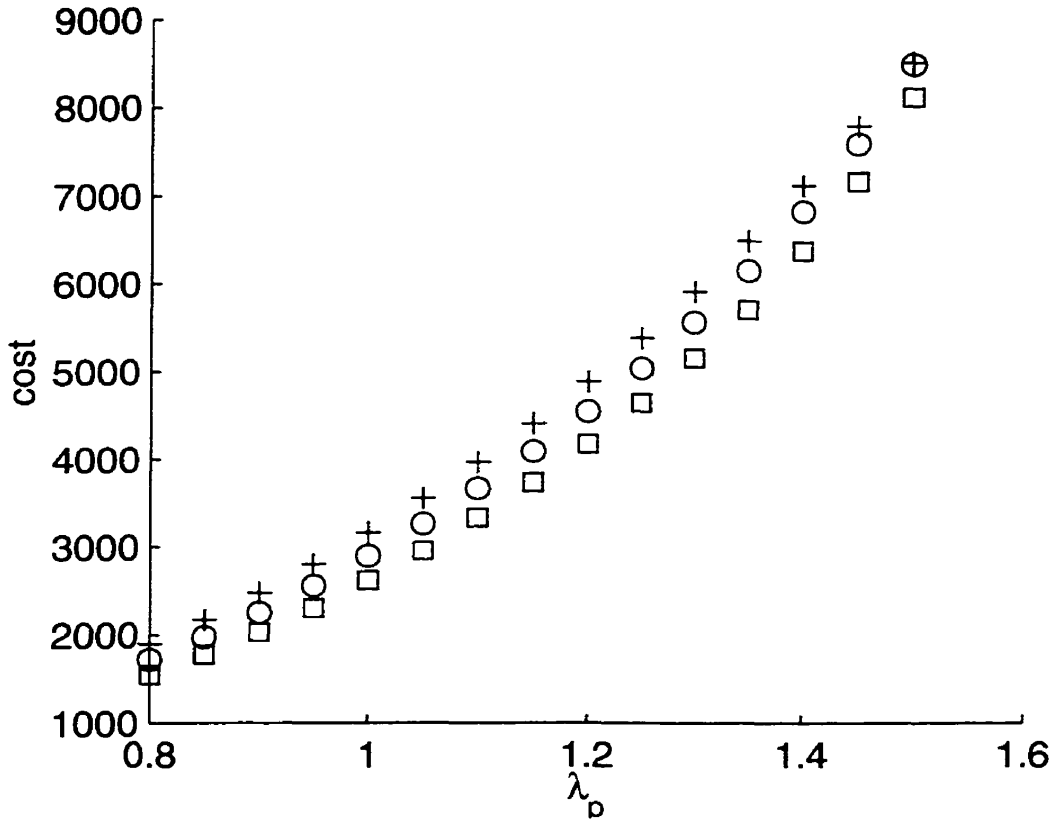


Figure 5.9: Cost versus current loading point for the 57-bus system when solving the traditional OPF problem. The symbols +, ∘, and □ indicate the use of constant power, current and impedance models, respectively.

tend to be set higher to reduce losses in the lines. The relative costs for the three models do not change greatly with increased loading.

As shown in Figure 5.10, incorporating the three load models into the traditional OPF problem for the 118-bus system results in similar characteristics as for the 57-bus system.

The different load models are then incorporated into the Voltage Stability Constrained OPF formulations presented in Chapters 3 and 4. A summary showing the maximum loading values obtained by solving the Maximum Distance to Collapse formulation for both the 57-bus and 118-bus systems is given in Tables 5.2 and 5.3. For both systems, when considering only generator limits at the critical point, using a constant impedance model gave the highest maximum loading level followed by the constant current model,

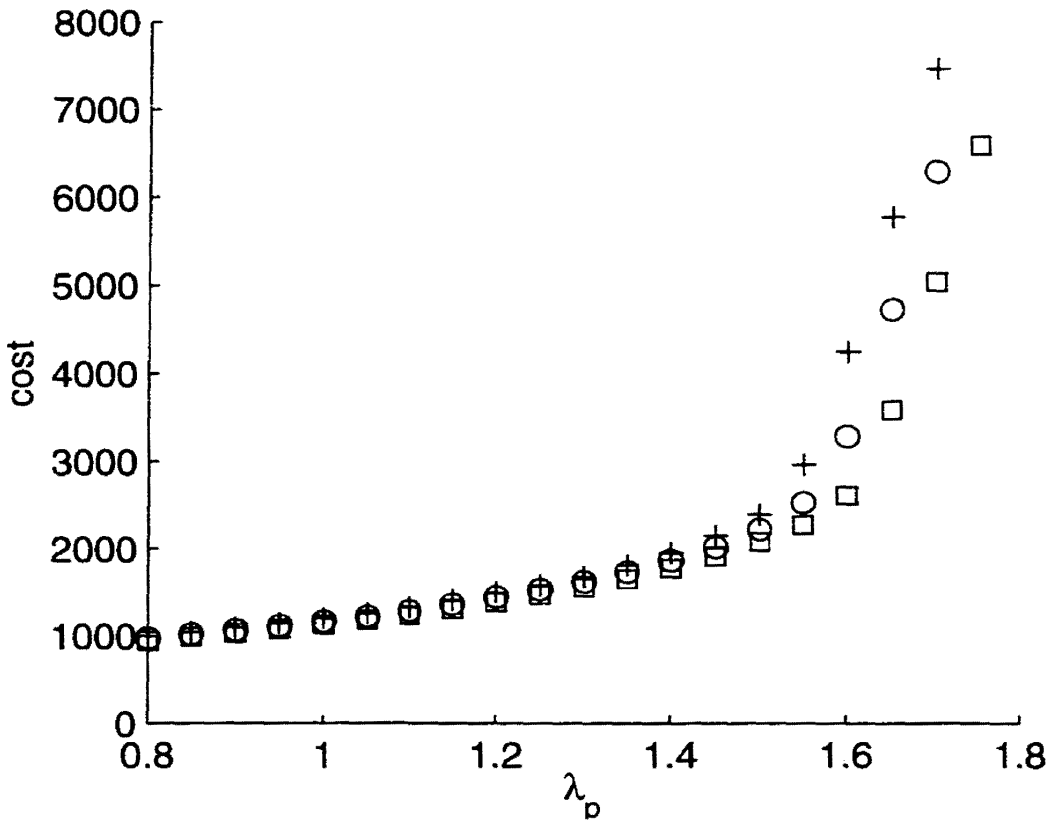


Figure 5.10: Cost versus current loading point for the 118-bus system when solving the traditional OPF problem. The symbols +, ∘, and □ indicate the use of constant power, current and impedance models, respectively.

Table 5.2: Maximum Loading λ_* for the 57-bus system found for the Maximum Distance to Collapse formulation.

	Constant Impedance load	Constant Current load	Constant Power load
Only Generator Limits at λ_*	3.8923	2.1285	1.5361
Operational Limits at λ_*	1.5403	1.5295	1.5361

then the constant power model, as expected.

An interesting result observed from these tables is the effect of voltage limits on the value of the maximum loading level. For example, for the 118-bus system, the difference between the results obtained for the three load models is greatly reduced when bus voltage limits are also placed on the maximum loading point. Furthermore, for the 57-bus system, when voltage limits are included in the problem, the maximum loading point λ_* for the constant power loads is slightly greater than when using constant current load model. This behavior can be explained as follows: When the load is modeled using voltage dependent models, the solution to the problem tends to lower terminal voltages, due to the fact that lower bus voltages result in less power consumption. However, when lower limits are placed on the magnitude of bus voltages, some generator voltage settings must be raised, resulting in increased real and reactive power demand, which leads to generator power limits becoming active, limiting λ_*. Therefore, a "balance" condition is reached for the voltage dependent loads, between the increases in λ_* from reduced power consumption with reduced voltages, and decreases in λ_* when voltages have to be increased to maintain minimum values.

Next, the Modified Maximum Distance to Collapse formulation is used for the two test systems. Figures 5.11 and 5.12 are plots of the maximum loading level λ_* versus the

Table 5.3: Maximum Loading λ_* for the 118-bus system found for the Maximum Distance to Collapse formulation.

	Constant Impedance load	Constant Current load	Constant Power load
Only Generator Limits at λ_*	6.6854	3.2442	2.1606
Operational Limits at λ_*	1.9245	1.8738	1.8253

current operating point λ_p for the 57-bus and 118-bus systems when applying the Modified Maximum Distance to Collapse formulation with full operating limits at the maximum loading point. For all three load models, the maximum loading level λ_* increases as the current operating point λ_p is increased, a characteristic observed and explained in Chapter 4 for constant power loads. The behavior of the voltage dependent loads (constant current and impedance loads) is due to the interaction between limits becoming active and the voltage dependency of the loads. When using these load models, the solution to the problem tends to lower voltage levels to reduce the power levels of the loads. However, bus voltages reaching lower limits, at the maximum loading point λ_*, force increases in voltage settings at the current operating point, resulting in some non-generator buses at the current operating point reaching upper voltage limits, similar to the behavior observed when using constant power load models.

The effect of limits on the behavior of the Modified Maximum Distance to Collapse formulation is further illustrated by modifying the limits of the 57-bus system. The modified limits are based on the limits used in [31]. Generally, the modified 57-bus system has higher maximum voltage limits and reduced lower voltage limits. Furthermore, some of the reactive power limits are higher, but the reactive power limit for the generator at Bus 1 is substantially reduced. No changes were applied to the active power limits.

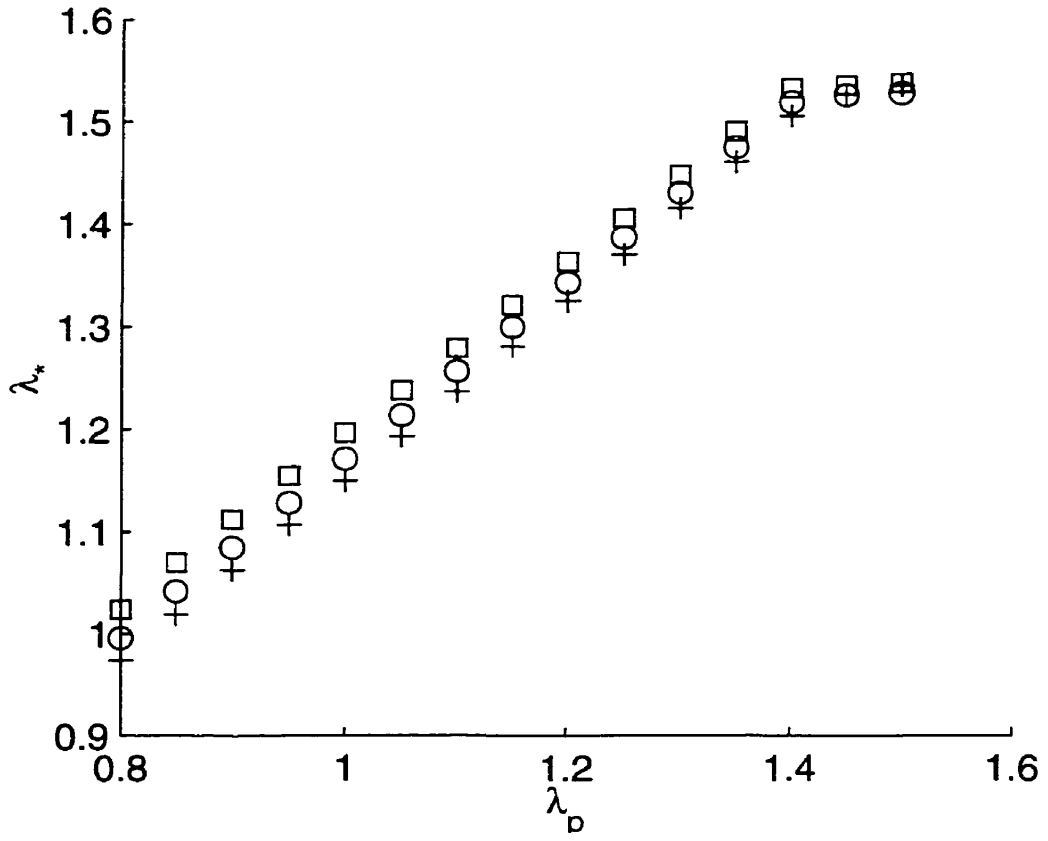


Figure 5.11: Maximum loading versus current loading point for the 57-bus system when maximizing the distance to collapse. The symbols +, ∘, and □ indicate the use of constant power, current and impedance models, respectively.

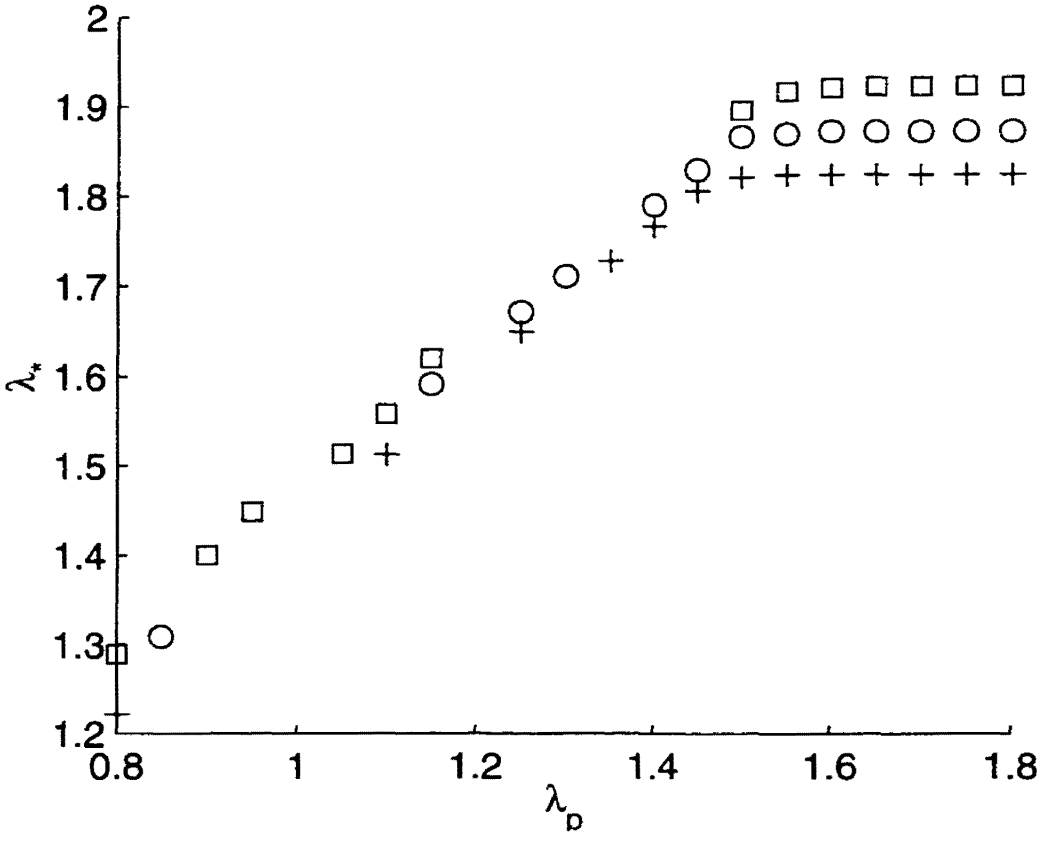


Figure 5.12: Maximum loading versus current loading point for the 118-bus system when maximizing the distance to collapse. The symbols +, ○, and □ indicate the use of constant power, current and impedance models, respectively.

Figure 5.13 illustrates the results obtained by applying the Modified Maximum Distance to Collapse formulation to the modified 57-bus system with only generator real and reactive power limits at the maximum loading point. For lower loading levels, all three load models, exhibit similar behavior as the original system. However, as the current loading point is increased, the maximum distance to collapse starts to decrease for the constant current and constant impedance models. This behavior can be explained as follows: When using constant current and impedance models, lower limits on the voltage at the current loading level tend to limit the maximum distance to collapse. As the loading level increases, generator voltage levels have to be increased to prevent voltage levels at non-generator buses from becoming too low at the current point. But increased generator voltage levels result in increased reactive power output from the generators (especially at the maximum loading point). The increased reactive power demand results in a lower stability margin as reactive power limits are reached (generator at Bus 1). For the constant current and constant impedance models, all the solutions obtained without voltage limits on the maximum loading point had one load bus voltage at a minimum setting. For any increases in load, this bus voltage would drop below an acceptable operating level. When using the constant power load model, power limits at the maximum operating point are reached at $\lambda_p = 0.9$ per unit limiting any further increases in the maximum loading point.

The effect of incorporating operational limits on the maximum loading point λ_* is shown in Figure 5.14 (for the modified 57-bus system) when solving the Modified Maximum Distance to Collapse formulation. For all three load models, incorporating lower voltage limits at the maximum loading point results in lower values of λ_*, but ensures that all loading points between the current and the maximum operating level are acceptable operating points. When using constant impedance load models, at low loading levels, similar characteristics as before are observed. A limit on a generator's reactive power output at the maximum loading point is reached at $\lambda_p = 0.85$, and no further improvements can be made to optimize the maximum loading point, with the maximum distance to collapse remaining constant for larger values of λ_p. For the constant current model, all generator reactive power upper limits are reached with the generator settings at the initial loading

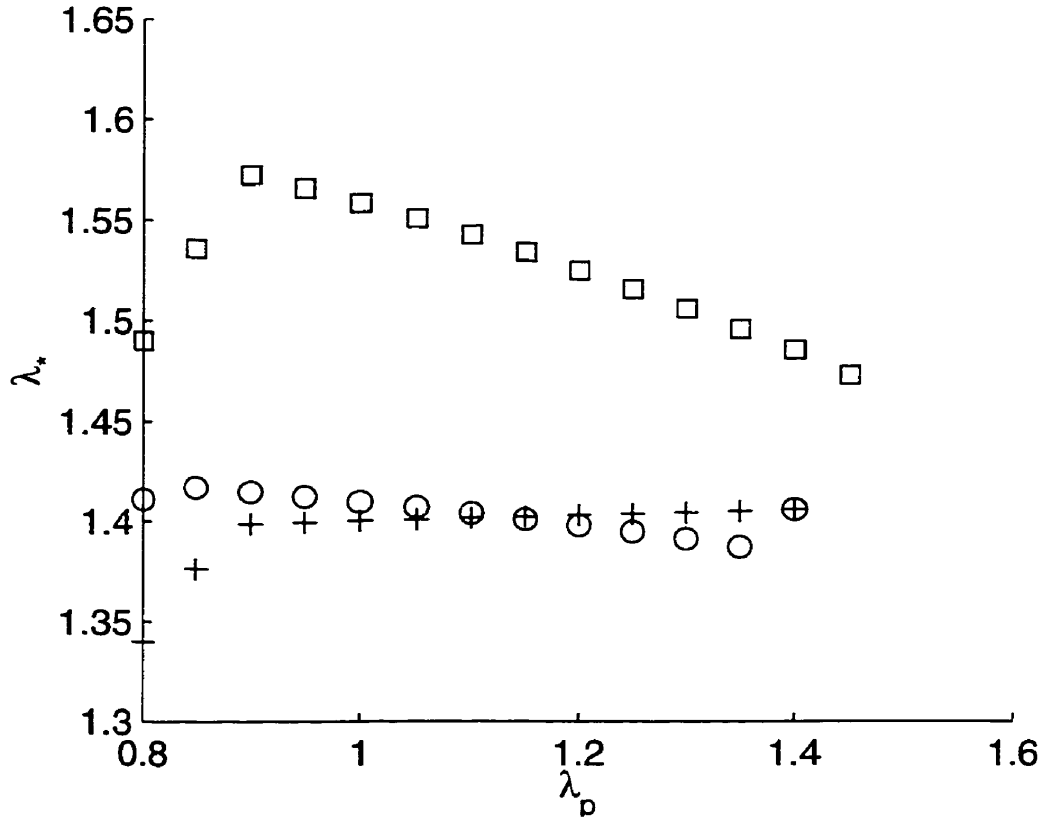


Figure 5.13: Maximum loading versus current loading point for the modified 57-bus system when maximizing the distance to collapse with generator real and reactive power limits at the critical point. The symbols +, ∘, and □ indicate the use of constant power, current and impedance models, respectively.

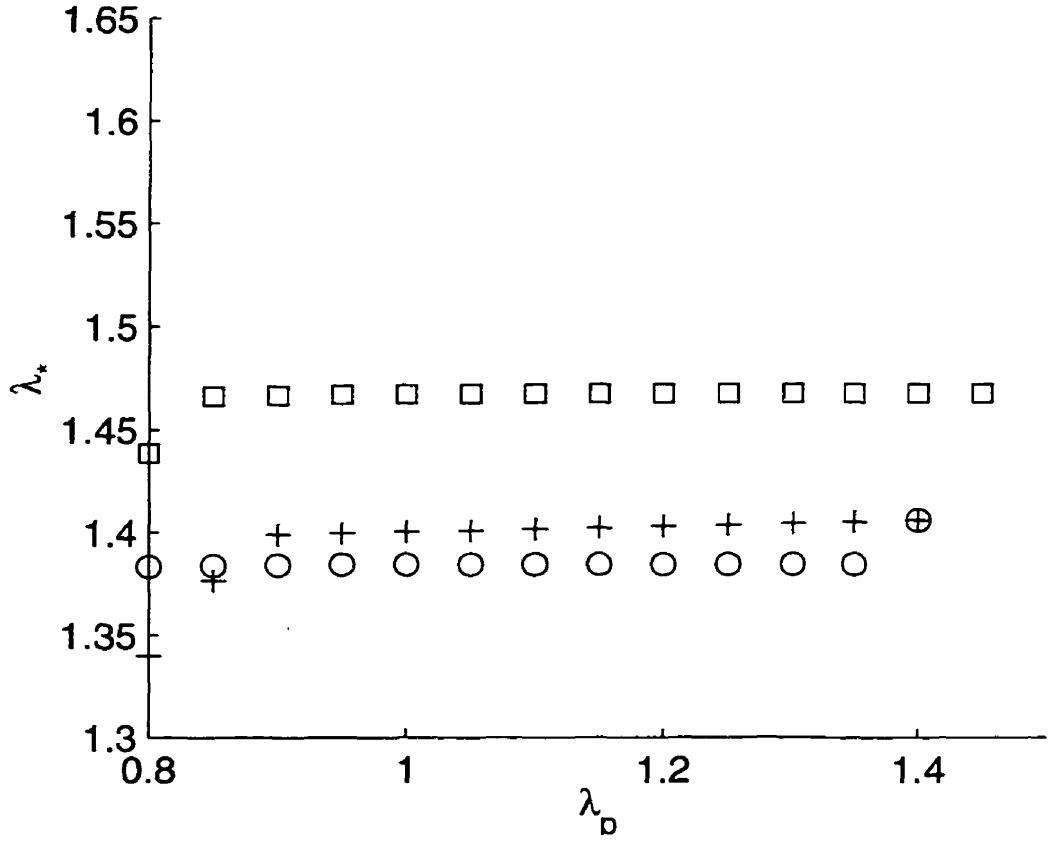


Figure 5.14: Maximum loading versus current loading point for the modified 57-bus system when maximizing the distance to collapse with operating limits at the critical point. The symbols +, ∘, and □ indicate the use of constant power, current and impedance models, respectively.

point, causing the value of λ_* to remain constant for all remaining values of λ_p. The negative slope of λ_* versus λ_p does not appear, because no voltages at the current loading point are at lower limits, as that would imply that those bus voltages would be below their operating limit at the critical loading point.

5.5.3 Static Var Compensator

Finally, the power flow SVC model is incorporated into both the traditional OPF and the VSC-OPF formulations. A SVC model was placed at Bus 31 of the 57-bus system using the SVC data presented in [71]. The single line diagram of the 57-bus system is given in Figure 4.1. The SVC was placed based on an analysis of the eigenvectors associated with the zero eigenvalue (saddle-node bifurcation) the system experiences at high loading levels [71].

Figure 5.15 shows the difference in total operating costs for the 57-bus system with the SVC controller in the system versus no SVC when solving the traditional OPF problem. As expected, the effect of the SVC on reducing operating costs is more significant at higher loading levels.

The effect of the SVC controller on the maximum loading level of the system when solving the Modified Maximum Distance to Collapse formulation with no limits being enforced at the maximum loading point is illustrated in Figure 5.16. As depicted, the SVC significantly increases the loadability of the system. Figure 5.17 shows the results obtained when enforcing limits at the maximum loading point for the Modified Maximum Distance to Collapse formulation. For all loading points the SVC enhances the stability margin, but the amount of improvement decreases because of limits. This further illustrates the significant effect of limits on these types of problems.

Incorporating the SVC controller into the various VSC-OPF problems resulted in similar characteristics as observed in Section 4.1.3, except that using the SVC model results in higher maximum loading levels and reduced costs, as expected. Figure 5.18 is a

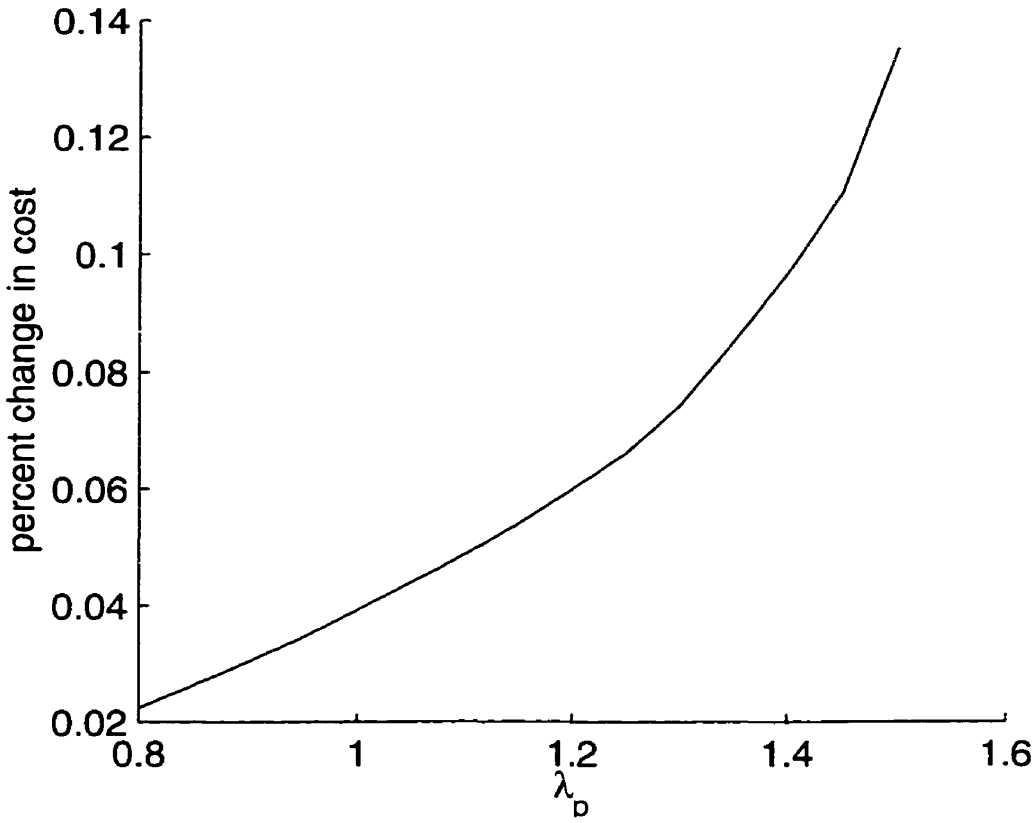


Figure 5.15: Difference in total operating costs with a SVC placed at Bus 31 of the 57-bus system versus no SVC when solving the traditional OPF problem.

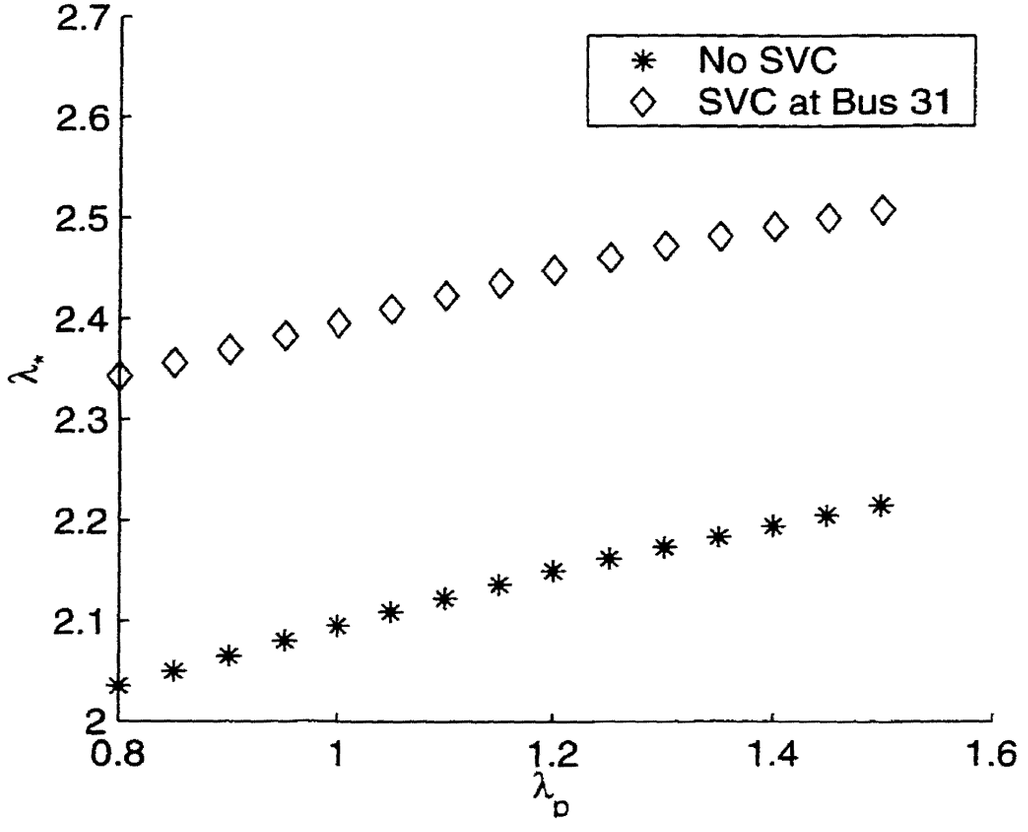


Figure 5.16: Difference in maximum loading point with a SVC placed at Bus 31 of the 57-bus system versus no SVC when solving the Modified Maximum Distance to Collapse formulation with no limits at the maximum loading point.

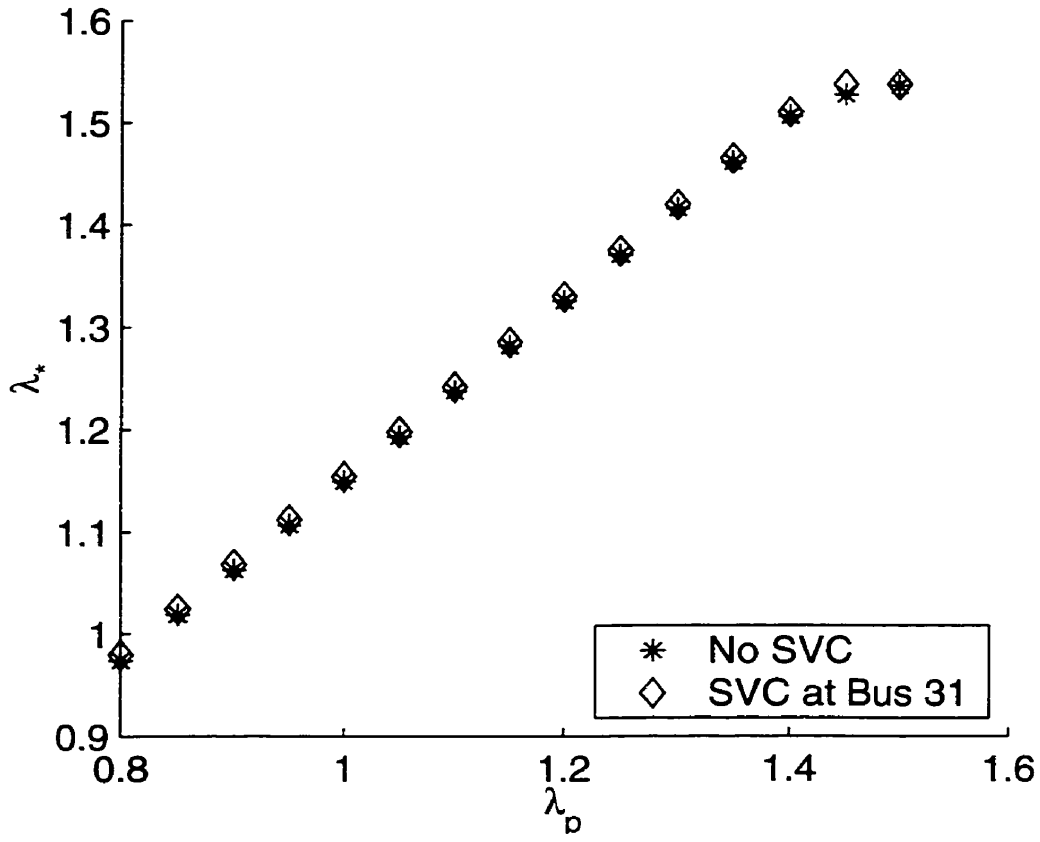


Figure 5.17: Difference in maximum loading point with a SVC placed at Bus 31 of the 57-bus system versus no SVC when solving the Modified Maximum Distance to Collapse formulation with operating limits at the maximum loading point.

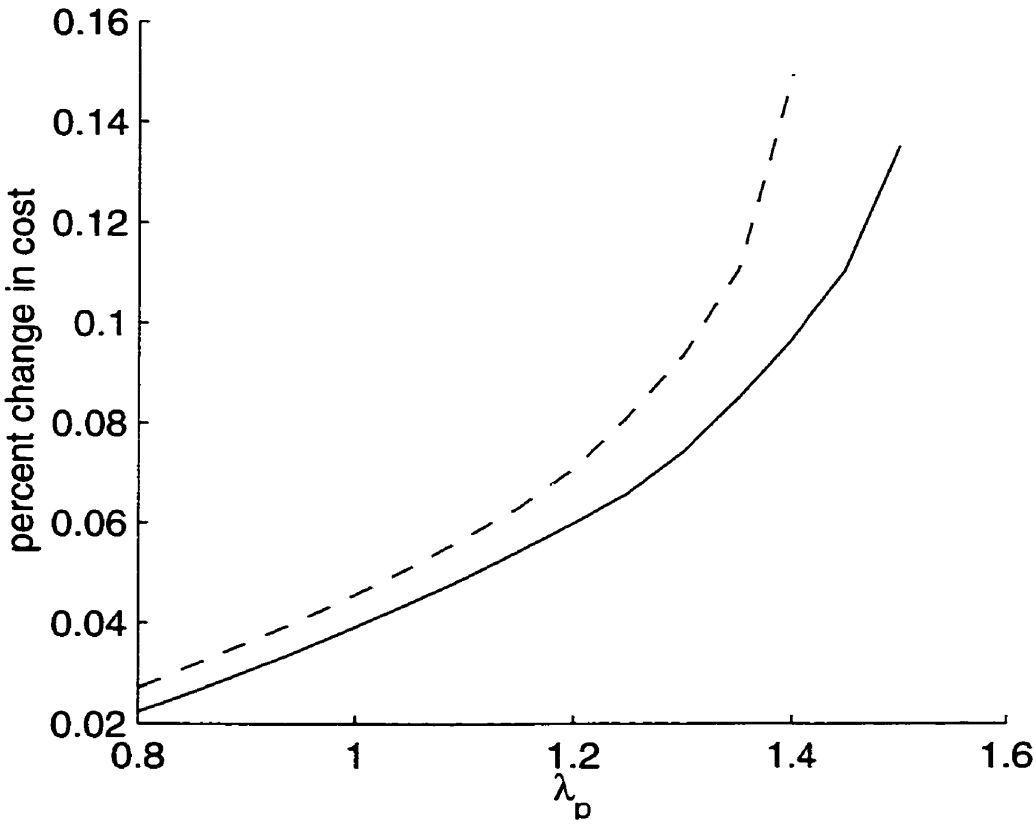


Figure 5.18: Difference in total operating costs with a SVC placed at Bus 31 of the 57-bus system versus no SVC when solving the Fixed Stability Margin VSC-OPF formulation (dashed line) and the traditional OPF problem (solid line) with operating limits at the maximum loading point.

plot of the reduction in the total operating costs by incorporating the SVC into the Fixed Stability Margin VSC-OPF formulation. The difference in the total operating costs when solving the traditional OPF problem is included in Figure 5.18 to demonstrate that when, considering both stability and operating costs, the benefits of incorporating the SVC are greater.

5.6 Summary of Results

In this chapter, a detailed generator model is incorporated into various voltage stability constrained optimal power flow problems. The results are compared to those obtained by

using a traditional OPF formulation. The use of a detailed generator model resulted in higher stability margins.

Three static load models are analyzed when applied to OPF and VSC-OPF problems. The characteristics of the load models are analyzed using various examples in order to demonstrate the effects of limits. The lowering of generator voltage settings to reduce generator power output when using constant impedance and constant current load models, indicates the need to include full operating limits on the current and the maximum loading point.

Finally, a load flow SVC model, is incorporated into both the traditional OPF problem and the VSC-OPF formulations. It was shown that incorporating the SVC resulted in lower operating costs, especially at higher loading levels. As expected, the SVC improved the maximum loading point, but limits at the maximum loading point reduced these stability "gains".

Chapter 6

Conclusions

6.1 Summary and Contributions

This thesis proposes a variety of formulations to perform voltage stability and optimal power flow studies concurrently.

In Chapter 2, the Optimal Power Flow problem is presented. Both a Primal-Dual Interior-Point and a Predictor-Corrector Interior Point method for non-linear optimization problems are presented to solve the OPF and Voltage Stability Constrained OPF problems presented in this thesis.

In Chapter 3, concepts and terminology of bifurcation analysis are described. Two traditional techniques for bifurcation analysis are presented. Issues related to optimization based approaches to voltage stability analysis, including the system model and the effect of control parameters are discussed. Finally, an optimization based approach is extended to formulate the Maximum Distance to Collapse and Maximum Distance to Saddle-node Bifurcation problems.

In Chapter 4, several methods for "pricing" voltage security in OPF formulations are proposed by incorporating voltage stability into traditional OPF problems, demonstrating its effect on operating costs. The results show the importance of including the current and maximum loading points in optimization procedures used for voltage stability analysis, as limits on these points significantly influence these types of studies. Furthermore, a method to include reactive power costs in an OPF problem is proposed. This formulation can be a very useful tool in the operation of electricity markets.

Finally, in Chapter 5, a detailed generator model is incorporated into various stability constrained optimal power flow problems. The results are compared to those obtained using a traditional OPF formulation. Furthermore, three load models are analyzed when applied to OPF and VSC-OPF problems. The characteristics of the load models are analyzed to demonstrate the effects of limits.

The main contributions of the thesis can be summarized as:

- Development of Voltage Stability Constrained Optimal Power Flow (VSC-OPF) formulations to incorporate voltage stability margins. The following VSC-OPF formulations are proposed:

  1. Hybrid VSC-OPF Formulation
  2. Linear Combination VSC-OPF Formulation
  3. Fixed Stability Margin VSC-OPF Formulation
  4. Goal VSC-OPF Formulation

  It was demonstrated that incorporating voltage stability into a traditional OPF problem results in higher operating costs.

- Development and implementation of a technique to incorporate reactive power pricing in electricity systems. This formulation and the Goal VSC-OPF formulation demonstrate methods to incorporate voltage stability and reactive power pricing in the operation of power systems.

- The inclusion of the current and maximum loading levels in optimization formulations for voltage stability analysis. The importance of this formulation is demonstrated by showing the influence of limits at the current and maximum loading points on these types of studies.

- Incorporation and analysis of detailed generator models, voltage dependent load models, and a Static Var Compensator model into the OPF and VSC-OPF formulations.

6.2 Directions for Future Work

Interesting directions for future work focus around the incorporation of the proposed VSC-OPF formulations in an electricity market environment. This would involve the determination of the *stability costs* in the operation of a power system, which is of great interest in these markets.

The non-linear interior point method written for the current research can be modified to allow for the investigation of the use of the Lagrangian Multipliers as indicators of the "cost" of stability with regards to some parameter limits. The use of Lagrangian Multipliers and the VSC-OPF formulations may also be used to determine placement locations for reactive support and FACTS controllers. Furthermore, since the proposed tools may have a direct application in the operation of electricity markets, other formulations of active and reactive power "costs" could be analyzed.

Bibliography

[1] "Power systems outages that occurred in the western interconnection on july 1996," technical report, Western Systems Coordinating Council (WSCC), September 1996.

[2] N. Mithulananthan. *Voltage Stability Study of the Sri Lankan Power System Grid.* Master's thesis, Asian Institute of Technology, Bangkok, Thailand, 1997.

[3] C. A. Cañizares, editor, "Voltage stability assessment, procedures and guides," technical report, IEEE/PES Power System Stability Subcommittee. Available at http://www.power.uwaterloo.ca.

[4] C. A. Cañizares, "Applications of optimization to voltage collapse analysis," Panel Session, Optimization Techniques in Voltage Collapse Analysis, IEEE/PES Summer Meeting, San Diego, CA, Available at http://www.power.uwaterloo.ca, July 1998.

[5] W. Rosehart, "Power system optimization with voltage stability constraints," Student poster session, 1998 IEEE/PES Summer Meeting, San Diego, CA, *IEEE Power Engineering Review*, Oct. 1998, pp. 14.

[6] W. Rosehart, C. Cañizares, and V.H. Quintana, "Optimal power flow incorporating voltage collapse constraints," Proc. of the 1999 IEEE/PES Summer Meeting, Edmonton, Alberta, July 1999, pp. 820-825.

[7] W. Rosehart, C. Cañizares, and V.H. Quintana, "Cost of voltage stability in electricity markets," Proc. of the 2000 IEEE/PES Summer Meeting, Seattle, Washington, July 2000.

[8] O.O. Obadina and G. J. Berg, "Determination of voltage stability limit in multimachine power systems," *IEEE Trans. Power Systems*, vol. 3, 1988, pp. 1545–1554.

[9] O.O. Obadina and G. J. Berg, "Var planning for power system security," *IEEE Trans. Power Systems*, vol. 4, 1989, pp. 677–686.

[10] C. A. Cañizares, "Calculating optimal system parameters to maximize the distance to saddle node bifurcations," *IEEE-Transactions on Circuits and Systems-I: Fundamental Theory and Applications*, vol. 45, no. 3, March 1998, pp. 225–237.

[11] T. Van Cutsem, "A method to compute reactive power margins with respect to voltage collapse," *IEEE Trans. Power Systems*, vol. 6, no. 1, 1991, pp. 145–156.

[12] C.J. Parker, I.F. Morrison, and D. Sutanto, "Application of an optimization method for determining the reactive margin from voltage collapse in reactive power planning," *IEEE Trans. Power Systems*, vol. 11, no. 3, August 1996, pp. 1473–1481.

[13] F. Alvarado, I. Dobson, and Y. Hu, "Computation of closest bifurcations in power systems," *IEEE Trans. Power Systems*, vol. 9, no. 2, May 1994, pp. 918–928.

[14] I. Dobson and L. Lu, "New methods for computing a closest saddle-node bifurcation and worst case load power margin for voltage collapse," *IEEE Trans. Power Systems*, vol. 8, August 1993, pp. 905–913.

[15] G.D. Irisarri, X. Wang, J. Tong, and S. Mokhtari, "Maximum loadability of power systems using interior point non-linear optimization method," *IEEE Trans. Power Systems*, vol. 12, no. 1, February 1997, pp. 162–172.

[16] D. Chattopadhyay and D. Gan, "Dispatch optimization incorporating transient and voltage stability constraints," Proc. of the 2000 IEEE/PES Summer Meeting, Seattle, Washington, July 2000, pp 516-521.

[17] C.D. Vournas, M. Karystianos, and N. G. Maratos, "Bifurcation points and loadability limits as solutions of constrained optimization problems," Proc. of the 2000 IEEE/PES Summer Meeting, Seattle, Washington, July 2000, pp 1883-1888.

[18] R. Seydel, *From Equilibrium to Chaos—Practical Bifurcation and Stability Analysis.* Elsevier Science, North-Holland, 1988.

[19] K.R.W. Bell, D.S. Kirschen, R.N. Allan, and P. Kelen, "Efficient Monte Carlo assessment of the value of security," *Proceedings of the 13th PSCC*, June 1999, pp. 81–86.

[20] E. Vaahedi, J Tamby, Y. Mansour, Li Wenjuan, and D. Sun, "Large scale voltage stability constrained optimal var planing and voltage stability planning," *IEEE Transactions on Power Systems*, February 1999, pp. 65–74.

[21] C. A. Cañizares, "On bifurcations, voltage collapse and load modeling," *IEEE Trans. Power Systems*, vol. 10, no. 1, February 1995, pp. 512–522.

[22] P. A. Löf, G. Andersson, and D.J. Hill, "Voltage dependent reactive power limits for voltage stability studies," *IEEE Trans. Power Systems*, vol. 10, no. 1, February 1995, pp. 220–228.

[23] N. G. Hingorani, "Flexible AC Transmission Systems," *IEEE Spectrum*, April 1993, pp. 40–45.

[24] C. A. Cañizares and Z. T. Faur, "Analysis of svc and tcsc controllers in voltage collapse," accepted for publication in IEEE Trans. Power Systems PE-200-PWRS-0-2-1998, March 1998.

[25] P. Kundur, *Power System Stability and Control.* McGraw Hill Publishing Company, New York, 1994.

[26] T. Van Cutsem and C. Vournas, *Voltage Stability of Electric Power Systems.* Kluwer Academic Publishers, Boston, 1998.

[27] W. Rosehart and C. Cañizares, "Bifurcation analysis of various power system models," *International Journal of Electrical Power and Energy Systems*, vol. 21, July 1999, pp. 171–182.

[28] J. Guckenheimer and Philip Holmes, *Nonlinear Oscillations, Dynamical Systems and Bifurcations of Vector Fields.* Springer-Verlag, New York, 1983.

[29] C. A. Cañizares, "Conditions for saddle-node bifurcations in ac/dc power systems," *Int. J. of Electric Power & Energy Systems*, vol. 17, no. 1, February 1995, pp. 61–68.

[30] A. A. P. Lerm, C. A. Cañizares, F. A. B. Lemos, and A. S. e Silva, "Multi-parameter bifurcation analysis of power systems," *Proceedings of the North American Power Symposium*, Cleveland, Ohio, October 1998, pp. 76–82.

[31] G. L. Torres, *Nonlinear Optimal Power Flow by Interior and Non-Interior Point Methods*, PhD thesis, University of Waterloo, Waterloo, Ontario, 1998.

[32] G. L. Torres and V. H. Quintana, "An interior-point method for nonlinear optimal power flow using voltage rectangular coordinates," *IEEE Transactions on Power Systems*, November 1998, pp. 1211–1218.

[33] K. M. Heal, M. L. Hansen, and K. M. Rickard, *Maple V, Learning Guide.* Springer-Verlag, New York, 1996.

[34] The Math Works Inc., Natick, Massachusetts, *MATLAB*, 1993.

[35] D. P. Bertsekas, *Nonlinear Programming.* Athena Scientific, Belmont, Massachusetts, 1995.

[36] H. W. Dommel and W. F. Tinney, "Optimal power flow solutions," *IEEE-Transactions on Power Apparatus and Systems*, vol. PAS-87, no. 10, October 1965, pp. 1866–1876.

[37] M. E. El-Hawary, "IEEE Tutorial Course: optimal power flow: Solution techniques, requirements, and challenges," IEEE Power Engineering Society 96 TP 111-0.

[38] M. Huneault and F. D. Galiana, "A survey of the optimal power flow literature," *IEEE Trans. on Power Systems*, vol. 6, no. 2, 1991, pp. 762–770.

[39] L. H. Fink and P. J. M. van Son, "On system control within a restructured industry," *IEEE Trans. Power Systems*, vol. 13, no. 2, May 1998, pp. 611–616.

[40] R. Vanderbei, "ALPO: Another linear program optimizer," *ORSA Journal on Computing*, vol. 5, no. 2, 1993, pp. 134–146.

[41] G. L. Torres and V. H. Quintana , "Nonlinear optimal power flow in rectangular form via a primal-dual logarithmic barrier interior point method," technical report 96-08, University of Waterloo, 1996.

[42] G. L. Torres and V. H. Quintana, "Optimal power flow via interior point methods: An educational tool in matlab," pp. 996–999 in [72].

[43] A. Vannelli, V. H. Quintana, and L. Vargas, "Interior point optimization methods: Theory implementations and engineering applications," *Canadian Journal of Electrical and Computer Engineering*, vol. 17, no. 2, 1992, pp. 84–94.

[44] H. Wei, H. Sasaki, and R. Yokoyama, "An application of interior point quadratic programming algorithm to power system optimization problems," *IEEE Transactions on Power Systems*, vol. 11, no. 1, February 1996, pp. 260–266.

[45] Y Wu, A. S. Debs, and R. E. Marsten, "A direct nonlinear predictor-corrector primal-dual interior point algorithm," *IEEE-Transactions on Power Systems*, vol. 9, no. 2, May 1994, pp. 876–883.

[46] X. Yan and V. H. Quintana, "An efficient predictor-corrector interior point algorithm for security-constrained economic dispatch," *IEEE-Transactions on Power Systems*, vol. 12, no. 2, 1997, pp. 803–810.

[47] W. D. Rosehart, C. A. Cañizares, and Anthony Vannelli, "Sequential methods for solving optimal power flow problems," *Proc. IEEE Canadian Conference on Electrical and Computer Engineering*, St. John's Newfoundland, May 1997, pp. 444–449.

[48] C. A. Cañizares and S. Hranilovic, "Transcritical and Hopf bifurcations in ac/dc systems," *Proc. Bulk Power System Voltage Phenomena III—Voltage Stability and Security*, August 1994, pp. 105–114.

[49] W. D. Rosehart and C. A. Cañizares, "Elimination of algebraic constraints in power system studies," *Proc. IEEE Canadian Conference on Electrical and Computer Engineering*, University of Waterloo, Waterloo, Ontario, May 1998, pp. 685–688.

[50] C. A. Cañizares, F. L. Alvarado, C. L. DeMarco, I. Dobson, and W. F. Long, "Point of collapse methods applied to ac/dc power systems," *IEEE Trans. Power Systems*, vol. 7, no. 2, May 1992, pp. 673–683.

[51] I. Dobson and L. Lu, "Voltage collapse precipitated by the immediate change in stability when generator reactive power limits are encountered," *IEEE Transactions on Circuits and Systems–I: Fundamental Theory and Applications*, vol. 39, no. 9, September 1992, pp. 762–766.

[52] C. A. Cañizares and F. L. Alvarado, "Point of collapse and continuation methods for large ac/dc systems," *IEEE Trans. Power Systems*, vol. 8, no. 1, February 1993, pp. 1–8.

[53] V. Ajjarapu and C. Christy, "The continuation power flow: A tool for steady state voltage stability analysis," *IEEE Trans. Power Systems*, vol. 7, no. 1, February 1992, pp. 416–423.

[54] H. D. Chiang, A. J. Flueck, K. S. Shah, and N. Balu, "CPFLOW: A practical tool for tracing power system steady-state stationary behavior due to load and generation variations," *IEEE Trans. Power Systems*, vol. 10, no. 2, May 1995, pp. 623–634.

[55] F. L. Alvarado and T. H. Jung, "Direct detection of voltage collapse conditions," pp. 5.23–5.38 in [60].

[56] C. A. Cañizares, A. Z. de Sousa, and V. H. Quintana, "Improving continuation methods for tracing bifurcation diagrams in power systems," pp. 349–358 in [61].

[57] K. Iba, H. Suzuki, M. Egawa, and T. Watanabe, "Calculation of critical loading conditions with noise curve using homotopy continuation method," *IEEE-Transactions on Power Systems*, vol. 6, no. 2, May 1991, pp. 584–593.

[58] C. A. Cañizares and F. Alvarado, Discussion to [11].

[59] L. H. Fink, editor, *Proc. Bulk Power System Voltage Phenomena II—Voltage Stability and Security*, ECC Inc., Fairfax, VA, August 1991.

[60] L. H. Fink, editor, *Proc. Bulk Power System Voltage Phenomena—Voltage Stability and Security*, EL-6183, EPRI, January 1989.

[61] L. H. Fink, editor, *Proc. Bulk Power System Voltage Phenomena III—Voltage Stability and Security*, ECC Inc., Fairfax, VA, August 1994.

[62] University of Washington Archive, http://www.ee.washington.edu/research/pstca.

[63] J. W. Lamont and J. Fu, "Cost analysis of reactive power support," *IEEE Transactions on Power Systems*, August 1999, pp. 890–898.

[64] R. Zimmerman and D. Gan, MATPOWER - Matlab routines for solving power flow problems. http://www.pserc.cornell.edu.

[65] C. A. Cañizares et. al, "Uwpflow: Continuation and direct methods to locate fold bifurcations in ac/dc/facts power systems," *University of Waterloo*, Available at: hppt://www.power.uwaterloo.ca, August 1998.

[66] D.H. Popovic, I.A. Hiskens, Y.V. Makarov, and D. J. Hill, "Investigation of load-tap changer interaction," *Electrical Power and Energy Systems*, vol. 18, no. 2, 1996, pp. 81–97.

[67] J. Arrillaga, C. P. Arnold, and B. J. Harker, *Computer Modeling of Electric Power Systems*. John Wiley and Sons, Chichester, 1983.

[68] P. C. Krause, *Analysis of Electric Machinery*. McGraw-Hill Inc., New York, 1986.

[69] S. Chapman, *Electric Machinery Fundamentals, Third Addition*. McGraw Hill, New York, 1998.

[70] R. Ramshaw and R. G. van Heeswijk, *Energy Conversion: Electric Motors and Generators*. Saunders College Publishing, Orlando, FL, 1990.

[71] Z. T. Faur and C. A. Cañizares, "Effects of FACTS devices on system loadability," *Proc. North American Power Symposium*, Bozeman, Montana, October 1995, pp. 520–524.

[72] T. Malkinson, editor, *Canadian Conference on Electrical and Computer Engineering*, The University of Calgary, Calgary, Alberta, May 1996.